

# **Polymeric Dispersions for the Protection of Limestone: Application on Noto and Comiso Stone**

**Facoltà di Scienze Matematiche, Fisiche e Naturali**

**Corso di laurea in Scienze e Tecnologie per la Conservazione dei Beni Culturali  
Erasmus Mundus Master in Archaeological Materials Science (ARCHMAT)**

**Iлона Viliunaite**  
**1723241**

Relatore  
Prof. Eugenio Caponetti



Correlatore  
Dr. Silvestro Antonio Ruffolo



Correlatore  
Prof. Giovanni Ettore Gigante



## Contents

I.	Introduction.....	5
a.	Weathering of the stone .....	5
i.	Action of water .....	5
ii.	Action of atmospheric gasses and pollution .....	6
iii.	Action of water soluble salts .....	7
iv.	Biological factors .....	8
b.	Stone conservation procedure and materials.....	9
i.	Cleaning .....	10
ii.	Consolidation .....	11
iii.	Protection .....	13
II.	Aim of the study.....	16
III.	Characterization techniques .....	18
a.	Mercury intrusion porosimetry and petrographic characterization .....	18
b.	X-ray diffraction (XRD) .....	18
c.	Colorimetry.....	18
d.	Liquid water absorption by capillarity .....	19
e.	Water vapor permeability.....	20
f.	Static contact angle .....	22
g.	Fourier Transformed Infrared (FT-IR) Spectroscopy .....	22
h.	Solid state Nuclear Magnetic Resonance (ss-NMR) Spectroscopy .....	23
i.	Scanning Electron Microscopy (SEM) .....	24
j.	X-ray Fluorescence (XRF).....	24
IV.	Materials .....	25
a.	Lithotypes .....	25
i.	Noto stone .....	26
ii.	Comiso stone.....	35
b.	Protective polymeric dispersions .....	42
i.	Fluoline HY .....	42
ii.	Silo 111 .....	45
iii.	Wacker 290 .....	47
V.	Sample preparation .....	49



VI.	Evaluation of the Effectiveness of the Treatment .....	52
a.	Noto stone .....	52
i.	Colorimetry .....	52
ii.	Liquid water absorption .....	53
iii.	Water vapour permeability.....	55
iv.	Static contact angle .....	56
v.	Total Reflectance FT-IR .....	56
vi.	ss-NMR .....	59
vii.	SEM-EDX.....	61
b.	Comiso stone.....	67
i.	Colorimetry .....	67
ii.	Liquid water absorption .....	68
iii.	Water vapor permeability.....	70
iv.	Static contact angle .....	70
v.	Total Reflectance FT-IR .....	71
vi.	ss-NMR .....	74
vii.	SEM-EDX.....	77
VII.	Samples treated till rejection with Silo 111 .....	82
a.	Colorimetry .....	82
b.	Liquid water absorption .....	83
c.	Contact angle .....	85
VIII.	Discussion .....	86
IX.	Conclusions.....	91
X.	Appendix.....	100

## ABSTRACT

Architectural heritage made of limestone faces a lot of threats due to the presence of water intrusions from various sources. This problem encouraged the development of hydrophobic polymeric dispersions for the protection of stone objects. In the following study, Noto and Comiso stone samples were selected and treated with three commercial protective polymeric dispersions of different chemical composition. Untreated samples were characterized by optical microscopy, porosimetry, XRD and XRF. An extensive characterization of the treated samples was performed in order to evaluate the changes in the stone properties upon treatment with the dispersions. According to UNI EN recommendations, several tests were performed in order to evaluate developed hydrophobic effects and chromatic changes. SEM-EDX was used to study the elemental composition of the surface and to observe changes in its morphology. Reflection FT-IR spectroscopy and ss-NMR gave insight about the polymer-substrate interactions.

From liquid water absorption measurement, on both Noto and Comiso stone, it was observed that Fluoline HY and Wacker 290 significantly reduced samples' ability to absorb liquid water, while Silo 111 did not show any significant impact. Reduction of water vapour permeability was observed in all cases, except on Comiso stone samples treated with the minimum amount of Wacker 290, which seems to have had the best performance in avoiding complete pore clogging. Fluoline HY, when the minimum amount was applied, gives also a low pores' filling while Silo 111 seems to obstruct to some extent the accessible porosity. SEM-EDX analysis confirmed the presence of polymer on the stone surface in all cases.

## I. Introduction

### a. Weathering of the stone

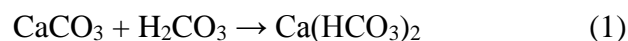
Cultural heritage is a broad definition that includes objects with different purpose of usage, which are made of various materials, like paper, metal, textile, stone and other organic and inorganic substances which differ not only in chemical composition but also in the way they react to surrounding environment and its changes. In this study the attention will be paid to cultural heritage objects made of stone.

Stone cultural heritage objects can undergo some degradation processes caused by factors of chemical, physical and biological origin. There could be marked out several causes of stone deterioration: action of water, action of atmospheric gasses and pollution, action of water-soluble salts, biological factors.

### i. Action of water

Water is a solvent which enables stone deterioration processes due to its ability to transport water soluble salts by stone capillaries, trigger biological activity at the interfaces between stone and the surrounding environment and, in some cases, physical deterioration which leads to loss of stone material. Water can be introduced into the monument or building through rain water, snow, hail, fog, condensation phenomena, can be sucked out from the ground by capillary absorption, as well appear due to the preparation processes of mortar during conservation or renovation works [1, 2]. An importance of the place where a building or a monument is located should not be forgotten. Water could be brought by the wind from various water basins like lakes, rivers, seas, together with salts and other possible contaminants, dissolved in water. The action of water can cause several types of damage: swelling, dissolution and washing away the rock-forming elements. The greater the frequency and continuity of the action of water the greater possible damage is caused.

The most fragile to dissolution by water are limestones and sandstones having a calcareous binder, due to the fact that water is able to remove calcium carbonate if the action of it is frequent and continuous. Another harmful additive present in water is carbon dioxide which forms a weak solution of carbonic acid which is able to transform calcium carbonate into calcium bicarbonate (1) which has dissolution capacity in water much higher than that of calcium carbonate (0.015 g/L of calcium carbonate, 1.66 g/L of calcium bicarbonate).



As compact limestones tend to have low porosity, their capability to dissolve in water is limited to the surface exposed to the direct contact. Meanwhile, light limestones and porous sandstones experience more damaging action due to the capability of calcium bicarbonate solution to penetrate into the pores and attack calcium carbonate in deeper layers causing greater damage.

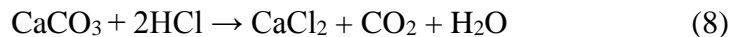
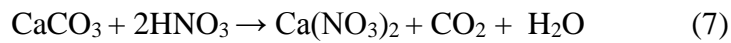
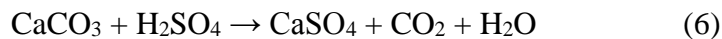
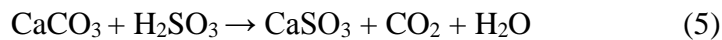
It is worth mentioning that the action of water can cause undesirable mechanical effects on a stone substrate which influences the stability of stone matrix. As some minerals strongly absorb water, they swell and become plastic [3]. Action of water on stone objects is so threatening that it requires deeper insight into this problem. As mentioned above, calcareous stones fall into a category which suffers a lot from the action of water and it has recently been studied [4]. This research has been centred on mechanical degradation processes which originate due to the presence of water in contact with stone objects, specifically calcarenites. During the experiment under artificial ageing conditions three main destructive processes have been observed: short term reduction in the strength of the stone, long term dissolution and chemical reduction in grain size. The results of the paper show the importance of proper protection of calcarenites from water which could be achieved using hydrophobic substances.

#### ii. Action of atmospheric gasses and pollution

Atmospheric pollution is a harmful consequence of modern society which affects everyday life of people, causes climate changes and is also detrimental for cultural heritage objects such as buildings and monuments. Carbon dioxide, sulphur and nitrogen oxides, hydrogen sulphide, water, dust and solid particles – all of these listed compounds can be described as pollution-related components causing damaging effects for cultural heritage, in this particular case, slow decomposition of stone. As a consequence, chemical reactions, like oxidation, reduction, hydration and dehydration, hydrolysis, carbonization may occur.

Air pollution may be gaseous, liquid or solid and mainly appears due to human activity, such as burning solid or liquid fuels, like petrol, which results in forming organic compounds and nitrogen oxides. Harmful but unfortunately very common atmospheric pollutant is sulphur dioxide, which is a result of oxidation of sulphur and its products. Hydrogen chloride and hydrogen fluoride could be listed as other by-products of industrial processes. Talking about solid pollution of the air, dust should not be forgotten, in particular, furnace ashes, coming from fine coal or coal-dust furnaces and peat-fired boiler houses. It is important to understand how above listed pollutants affect stone and what consequences could bring

upon their contact at the stone interface. It is important to mention that gasses emitted into the environment, like sulphur (2, 3) or nitrogen oxides (4), form acid solutions with water, which deteriorate stones due to the formation of much more soluble products: calcium sulfite (5), calcium sulfate (6), calcium nitrate (7), calcium chloride (8), comparing to calcium carbonate of non-deteriorated stone with dissolution capacities of 0.045 g/L, 2.1 g/L, 1212 g/L and 745 g/L respectively, while the one of calcium carbonate is 0.015 g/L. Starting from the surface, corrosion process slowly goes deeper into the stone transforming inner layers into new compounds.



Solid particles as furnace dust mentioned before are involved in slightly different deterioration mechanism but unfortunately it causes not less damage than gaseous pollutants. Action of dust can be direct or indirect. The first one involves sulphur dioxide absorbed by soot, which results in acidic decomposition of carbonates when deposited on the stone surface (5). Nevertheless, the indirect action can be more harmful due to condensation of water vapour when water gets saturated with aggressive substances and can penetrate the stone causing destruction of inner layers. Furthermore, dust can deposit on stone surfaces not only causing deterioration but also ruining the aesthetic appearance of the building or monument [3]. It is worth mentioning that atmospheric pollutants present in modern environment, especially in urban areas, can encourage growth of microorganisms which cause biological deterioration of stone artworks [5].

### iii. Action of water soluble salts

One of the most common challenges that stone conservators have to face is the action of water-soluble salts, in particular, sulphates, chlorides and nitrates [6]. Transported by water, dissolved salts can

penetrate into deeper layers of the stone or come directly from the soil by capillary absorption up to the surface. This action can form stains, efflorescence, damp patches, fluffy deposits, glassy coatings, etc. During water evaporation due to the drying of rock, crystallization process of salts occurs generating a high pressure inside stone pores, which is particularly dangerous because the progressive expansion of the crystals can be enormous, resulting in the cracking of the pore walls and bringing a high degree of degradation or even loss of a part of the stone material [3]. Salts to the stone objects can be introduced from various sources, like air pollution, de-icing salts, soil, sea spray, inappropriate treatments or interaction between building materials [7]. Nitrates, in particular, can be of biological origin when the stone object is in contact with animal excrements, for example pigeon droppings which are a very common problem in urban areas. Recent studies showed that it contains 4 % of water-soluble salts commonly found on buildings [8]. Due to the reasons mentioned above it is important to understand what harm could be done for precious objects and how it occurs. Solutions of water soluble salts get inside the stone body through its capillary system. Several degradation mechanisms can be recognized due to water soluble inorganic salts, like chemical reactions with the stone components, enhanced hygroscopic water absorption, salt hydration, salt's leaching [9]. Salt crystallization could be stated as one of the most harmful degradation mechanisms and can occur in two different ways. If the salt solution migrates to the stone surface faster than its drying time, the crystallization starts on the stone surface and results in efflorescence – visible deposit of salts on the stone surface which damages aesthetic appearance of the monument. On the other hand, if the migration of salt solution is slower than its drying time, crystallization starts inside the pores without causing any visible changes and the force of growing crystals can break the stone surface and results in mechanical deterioration as reported before [10].

#### iv. Biological factors

Microorganisms could be divided into two categories: autotrophic (algae, lichens, chemolithotrophic bacteria, higher plants) and heterotrophic (above fungi and bacteria) microorganisms [3]. Deterioration by microorganisms often results in an undesirable staining effect on the stone surfaces, caused by biogenic pigments. The process of biodeterioration and growth of microorganisms is strongly influenced by the availability of water, which depends not only on the properties of the lithotype, like porosity, pore size distribution and permeability to water, but also on the conditions of the object exposure to harmful substances: outdoors or indoors, rural or industrial area, etc. More polluted areas are far more favourable



for the development of stone-colonizing species as atmospheric pollutants such as nitrogen compounds, hydrocarbons and others from natural or anthropogenic sources satisfy their nutrients demand [11]. Photosynthetic microorganisms could be considered, due to their phototrophic nature, as potentially the most aggressive due to their capability to easily develop on the stone surface causing coloured patinas and incrustations. Nevertheless, aesthetic damage is not the only problem caused by these microorganisms. It is very important to stress that they not only participate in stone deterioration processes directly but also indirectly by supporting the growth of other microorganisms [12].

Talking about biological factors which can cause a deterioration of cultural heritage objects, it is important to stress the possible damage caused by fungi due to their enzymatic activity and ability to cause deterioration to all types of organic and inorganic materials like pigments, dyes, textiles, leather, paper, glue and others used for art objects. In outdoor environments, fungi and lichens are the most important causes of deterioration of stone, plaster and mortar objects. Fungi are also resistant to biocides or other anti-microbial treatments because of their thick cell walls. Granite, marble and calcareous limestone often suffer from black fungi which grows deep inside the pores and due to which biopitting phenomena occurs, covering the stone with black spots. Black fungi can often be found in caves or catacombs and are particularly dangerous due to deep penetration into stones bulk [13].

Lichens are another group of organisms causing stone biodegradation due to physical and chemical processes that they cause on mineral substrate. Physical effects of lichens include hyphal penetration through stone fissures and voids, causing mechanical damage and accelerating other kinds of weathering like disaggregation and detachment of mineral rock grains. Talking about chemical processes caused by lichens, it is necessary to mention solubilisation phenomena, like acidolysis, complexolysis, alcalinolysis which are responsible for the formation of oxalic acid, metal complexes and alkaline compounds [14].

All these biological threats should be taken into account by conservators in order to effectively plan a conservation procedure.

#### b. Stone conservation procedure and materials

As listed above, there are a lot of potential risks that stone objects placed in outdoor environments experience every day. This is why a properly selected conservation methodology is a key point for preservation of cultural heritage objects made of stone. Depending on the conservation state of a

particular object, a conservation procedure usually consists of three phases: cleaning, consolidation and protection.

#### i. Cleaning

Cleaning is the first and necessary step in conservation practice to remove dirt, crusts and other kinds of contamination in order to prepare the surface for further conservation. Cleaning procedure can be classified according to the method used in two types – mechanical and chemical - the choice of which depends on the nature of the material that needs to be cleaned and the desirable post-cleaning effects.

Biological organisms are very common contaminants, dwelling on stone monuments in outdoor environment. For this reason removing them often is a requirement for stone conservators. In a recent study [15], the removal of sulphated black crusts by using mechanical, chemical and laser cleaning methods has been discussed. As a mechanical method, a procedure based on an air-water-micro granule mixture under low pressure, called Hydrogommage<sup>®</sup> was used. In order to test chemical method authors applied nine cleaning treatments using different reagents on the surface of granite. Laser cleaning was performed using 355 nm Nd:YVO<sub>4</sub> nanosecond laser. This study proved that chemical methods are more effective than mechanical and laser cleaning, although none of the three methods completely managed to remove a black crust without giving unwanted effects, such as residues after chemical and mechanical cleaning and melting of biotite present on the stone surface when laser cleaning was used. Another research about the removal of black crusts was done on a limestone using laser cleaning and laser-induced breakdown spectroscopy (LIBS) [16]. In this case the cleaning procedure showed high cleaning efficiency and selectivity, being able to carefully control the cleaning operation. Laser coupled with spectroscopic technique allowed researchers to analyse changes in the structure of the layers while cleaning, ensuring a properly definition of the end point of the cleaning, without risking to modify the surface morphology of the substrate. Comparing these two studies [15, 16] it could be stated that the efficiency of the same method strongly depends on the origin of the substrate and its interactions with the contaminant.

Another promising method for various cultural heritage objects is plasma cleaning. First started to be used for metal artefacts, this contactless method now shows good sensibility and cleaning efficiency in removal of black crusts, graffiti paint and aged protective polymers from stone substrates [17]. Being a relatively new cleaning method, it exposes some drawbacks, such as deposition of metallic particles

from the torch which causes chromatic alterations of the stone surface. Plasma cleaning still remains a relatively new technique which requires more investigations to be done.

Nowadays very common, most of the times intentional, destruction of monuments' aesthetic appearance are graffiti. The graffiti spray consists of pigment, a binding media and the solvent, both of which usually are synthetic organic substances. Due to the presence of a solvent, paint can easily penetrate into pores of the stone substrate. Because of this reason, the removal of this kind of material still remains a challenge for conservators and restorers and requires a usage of chemical, physical and biological methods. Chemical methods refer to the usage of various solvents, like ammonia, isopropyl alcohol, acetone or white spirit for fresh graffiti due to paint insolubility in water. Alkaline compounds could be used for the removal of wax based substances like crayons or lipstick, although it is necessary to neutralize it with a weak acid and rinse with water to avoid damage for the stone. These above mentioned methods should be seriously considered before the application due to possible staining or dissolving of a monument surface, as well as atmospheric pollution should be taken into account, especially in the case of volatile organic compounds (VOC). Physical methods are considered as traditional and include mechanical cleaning of the surface with abrasive dust, scalpel, water or sand blasting. Although these techniques should be chosen according to the origin of the stone substrate, and should be used at mild conditions and by experienced conservator in order to avoid bigger damage of the structure. Novel approaches have been recently taken into account, in particular, the usage of microorganisms. This approach exploit their metabolic growth activity for efficiently degrading pollutants. The field of biological cleaning techniques still requires further investigation [18, 19]. Nowadays, more and more researches in cultural heritage field focus on preventive conservation methods in order to make the surface of stone monument resistant to graffiti, such as anti-graffiti protective substances [20] or self-cleaning products [21].

## ii. Consolidation

Consolidation is a necessary procedure that must be performed if an object is significantly damaged, tends to powder or there is a risk of collapse. Often the consolidation must be performed before the cleaning, in that case it is defined as pre-consolidation. In case of stone cultural heritage objects, one of the main reasons why consolidation becomes necessary is prolonged contact with water soluble salts which are introduced into the stone due to its capillarity. The role of consolidant is to reduce the stone porosity by filling up small pores of the stone in which water tends to be absorbed and retain for long

periods. For a successful consolidation procedure a number of factors regarding the stone must be taken into account: properties, composition, state of conservation, degradation processes. These factors justified the demand of suitable stone consolidants and resulted in a high availability of commercial products of inorganic and organic origin, like calcium or barium hydroxide, alkoxysilanes, fluoropolymers, acrylic and epoxy resins [22].

The application of inorganic materials, like hydroxide particles, became very popular in conservation practice after the invention of Ferroni-Dini method which includes the application of ammonium carbonate and barium hydroxide aqueous solutions for removal of formed gypsum and consolidation of the object without changing chemical composition of the artefact [23]. In a recent study [24] barium hydroxide was tested as a probable consolidant for highly porous limestones. It was proved that barium hydroxide acts in two ways: through carbonation with atmospheric CO<sub>2</sub> and by replacing calcium for barium in the calcite lattice followed by secondary consolidation action when the carbonation of released calcium hydroxide occurs. This consolidation method turned out to be efficient due to the compatibility with the substrate although small penetration depth should be taken into consideration. The way to reduce these limitations could be the usage of hydroxide nanoparticles as the particle size increases the reactivity of the consolidant and its penetration through stone pores [25]. Talking about stone rich in silica, like sandstone, ethyl silicates (silicon alkoxides) are worth to mention as very promising consolidation materials due to their compatibility and ability to bind to the substrate. On the other hand, some limitations and drawbacks were noticed during the studies, such as cracking, shrinkage and pore size distribution. Researches try to solve these problems by modification of original product with nanoparticles, which increase material hardness and forms desired mesoporosity [26]. Another way to solve ethyl silicate issues, mainly incompatibility with carbonate materials, by suggesting new product for the treatment was described in the study [27]. In this case phosphate-based product – diammonium hydrogen phosphate, was suggested as an alternative for ethyl silicate, due to the formation of hydroxyapatite inside the pores of the stone when chemical reaction between calcium and phosphate ions takes place. Higher compatibility with the substrate, good ability to restore mechanical properties was achieved and no alterations in water transport properties occurred. Phosphate-based treatment also presented acceptable durability results after artificial ageing tests: wetting-drying, freezing-thawing and salt crystallization [28].

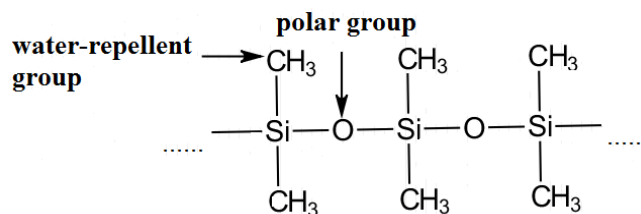
### iii. Protection

The aim of above mentioned consolidation procedure is to improve the cohesion and hardness of the damaged stone substrate. Due to the damaging action of water, another property is required for stone objects – hydrophobicity, which most often cannot be achieved with consolidants. It results in demand of other kind of protective conservation products which would give hydrophobic effect and at the same time leave stone porous system open for free water vapour flow through the substrate along with no chromatic alterations, reversibility and chemical stability. Nowadays polymeric materials dominate in the field of conservation and get a lot of interest from researchers. Protective product could either penetrate deep into the stone material or form a coating on the surface, which depends on the molecular size, used solvent or application procedure [29]. The usage of acrylic polymers is well known in conservation practice as protectives and consolidants. One of the most widely used consolidation and protection acrylic-based product in many countries is Paraloid B72, whose active compound is a copolymer of ethyl methacrylate and methyl acrylate, well known for its good adhesive power, transparency and solubility in several solvents. In spite of that, some limitations have been noticed through various researches undertaken during long years of usage, like poor penetration into porous and non-porous stones, reduced reversibility of aged polymer as well as lower hydro repellency in comparison to silicone polymers [30]. It led to the usage of acrylic-silicone mixtures, for example the “Bologna Cocktail”, composed of Paraloid B72 and methyl siloxanes which was very extensively used as a stone conservation product for last couple of decades because of suitable penetration depth and good stability when exposed to atmospheric pollutants, but it also presents an important drawback – reduced reversibility after artificial aging in comparing with Paraloid B72 alone [31]. In order to obtain the best protective properties various products of different chemical origin have been introduced to the market, like previously mentioned acrylic polymers, along with silica-based or fluorine-based substances.

Nowadays organo-silicon compounds, so called silicones, get a lot of restorers’ attention as water repellents as they exhibit large amount of positive features: transparency, resistance to atmospheric pollutants, high water repellency. Often, silica-based products are composed of various mixtures of compounds such as silanes and siloxanes.

Silanes are a class of compounds which can be described with the general formula  $\text{Si}_n\text{H}_{2n+2}$ , like their carbon analogues - alkanes. The major difference between compounds belonging to those two chemical

classes is the bond strength. Si-Si bonds of silanes are much less strong than C-C bonds of alkanes. This feature led to the wide usage of much durable siloxane compounds, in which are present much stronger Si-O-Si bonds. Polysiloxanes can be obtained by hydrolysis and polycondensation reactions of monomers, like alkyl- or phenylchlorosilanes, alkoxy silanes, alkyl- and phenylalkoxy silanes. Depending on the used monomers, polysiloxanes of different molecular size, structure and properties can be obtained. In order to understand how the desired water-repellent effect is obtained on the substrate, it is necessary to take a closer look into the chemical structure of a silicone (*Fig. 1*). As it can be noticed, water-repellent properties occur due to the dipole orientation of the coating over the substrate, because polar groups are turned towards the substrate while hydrophobic groups are oriented outside [3]. Also the stability of organo-silicon coatings can be explained through the presence of polar groups. Having low electronegativity, silicon forms very polarized Si-O bond with oxygen having a high bond energy (452 kJ/mol) higher than the one of a Si-C bond (318 kJ/mol) and the one of a Si-Si bond, which is fairly weak (193 kJ/mol). Featuring this high bond energy, a Si-O bond is very resistant to bond cleavage [32].



**Fig. 1.** The structure of organo-silicon compound

Silicone films work forming a hydrophobic network by covering separate stone grains and are bonded to the monument's surface by covalent bond [33].

Fluorine containing polymer science is a rather new field of research which began with an accidental discovery of polytetrafluoroethylene (PTFE), better known by its commercial name Teflon. Outstanding properties of PTFE encouraged researches to incorporate fluorine into other polymers [34]. Fluoropolymers tend to exhibit high thermostability, water and oil repellency, chemical inertness which makes it suitable for coatings. Fluoro-copolymers are widely used fluorine-containing products. A general idea of copolymers' working principle is to exploit the specific properties that constituting monomers have. The presence of fluorine atom makes a monomer a good electron acceptor. The most often used monomers are commercially available fluoroalkenes, like tetrafluoroethylene, vinylidene fluoride, hexafluoropropene, 3,3,3-trifluoropropene and perfluoroalkyl vinyl ether. It is common to find

vinylidene fluoride as a component of fluorinated copolymers too. It is a non-toxic, non-hazardous, environmentally friendly compound, resistant to acid and solvents, moreover, it can be easily polymerized [35]. Hydrophobic effect develops on the surface due to the small atomic radius and high electronegativity of fluorine atom, which leads to the formation of strong covalent bond between fluorine and carbon resulting in the reduction of surface energy and surface tension. Fluorine-based coatings are bonded to the substrate's surface by weak Van der Waals forces [33]. The wide usage of fluorinated protective products can be confirmed by recent researches. For example, a study [36] presents promising results in development of self-cleaning superhydrophobic coatings of fluoroalkylsilanes provided of a hydrophobic fluoroalkyl group as end group.

## **II. Aim of the study**

Stone artefacts are a wide class of cultural heritage which plays an important role by representing the legacy of past generations in form of sculptures, monuments and buildings. Precious stone objects, even though from the first look seem to be resistant to weathering, in reality face a lot of threats. One of the most harmful is the presence of water coming from various sources, which transports water soluble salts and other contaminants to the stone surface. This is why in a lot of cases the most desirable effect for commercially available protective substances is hydrophobicity.

Architectural heritage has a significant importance all over the world and Sicily is not an exception. Widely known and used stone quarries in this region were the ones of Val di Noto area, which served as a source of building materials for the reconstruction of the cities in Baroque style, after an earthquake which took place in 1693. Because of its significant meaning for Sicilian architectural heritage, two stones – Comiso and Noto were selected for the analysis.

The aim of the study is to analyse polymer-substrate interaction and the properties at the interface upon application of three polymeric dispersions on the stones, in order to understand the working principle of commercial polymeric products and how the hydrophobic effect develops on the stones' surface. These studies should also allow to find a suitable protective material for Comiso and Noto stones which shows good hydrophobic properties, permeability to water vapour and does not alter chromatic properties of the stone surface more than acceptable by international standards.

Regarding the protective commercial products, two different groups of polymeric dispersions have been chosen: silica-based (Silo 111 and Wacker 290) and fluorine-based (Fluoline HY). The purpose of selecting materials of different chemical origin is to understand the differences of the mechanism in which protective properties are developed. Two silica-based products were chosen because of their different chemical composition: Silo 111 is composed of low molecular weight organosiloxane oligomers while Wacker 290 is based on a mixture of silane and siloxane. In case of fluorine-based products, Fluoline HY is a ready to use protective based on fluoro-copolymers. Concentrations of the active content of products will be kept the same within the group: 10% (w/w) Silo 111 and 10 % (w/w) Wacker 290, 3 % (w/w) Fluoline HY. Two different amounts, which fall into the yield range suggested by the manufacturer, will be applied on the stones' surface by brush.



The effectiveness of products will be evaluated by several surface analysis techniques: SEM-EDX, FT-IR, along with liquid water absorption by capillarity, colorimetry, contact angle measurements and bulk analysis techniques: ss-NMR, water vapour permeability test. Untreated stone will be characterized by mercury intrusion porosimetry, optical microscopy and XRD.

### III. Characterization techniques

#### *a. Mercury intrusion porosimetry and petrographic characterization*

Mercury intrusion porosimetry was performed on untreated Noto stone sample using Micromeritics AutoPore IV 9500 Series pore size analyzer in order to characterize material porosity and measure the pore size by applying different pressure levels to the sample immersed in mercury. The pressure required to intrude mercury into the sample's pores is inversely proportional to the size of the pores.

Petrographic characterization was performed by using Axioskop 40 optical microscope equipped with the DeltaPix InSight software.

#### *b. X-ray diffraction (XRD)*

Small amount of specimen was obtained from the untreated stone sample using a hammer and a screwdriver, and grinded until fine powder. XRD measurements were conducted by a Philips PW 1050/39 diffractometer in the Bragg-Brentano geometry using Ni-filtered Cu K $\alpha$  radiation ( $\lambda = 1.54056 \text{ \AA}$ ) in the 2theta range 3-70 with a step of  $0.05^\circ$  and a time for step of 15 seconds. The X-ray generator worked at power of 40 kV and 30 mA, and the resolution of the instrument (divergent and antiscatter slits of  $0.5^\circ$ ) was determined using R-SiO<sub>2</sub> and R-Al<sub>2</sub>O<sub>3</sub> standards free from the effect of reduced crystallite size and lattice defects. The obtained XRD patterns were analyzed by using X'Pert High Score software.

#### *c. Colorimetry*

The main purpose of the technique is to evaluate chromatic alterations by calculating total color difference ( $\Delta E$ ) value between two measurements. For this reason three main parameters have to be measured: L\* - the lightness coordinate, a\* - the red/green coordinate, b\* - the yellow/blue coordinate.

In the case of Noto and Comiso stone samples, colorimetric measurements were performed before and after the treatment. Due to the inhomogeneity of stone colour, measurements were carried out on 10 randomly selected points of each sample, following UNI EN 15886 normative [37].

Results were obtained using Ocean Optics spectrometer equipped with DH-mini light source and USB 2000 + XR1 detector. Data were obtained applying the following experimental parameters: CIE standard illuminant D65, CIE standard colorimetric observer 10°, reference system colour space CIE x, y, Y and L\*, a\*, b\*.

The results were expressed representing averaged values of  $L^*$ ,  $a^*$ ,  $b^*$  and evaluating the degree of chromatic alterations from  $\Delta E$  value, calculated from the equation (9):

$$\Delta E^*_{2,1} = \sqrt{(\Delta L^{*2} + \Delta a^{*2} + \Delta b^{*2})} \quad (9),$$

$$\Delta L^* = L^*_2 - L^*_1 \quad (10),$$

$$\Delta a^* = a^*_2 - a^*_1 \quad (11),$$

$$\Delta b^* = b^*_2 - b^*_1 \quad (12),$$

where:

$L^*_1, a^*_1, b^*_1$  – parameters obtained from samples before the treatment,

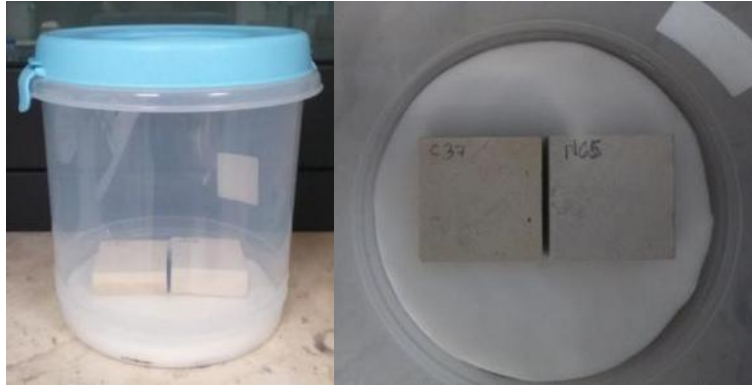
$L^*_2, a^*_2, b^*_2$  – parameters obtained from samples after the treatment.

#### *d. Liquid water absorption by capillarity*

The procedure indicated in the UNI EN 15801 normative [38] was applied in order to evaluate the capability of stone samples to absorb liquid water by capillarity.

For the measurement, round plastic containers with a diameter of 15 cm were used. 1 cm thickness filter paper was placed on the bottom of containers as a bedding layer and soaked in distilled water, maintaining a constant water level of 0.5 cm. Samples were placed in containers having the side to be treated in contact with the bedding layer. Samples were weighted after time intervals of 10, 20, 30, 60, 240, 360, 1440, 2880, 4320 and 5760 minutes. The experiment was ended when the mass difference between two successive weightings was not greater than 1 %.

The results were expressed in the form of graphs of water absorbed by the specimen per unit area  $Q$  ( $\text{g}/\text{cm}^2$ ) as a function of a square root of time  $t^{1/2}$  ( $\text{s}^{1/2}$ ).



**Fig. 2.** Liquid water absorption by capillarity

**e.** *Water vapor permeability*

The effect of protective polymeric dispersions on microporosity of the stone specimens was evaluated according to the UNI EN 15803 normative [39], where the water vapour flow through the stone specimen subjected to different partial water vapour pressures is measured.

Treated Noto and Comiso stone samples of the size 5x5x1 cm were tested along with two untreated samples taken as a reference. Before the measurement, selected samples were kept in the desiccator at  $23 \pm 3$  °C and  $50 \pm 3$  % relative humidity until constant mass was reached. Temperature and humidity were monitored during pre-conditioning and throughout the experiment.

At the beginning of the experiment, the test cup was filled with deionized water and the sample was mounted in the test cup with the face to be tested upwards. The principle of the wet cup system is to test the behaviour of materials under high humidity conditions.

In order to keep the same climatic conditions throughout the experiment, the desiccator, filled with a saturated  $\text{Ca}(\text{NO}_3)_2 \cdot 4\text{H}_2\text{O}$  salt solution, which gives constant relative humidity, was used. Temperature and RH have been continuously monitored during the experiment. Sample and cup assembly were weighted every 24 hours for five days and the diagram, in which the cumulative mass change per unit area is plotted versus time was drawn, in order to determine the steady state of water vapour diffusion flow through the specimen.



**Fig. 3.** Water vapor permeability measurement.

Cumulative mass change  $\Delta m_i$  was calculated for each set of successive weightings of the specimens, according to the equation (14):

$$|\Delta m_i| = m_i - m_0 \quad (14),$$

where:

$m_0$  – the mass of test assembly at the time  $t_0$ ,

$m_i$  - the mass of test assembly at the time  $t_i$ .

Water vapour permeance  $W_p$  was calculated according to the equation (15):

$$W_p = G / (A \times \Delta p_v) \quad (15),$$

where:

$G$  – the slope of the linear section of the curve presenting the mass change ( $\Delta m_i$ ) versus time (t) versus time (t)

$\Delta p_v$  value was calculated from the mean of temperature and relative humidity measured over the experiment, as the difference between the vapour pressure of pure water at operative T and the vapour pressure of water in equilibrium with the saturated calcium nitrate solution, at operative T.

$A$  – a surface area of the sample.

Water vapour permeability was calculated according to the equation (16):

$$(\delta_p) = W_p \times D \quad (16),$$

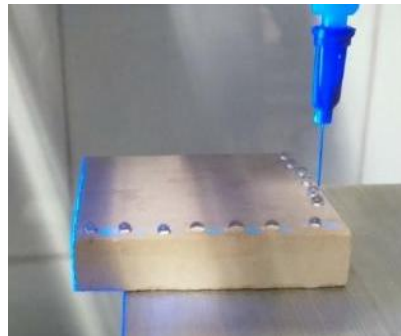
where:

D – the mean thickness of the specimen.

Obtained water vapour permeability ( $\delta_p$ ) values of treated samples were expressed as a percentage from the values of untreated samples, which were equated to 100 %.

#### *f. Static contact angle*

The test procedure was done following the UNI EN 15802 normative [40] in order to evaluate the hydrophobicity of the treated stone surface by measuring static contact angle on Noto and Comiso stones' samples, before and after the treatment. One untreated sample of each stone was measured as a reference for the evaluation of hydrophobic effect obtained due to the treatment.



**Fig. 4.** Static contact angle measurement

Measurements were done using a contact angle and surface tension instrument FTA1000 C Class. Before the procedure, a micro-pipette was filled with deionized water and a sample was placed on a sample holder, putting the test surface in a horizontal position. The contact angle of the drop deposited on a stone surface was measured after 10 seconds. In order to have a good average appraisal, 15 measurements on each sample surface were performed. Obtained values were averaged and standard deviation calculated.

#### *g. Fourier Transformed Infrared (FT-IR) Spectroscopy*

Attenuated Total Reflectance (ATR) infrared Spectroscopy was carried out in order to characterize the film polymer films of Fluoline HY and Wacker 290 obtained after solvent evaporation by solvent-

casting method, while spectrum of Silo 111 was obtained on a liquid sample of the polymer, after solvent evaporation.

Attenuated Total Reflectance (ATR) infrared spectra were acquired on protective polymeric dispersions using a VERTEX 70V FT-IR spectrophotometer equipped with a Platinum ATR unit. Spectra were acquired in the range 5800-40  $\text{cm}^{-1}$  at a resolution of 2  $\text{cm}^{-1}$ , collecting and averaging 50 scans. The operations were performed using the software OPUS 7.5<sup>®</sup>. ATR correction was applied to the spectra after acquisition.

Total Reflectance FT-IR Spectroscopy were carried out in order to characterize the stone samples' surface in a non-destructive and fast way, so this technique is not harmful for artworks and ideal to make in situ measurements. Spectra were obtained on untreated and treated stone samples using a portable Bruker ALPHA spectrophotometer. No sample preparation was required. The spectrophotometer is made up of a Globar IR radiation source, a Rocksolid<sup>®</sup> interferometer and a DTGS (Deuterated TriGlycine Sulphate) detector. The overall dimensions of the instrument are 30x12x20 cm. Spectra were acquired in the range 5900-360  $\text{cm}^{-1}$  at a resolution of 4  $\text{cm}^{-1}$ . The spectrophotometer allowed an excellent signal to noise ratio throughout the range used even for short acquisition time as long as 60 sec (the acquisition time used for data collection in the present work). The operations were performed using the software OPUS 7.5<sup>®</sup>.

The spot size on the investigated sample was of 1 cm area. The instrument was kept perpendicular to the sample surface (normal geometry) using a Manfrotto tripod equipped with a special frame which support the instrument and avoid vibrations during measurements. The instrument is kept in contact with the point analyzed. The total reflectivity, R due to the combined diffuse and specular components, was collected over 1 minute using the spectrum from a golden mirror plate for background correction. Spectra were expressed as function of pseudo-absorbance  $A'$  where  $A' = \log(1/R)$ .

#### *h. Solid state Nuclear Magnetic Resonance (ss-NMR) Spectroscopy*

In this work, treated Noto and Comiso stone samples along with protective polymeric formulation Fluoline HY were analysed by *ss-NMR Spectroscopy* in order to investigate the possible molecular interactions between stone substrate and the polymer.

Solid-state NMR spectra were obtained on Fluoline HY polymer film and Noto and Comiso stone samples treated with maximum amount of Fluoline HY using Bruker Avance II 400 MHz (9.4 T)

spectrometer at the room temperature, acquiring direct-polarization (DP)  $^{19}\text{F}$  magic angle spinning (MAS) spectra.  $^{19}\text{F}$  DP MAS NMR experiments were performed with following parameters: MAS rotation speed of 10 kHz, 128 scans, repetition delay of 4 s, excitation pulse length of 4  $\mu\text{s}$ . All samples were ground to fine powder.

*i. Scanning Electron Microscopy (SEM)*

SEM-EDX (Energy Dispersive X-Ray spectroscopy) measurements were performed on untreated and treated with protective polymeric dispersions Noto and Comiso stone samples, in order to analyze surface morphology changes and elemental composition which could occur due to the treatment. Analysis was performed with PHENOM ProX Desktop Scanning electron microscope equipped with an energy dispersive X-ray spectroscopy (EDAX) detector.

*j. X-ray Fluorescence (XRF)*

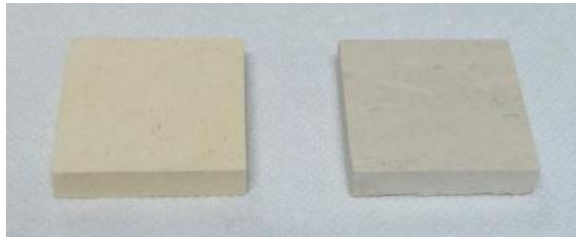
Energy dispersive X-Ray fluorescence analysis was performed with portable spectrometer Tracer III SD Bruker AXS operating at 40 kV and 11  $\mu\text{A}$ . The instrument is equipped with a Rhodium Target X-Ray tube source, a silicon drift X-Flash SDD detector with Peltier cooling system and 3-4 mm diameter spot, two different filters allowing a good sensitivity both at lower and higher energies (up to Ba K - lines). Each spectrum was acquired for 60 s. The energy resolution of the spectrometer was 150 eV at 5.9 keV. Vacuum was not applied at the head of the instrument. Under these conditions the portable instrument allows the detection of elements with atomic number higher than Na ( $Z > 11$ ). The sample surface was placed in contact with the window of the instrument. Data was acquired with S1PXRF® Software, while the analysis of spectra was performed using ARTAX® X-ray software.



#### IV. Materials

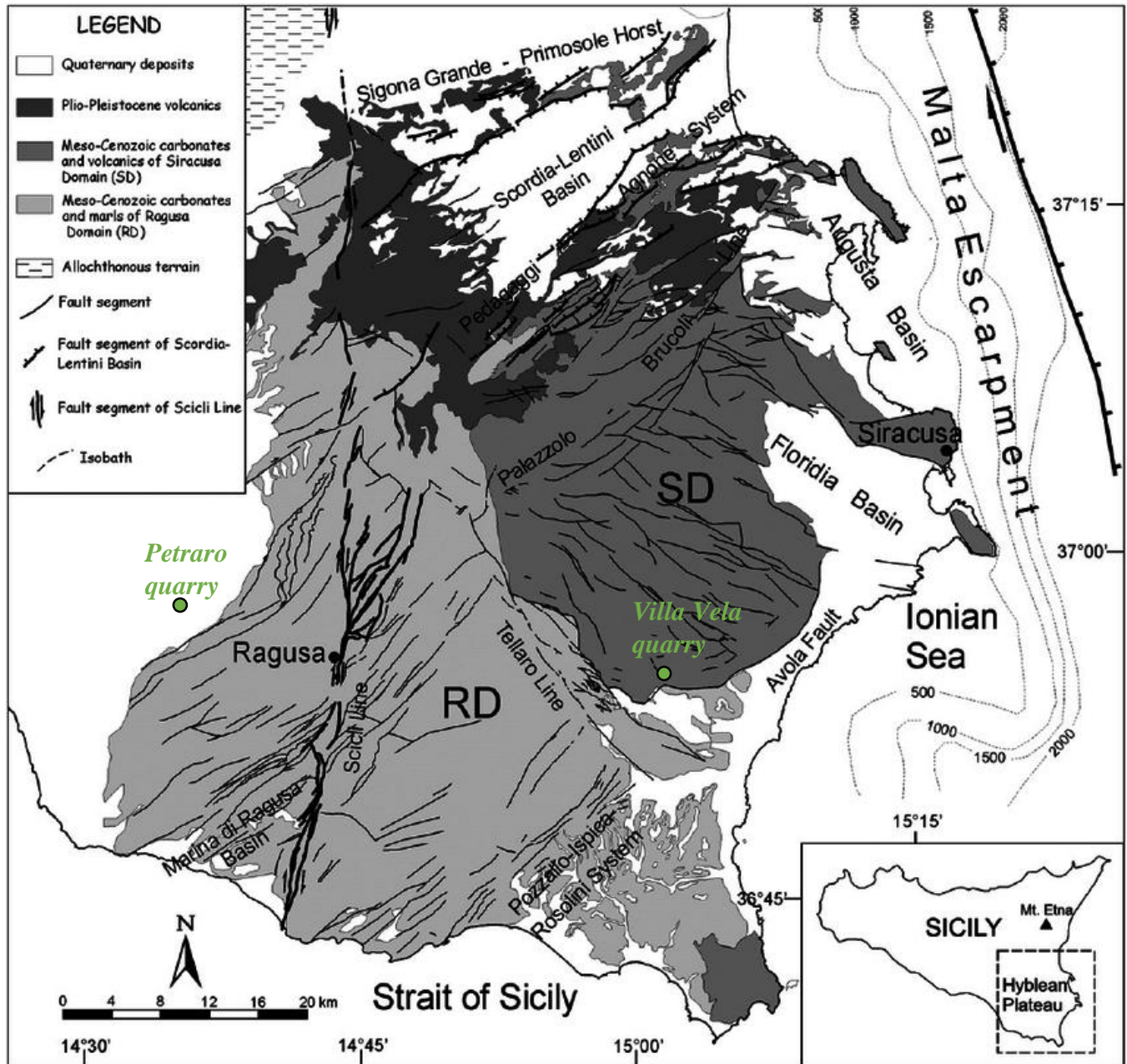
##### a. Lithotypes

The architecture of Val di Noto area of southeastern Sicily can be easily distinguished from other parts of the region due to the presence of buildings presenting Baroque style, as a consequence of an earthquake which took place in 1693 and caused strong damage in this part of Sicily. Another distinctive feature is the building material used for the reconstruction – whitish carbonate rocks supplied from local quarries of the region, characterized by good mechanical properties and easy workability, which made them suitable for reconstructing structural and decorative elements [41]. In the present work, Noto and Comiso stone samples were used for the analysis.



**Fig. 5.** Comiso and Noto stone samples

Noto stone samples were obtained from Vila Vella quarry, while Comiso stone samples – from Petraro quarry. According to the tectonic sketch map (*Fig. 6*), Noto stone belongs to Meso-Cenozoic carbonates formation of Siracusa domain. Comiso stone falls into Quaternary deposits formation. This sedimentological division leads to the hypothesis that selected calcarenites have different properties and composition.



**Fig. 6.** Tectonic sketch map of Hyblean Plateau southeastern Sicily [42]

- i. Noto stone
  - 1. Context

Noto stone is a pale cream calcarenite which comes from the quarries near the city of Noto which is an important Baroque urban center in southeastern Sicily. The city was reconstructed in baroque style using Noto stone after an earthquake which caused a lot of damage in 1693. One of well-known examples of

this building practice was the Cathedral of Noto which was originally constructed and then reconstructed after an earthquake in 1900 using Noto stone [43-45]. The stone is still currently used as a building material [46]. The study [47] reveals that the Palazzolo Formation calcarenite, commonly known as Noto, has been extracted from several quarries which corresponds to different features of calcarenite such as hue of colour, mechanical resistance, the ability to absorb water, heterogeneity of degradation forms that can be observed on the monuments. Salt crystallization, bioturbation, and the occurrence of expandable clay minerals could be listed as main causes of stone deterioration. For this reason it is important to test innovative protective materials. In the article [46] the authors performed a study of three commercially available substances: fluorinated elastomer copolymer Akeogard LTX, a micro-emulsion Akeogard ME, composed of vinylidene copolymer fluoro-hexafluoropropene-tetrafluoropropene and, well known in conservation practice, an acrylic resin Paraloid B72 in order to assess their protective effectiveness from salt crystallization and stability to UV radiation. Both fluorinated products did not show good protective properties although chromatic alterations after artificial aging were not significant and not visible with the naked eye. Studies revealed that Paraloid B72 shows good protective properties against salt crystallization however it is sensitive to UV radiation which causes greater chromatic alterations than acceptable. Another recent study [48] on Noto stone was made by incorporating relatively innovative material: TiO<sub>2</sub> nanoparticles. The aim of this study was to find the best binder for nanoparticles from commercially available protectives: toluene solution of Paraloid B72, hydroalcoholic emulsion of Akeogard P, an aqueous emulsion of acrylic polymer Fosbuild and evaluate the effectiveness of the treatment by applying prepared dispersions on Carrara marble and Noto calcarenite. The best results in terms of hydrophobicity, self-cleaning properties and durability were achieved when Fosbuild acrylic water suspension was used as a binder for TiO<sub>2</sub> nanoparticles, while Paraloid B72 presented unsatisfying results as a protective substance. The eligibility of TiO<sub>2</sub> nanoparticles in the state of nanosols for conservation of Noto stone was investigated also in another study [49]. In this case, the main tested factor was pH value of the nanosol and its' influence to protective properties of the coating.

## 2. Stone characterization

Noto stone samples were characterized by several analysis techniques in order to understand mineralogical and chemical composition of this type of stone.

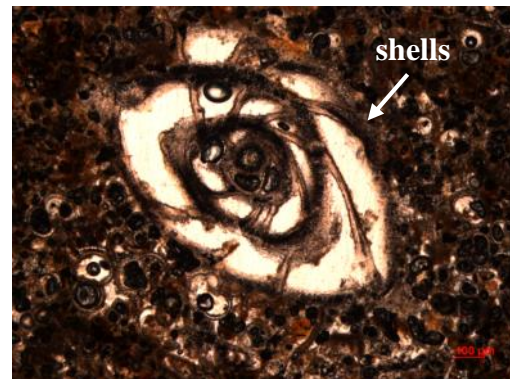
According to mercury intrusion porosimetry results, the porosity of Noto stone is  $14.48 \pm 0.54$  % and the average pore diameter is equal to  $0.10 \pm 0.02$   $\mu\text{m}$ .

Petrographic characterization was done using light polarizing device in order to change natural light to linearly polarized light. The results were obtained in two states: 1) crossed nicols - when primary light polarizing device (polarizer) and secondary light polarizing device (analyzer) are perpendicular to each other; 2) parallel nicols – when polarizer and analyzer are in linear position to each other [50]. The materials were characterized according to two most commonly used carbonate classifications - Dunham and Folk which subdivide limestones according to their matrix content. According to Dunham, if limestone is composed of grains that touch one another without presence of mud, such stone is called grainstone. If carbonate matrix also contains mud but the part of grains in it makes more than 10 %, the sediment is called wackestone, if less than 10 % - mudstone [51]. Folk classification defines limestones according to whether they have micrite or sparite matrix, in this case, carbonate rocks with micrite matrix contain microcrystalline calcite mud with particles smaller than 5 microns, while sparite matrix is composed of coarse calcite cement crystals [52]. Carbonate grains can be classified as skeletal and non-skeletal. Skeletal grains include whole or fragmented remains of calcareous plants and animals, like corals, mollusks, calcified algae, echinoderms, arthropods, etc. While non-skeletal grains include ooids, peloids, pisoids and clasts [53].

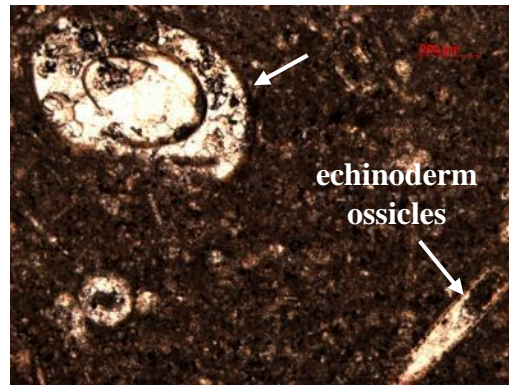
Obtained results revealed that Noto stone is a biocalcarenite, characterized by bioclastic inclusions (shell fragments and other organic remains) in inorganic carbonate matrix. The micrographs, shot using parallel nicols, allowed to operate a petrographic characterization according to Dunham and Folk classifications. Noto stone has been classified as a wackestone and biomicrite. From the images (*Fig. 7*), bioclastic inclusions, such as peloids (*Fig. 7. a*)), shells (*Fig. 7. b*)), ooids (*Fig. 7. c*)) and echinoderm ossicles (*Fig. 7. c*)) could be observed.



a)



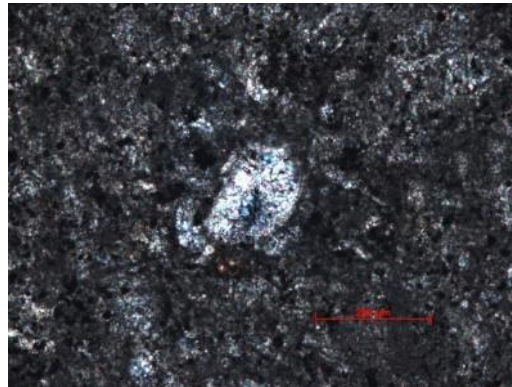
b)



c)

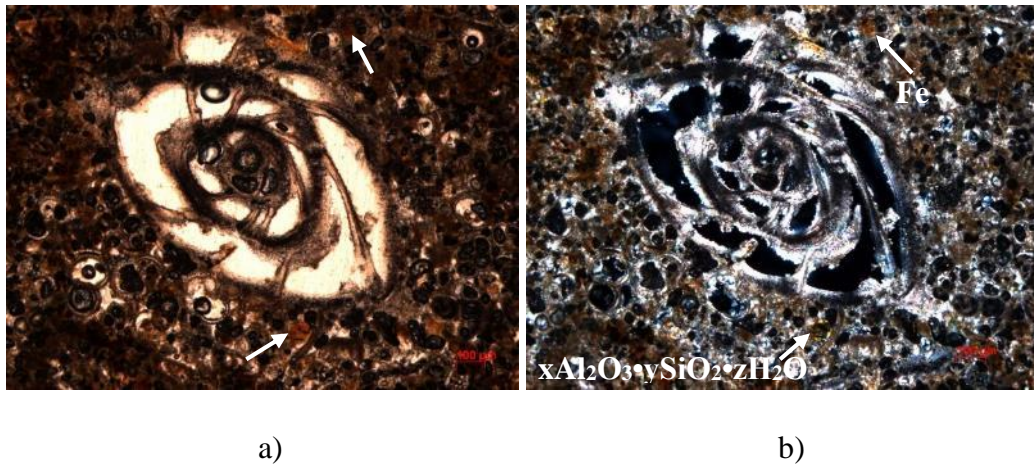
**Fig. 7.** Micrographs of Noto stone thin section using parallel nicols

The micrographs shot using crossed nicols (*Fig. 8.*) show well the high birefringence of calcite crystals, as multiple interference colours could be seen, defining calcite a high order mineral.



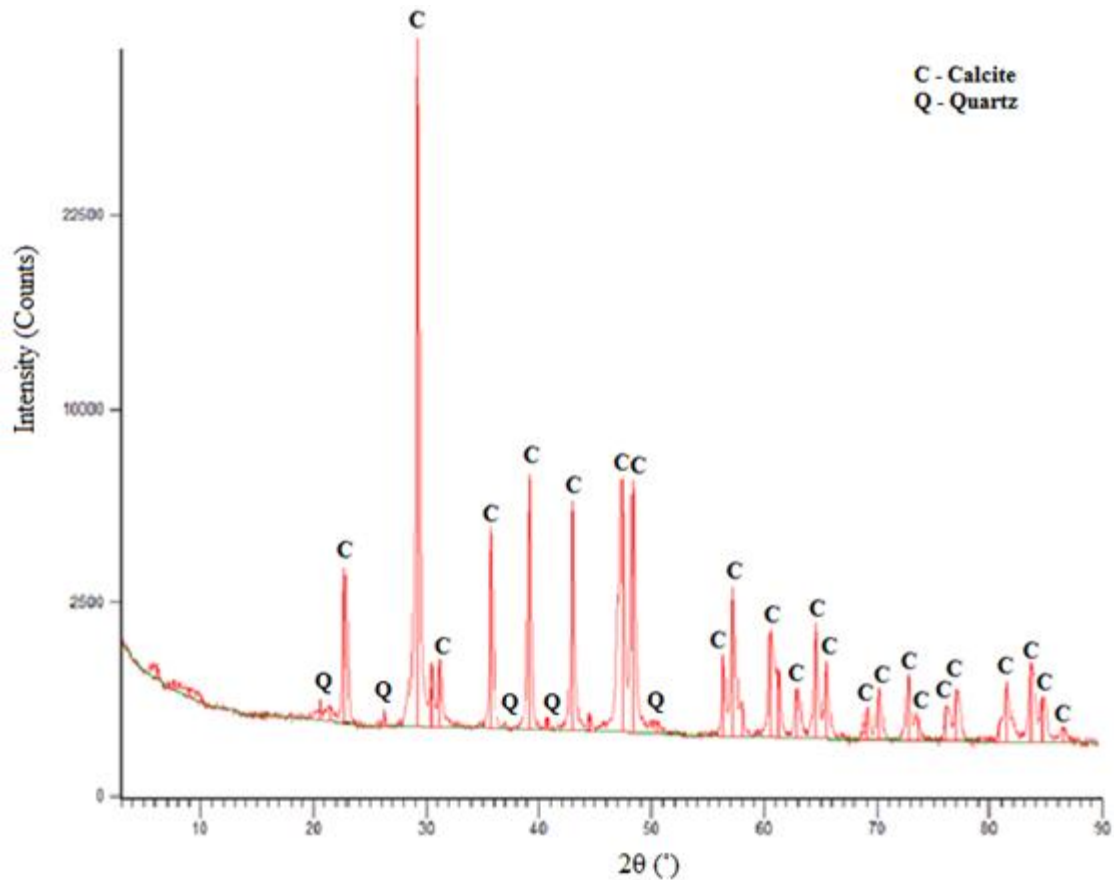
**Fig. 8.** The micrograph of Noto stone thin section using crossed nicols.

Polarized light microscopy also allows to obtain information about minor crystalline phases, such as iron (Fe) and aluminium silicate crystals ( $x\text{Al}_2\text{O}_3 \cdot y\text{SiO}_2 \cdot z\text{H}_2\text{O}$ ). In figure 9 micrographs shot using parallel and crossed nicols are presented side by side, which allows to see the difference in a colour of some particular parts of the sample, marked with arrows. With parallel nicols both marked areas present the same behaviour - dark brown colour, while with crossed nicols, some crystals turn light green indicating aluminium silicate, while the rest remain brown, which could be ascribed to iron crystals.



**Fig. 9.** The micrograph of Comiso stone thin section using: a) parallel nicols, b) crossed nicols

X-ray diffraction (XRD) is a useful technique for identifying the mineralogical composition of the sample. As it is clear from the XRD pattern (*Fig. 10*), the major crystalline phase of Noto stone is calcite ( $\text{CaCO}_3$ ). Quartz ( $\text{SiO}_2$ ) can be identified as a minor phase.



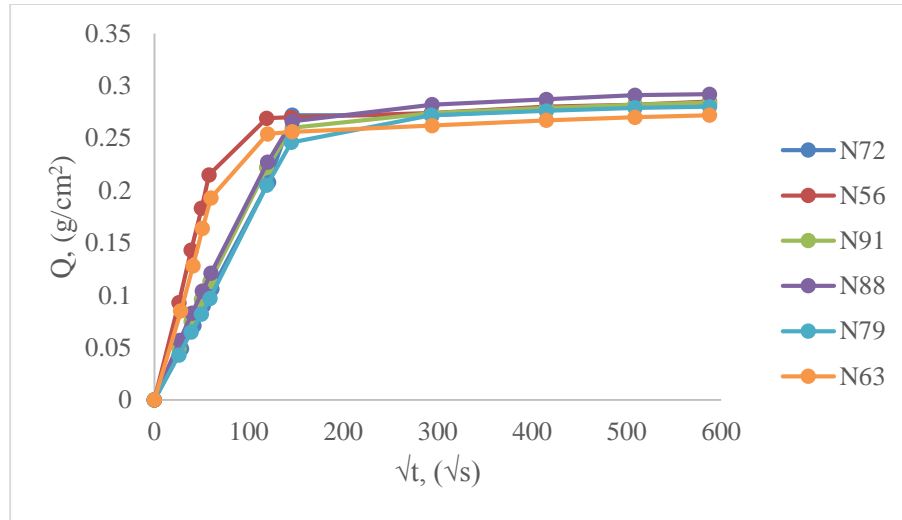
**Fig. 10.** XRD spectrum of Noto stone sample.

Colorimetric measurements were performed on all selected for the analysis Noto stone samples before the treatment and obtained chromatic parameters ( $L^*$ ,  $a^*$ ,  $b^*$ ) were compared within the group (*Table 1*). Differences in all measured parameters could be observed, which proposes the conclusion that color of the stone surface is not completely homogeneous.

**Table 1.** Chromatic parameters of untreated Noto stone samples

Sample name	$L^*$	$a^*$	$b^*$
N72	$82.97 \pm 0.94$	$0.45 \pm 0.56$	$8.71 \pm 1.32$
N56	$80.57 \pm 1.62$	$1.89 \pm 0.24$	$10.26 \pm 0.45$
N91	$82.54 \pm 1.47$	$0.58 \pm 0.62$	$9.60 \pm 1.2$
N88	$80.21 \pm 2.73$	$1.63 \pm 0.69$	$11.44 \pm 1.57$
N79	$79.39 \pm 2.46$	$1.52 \pm 0.77$	$10.62 \pm 1.76$
N63	$79.86 \pm 1.27$	$1.57 \pm 0.26$	$10.09 \pm 1.11$

Liquid water absorption by capillarity measurement was performed on untreated samples and obtained liquid water absorption curves were compared among each other (*Fig. 11*). Some absorption curves show different behaviour, especially in time interval 0-146  $\sqrt{s}$ , which could suggest a hypothesis about inhomogeneous distribution of capillary system in Noto stone.



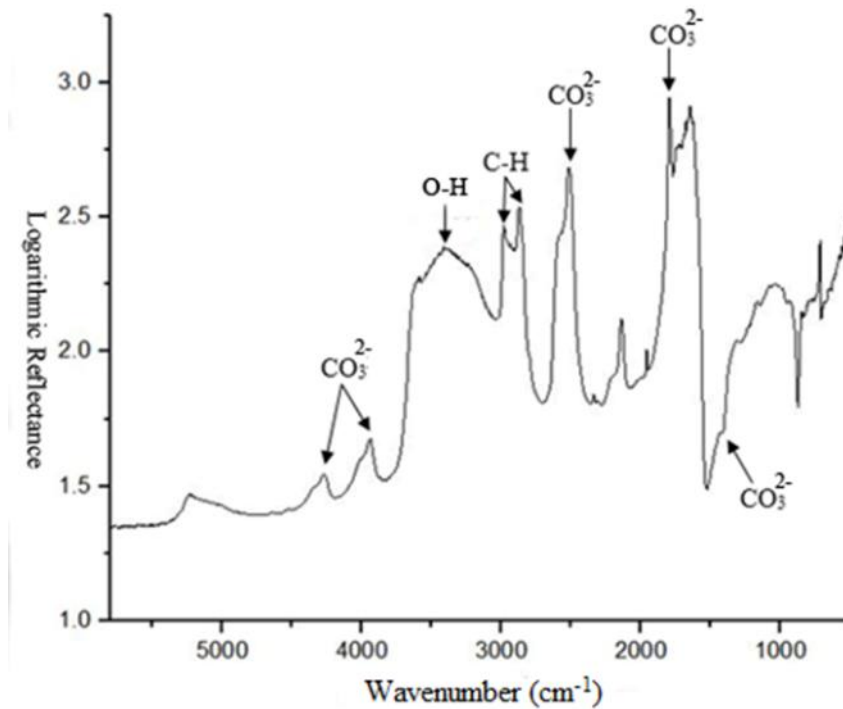
**Fig. 11.** Liquid water absorption by capillarity as a function of square root of time of untreated Noto stone samples

Water vapour permeability ( $\delta_p$ ) was calculated from obtained results during measurement: water vapour flow rate ( $G$ ), vapour transmission rate ( $g$ ), water vapour permeance ( $W_p$ ). Water vapour permeability of the untreated Noto stone sample was equal to  $1.64 \cdot 10^{-13} \text{ kg}/(\text{m} \cdot \text{s} \cdot \text{Pa})$ . For the calculation of water vapour permeability relative reduction, this obtained value will be taken as reference.

Static contact angle of the untreated sample was measured 15 times throughout the surface. The obtained value was averaged in order to take into account possible surface inhomogeneity and was equal to  $23.43 \pm 5.47^\circ$ , which is less than  $90^\circ$  and proves the surface to be hydrophilic.

The molecular composition of Noto stone sample was analyzed applying reflectance FT-IR technique. The spectrum (*Fig. 12*) presents the behaviour characteristic to carbonates:

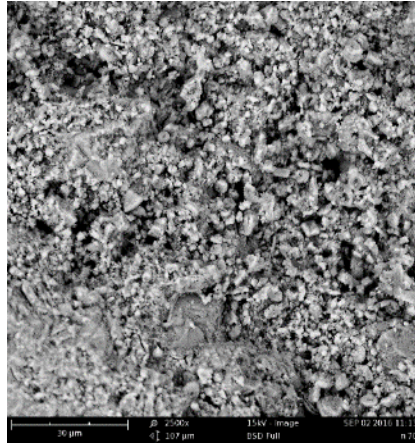




**Fig. 12.** Reflectance spectrum of an untreated Noto stone sample

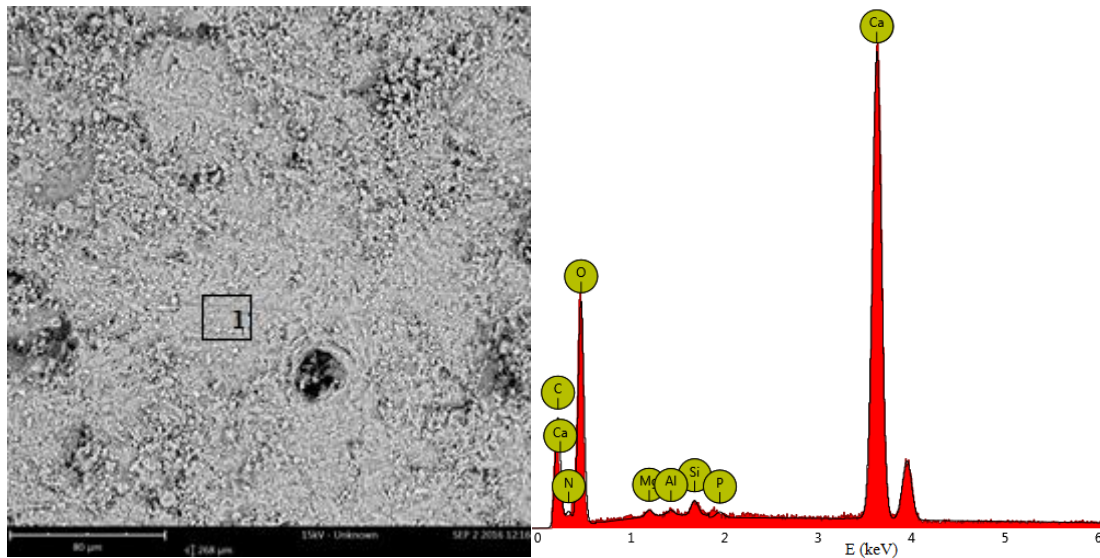
The reflectance FT-IR spectrum of an untreated Noto stone sample shows an inverted band at  $1400\text{ cm}^{-1}$ , due to the presence of the  $\text{CO}_3^{2-}$  group, together with combination bands at  $2524$  and  $1794\text{ cm}^{-1}$ , which are characteristic of calcite ( $\text{CaCO}_3$ ). C-H stretching bands can be identified as well at  $2983$  and  $2873\text{ cm}^{-1}$ , which could indicate the presence of organic inclusions in the stone matrix [54]. Also, two calcite bands could be seen in the region between  $4300$  and  $3900\text{ cm}^{-1}$ , more specifically – an overtone at  $4274\text{ cm}^{-1}$  and a combination band at  $3940\text{ cm}^{-1}$  [55]. A broad vibration band, present at  $3403\text{ cm}^{-1}$ , may be attributed to the presence of water in the sample analyzed [56].

The surface morphology studies and elemental composition of the sample was obtained performing SEM-EDX measurement. The image of the sample's surface (*Fig. 13*) shows the presence of grains of different size and clearly visible surface roughness.



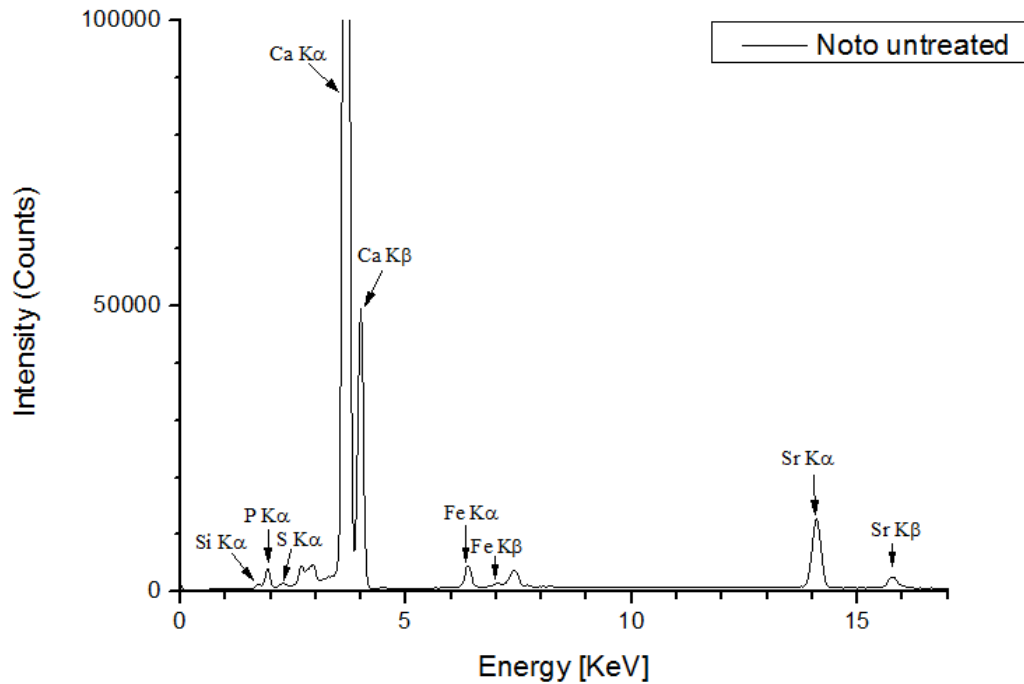
**Fig. 13.** SEM image of untreated Noto stone sample (magnification x2500).

The spectrum of the marked area (*Fig. 14*) reveals that the sample consists of calcium (Ca), oxygen (O), carbon (C), magnesium (Mg), aluminium (Al), phosphorus (P) and silicon (Si).



**Fig. 14.** Elemental composition of untreated Noto stone sample

In addition to SEM-EDX analysis, XRF was performed as a supporting measurement. Presented spectrum (*Fig. 15*) shows the presence of such elements: Ca, Fe, P, sulphur (S), Si, strontium (Sr), titanium (Ti). The most intense for the untreated sample is calcium peak, representing both  $K\alpha$  and  $K\beta$  transition lines.



**Fig 15.** XRF spectrum of untreated Noto stone sample.

XRF analysis aided in revealing the presence of Fe, S, Sr and Ti which were not visible with SEM-EDX.

The surface and bulk analysis techniques listed above allowed to extensively characterize Noto stone samples used for the study and revealed them to be inhomogeneous in surface color and capillary distribution. The major component of the material was proven to be calcite with the presence of quartz in the stone matrix along with chemical elements such as Fe, S, P, Ti, Al, Si, Sr and bioclastic inclusions of marine origin.

ii. Comiso stone

1. Context

Comiso calcarenite can be extracted from the quarries located in the southeastern part of Sicily and was used as a material for buildings and monuments in Val di Noto area, included in the UNESCO World Heritage List [47], to which belong Catania, Syracuse, Noto, Ragusa and Modica. Due to the value of cultural heritage objects made from this type of stone, it is important to ensure their proper protection from deterioration and possible loss in the future. Several studies have been done in order to achieve this goal. Innovative treatment with nanocrystalline  $\text{TiO}_2$  was applied on Comiso stone to obtain a suitable self-cleaning photocatalytic coating [57]. The treatment did not cause any chromatic alterations.

Moreover, a satisfactory self-cleaning effect was achieved, although the coating did not prevent salt crystallization. A different approach to the conservation of Comiso stone was presented in another article [58]. In this case, the authors tried to investigate the efficiency of polymeric coating obtained by using an *in situ* polymerization, impregnating the stone with a mixture of monomers. The study has been conducted on several different types of stones but only Comiso stone presented acceptable results.

Due to the fact that both Noto and Comiso stones are limestones, they suffer from deterioration processes characteristic to this type of rock. Being of highly porous and hydrophilic nature, limestones are sensitive to acid rain and environmental pollutants [59].

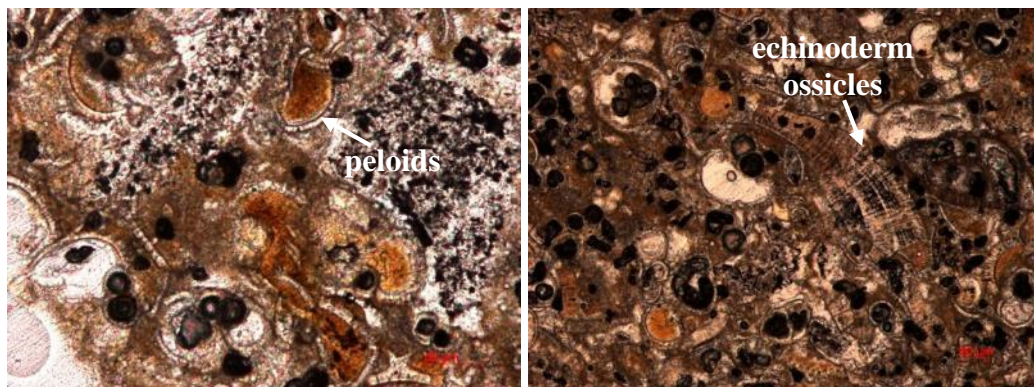
## 2. Stone characterization

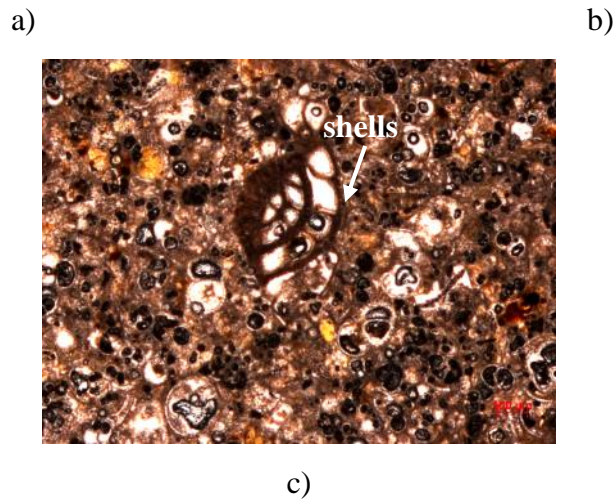
In order to understand the mineralogical composition of Comiso stone sample, petrographic analysis with optical microscope and XRD measurement were performed. Porosity of the material was evaluated by mercury intrusion porosimetry, molecular and elemental composition was analyzed with reflectance FT-IR and SEM-EDX techniques respectively.

According to the results, the porosity of Comiso stone is  $40.1 \pm 1.07$  % and the average pore diameter  $0.35 \pm 0.01$   $\mu\text{m}$ .

From the obtained results it could be stated that Comiso stone is a biocalcarenite, characterized by bioclastic inclusions, such as peloids (*Fig. 16. a*)), echinoderm ossicles (*Fig. 16. b*)), shells (*Fig. 16. c*)) in inorganic carbonate matrix.

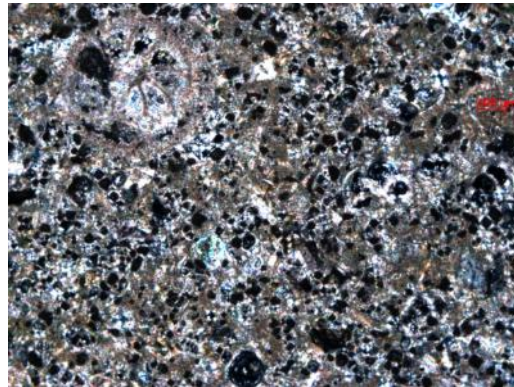
The micrographs, shot using parallel nicols, allowed to operate a petrographic characterization according to Dunham and Folk classifications. Comiso stone has been classified as a grainstone according to Dunham and biosparite according to Folk classification.





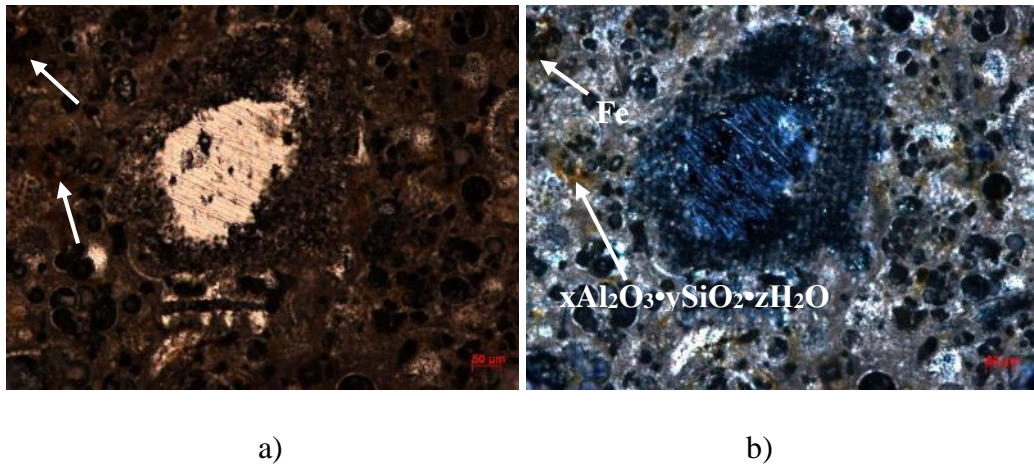
**Fig. 16.** The micrograph of Comiso stone thin section using parallel nicols

The micrographs shot using crossed nicols (*Fig. 17*) show high birefringence of calcite crystals, recognizable from multiple interference colours, which prove calcite to be a main mineral.



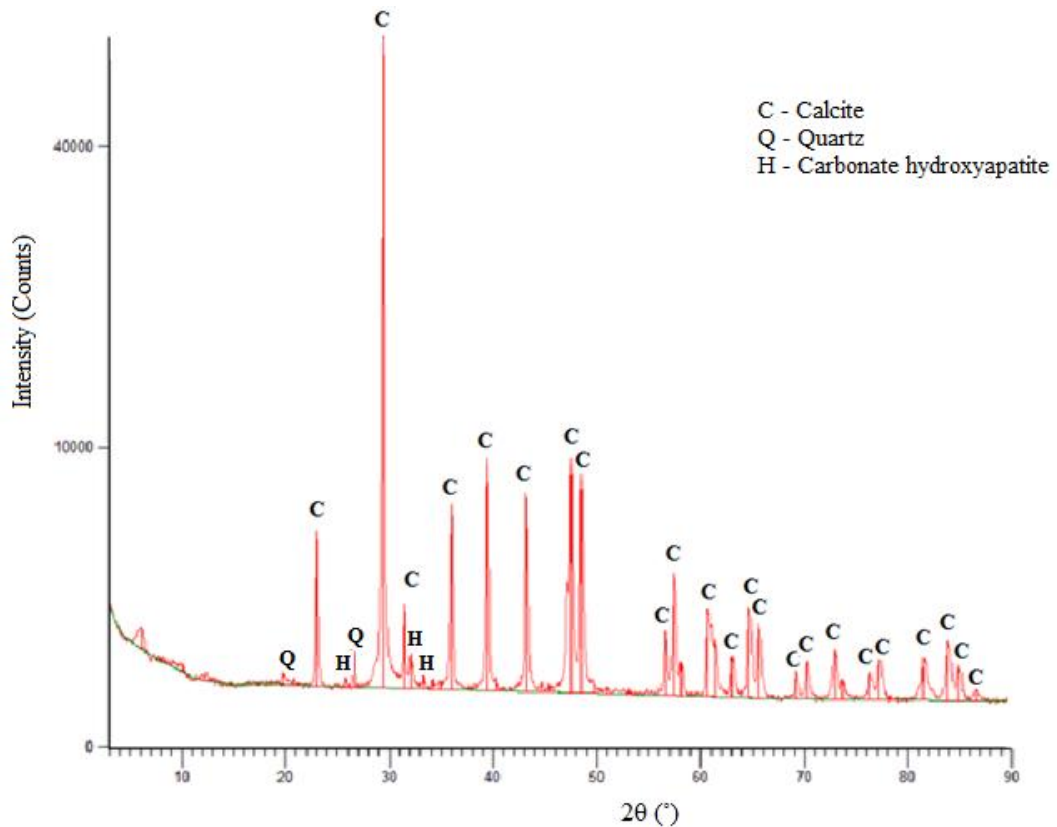
**Fig. 17.** The micrograph of Comiso stone thin section using crossed nicols.

Polarized light microscopy, combining images obtained using both, parallel and crossed nicols, allowed to distinguish crystals of iron (Fe) and aluminium silicate ( $x\text{Al}_2\text{O}_3 \cdot y\text{SiO}_2 \cdot z\text{H}_2\text{O}$ ) (*Fig. 18.*). With parallel nicols, both iron and aluminium silicate crystals have a dark brown colour and cannot be easily distinguished from each other (*Fig. 18. a)*), while using crossed nicols, aluminium silicate crystals from dark brown turn into light green, iron crystals remain brown and in this way can be distinguished (*Fig. 18. b)*).



**Fig. 18.** The micrograph of Comiso stone thin section using: a) parallel nicols, b) crossed nicols

The XRD analysis result is presented in figure 19. As the measurement revealed, Comiso stone is mainly composed of calcite ( $\text{CaCO}_3$ ) with small amounts of quartz ( $\text{SiO}_2$ ) and carbonate-hydroxyapatite ( $\text{Ca}_{10}(\text{PO}_4)_3(\text{CO}_3)_3(\text{OH})_2$ ).



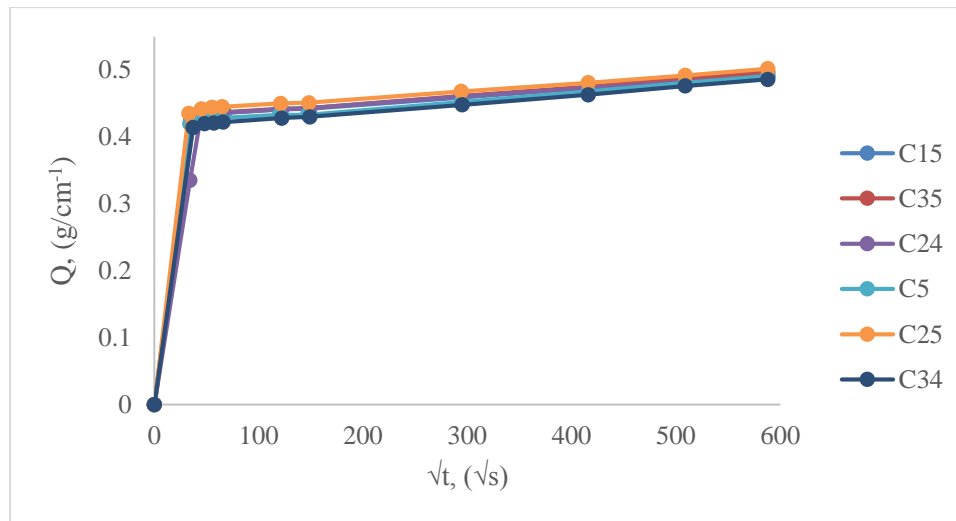
**Fig. 19.** XRD spectrum of Comiso stone

Colorimetric measurements were performed on all untreated Comiso stone samples selected for the study. Chromatic parameters are presented in table 2. It could be observed, that measured chromatic parameters vary between samples, even though all of them belong to the same type of stone. These results suggest that the stone surface colour is not completely homogeneous.

**Table 2.** Chromatic parameters of untreated Comiso stone samples

Sample name	L*	a*	b*
C25	84.79 ± 1.08	1.4 ± 0.49	13.82 ± 0.7
C34	81.69 ± 1.29	1.7 ± 0.65	14.74 ± 1.04
C15	82.24 ± 0.74	1.61 ± 0.41	14.68 ± 1.31
C35	85.38 ± 1.25	1.4 ± 0.39	13.66 ± 0.86
C24	84.74 ± 1.28	1.7 ± 0.47	14.17 ± 0.85
C5	84.96 ± 1.03	1.39 ± 0.39	14.62 ± 0.66

Liquid water absorption by capillarity was performed on the same samples, in order to see the tendency in the amount of absorbed liquid water within the group of samples of the same stone type. Absorption curves (Fig. 20) show almost identical patterns which could be referred to the homogeneous distribution of capillary system of the stone.

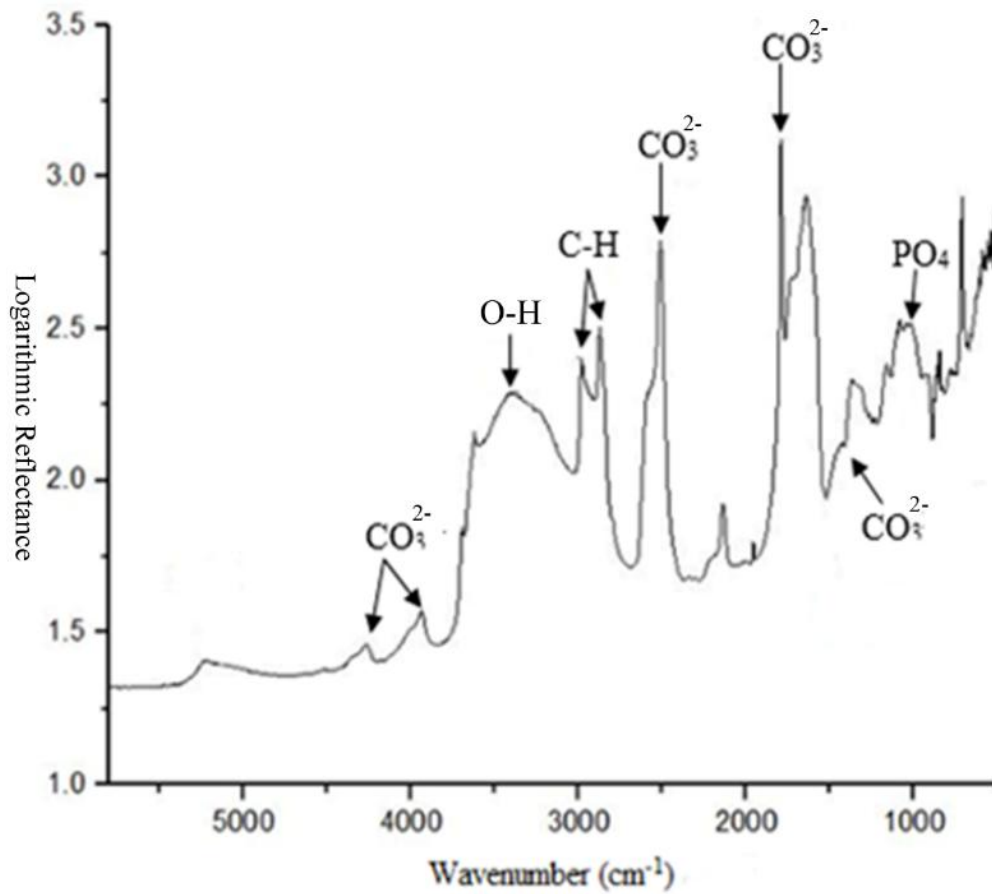


**Fig. 20.** Liquid water absorption by capillarity as a function of square root of time of untreated Comiso stone samples

Water vapor permeability ( $\delta_p$ ) was calculated from the experimental data and the obtained value is equal to  $2.73 \cdot 10^{-13} \text{ kg}/(\text{m} \cdot \text{s} \cdot \text{Pa})$ .

Static contact angle value of untreated Comiso stone samples has been proven to be equal to  $0^\circ$  because of the very short time the water drop stayed on their surface, considering its highly hydrophilic character.

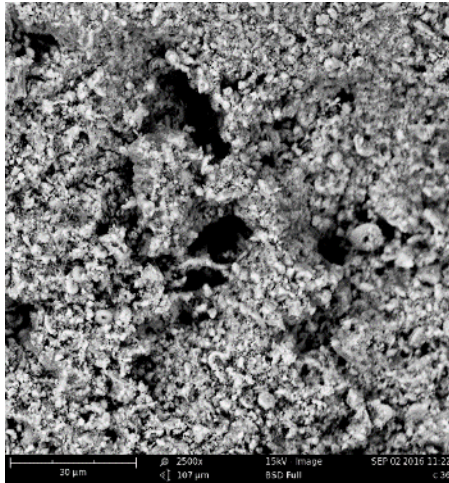
The reflectance FT-IR spectrum obtained on untreated Comiso stone samples (*Fig. 21*) shows a peak at  $1400 \text{ cm}^{-1}$ , together with combination bands at  $2524 \text{ cm}^{-1}$  and  $1803 \text{ cm}^{-1}$  represents group vibration of the calcite  $\text{CO}_3^{2-}$  ion. C-H stretching bands identified at  $2983$  and  $2873 \text{ cm}^{-1}$  indicate the presence of organic content in the stone matrix [54]. An overtone and a combination band of calcite could be observed at  $4273 \text{ cm}^{-1}$  and  $3942 \text{ cm}^{-1}$  respectively [55]. A combination band, attributed to water, is present at  $3403 \text{ cm}^{-1}$  [56]. The band at  $1034 \text{ cm}^{-1}$  could be assigned to a  $\text{PO}_4^{3-}$  ion, possibly of hydroxyapatite [60].





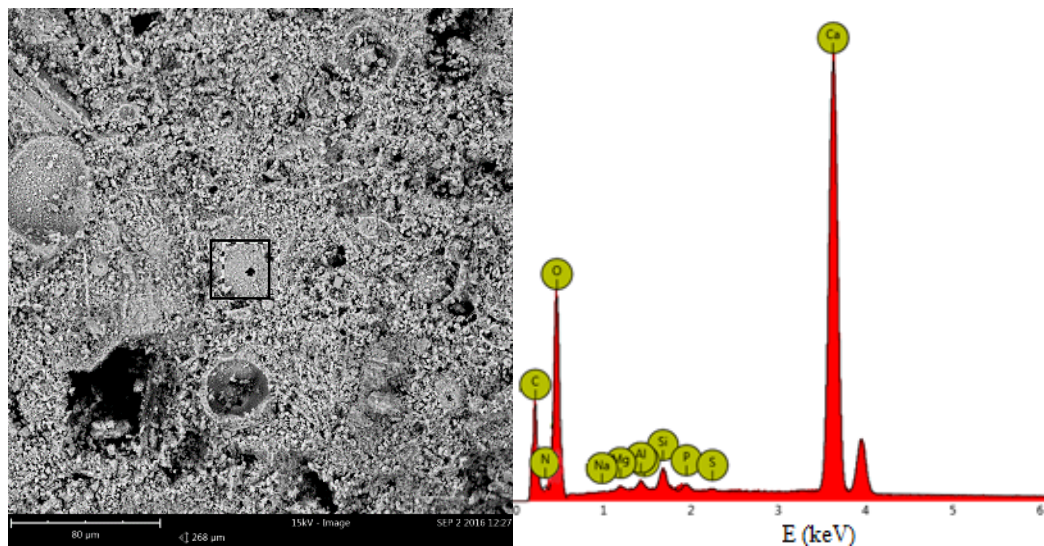
**Fig. 21.** Reflectance spectrum of untreated Comiso stone sample

The information about morphological structure and elemental composition of the sample was obtained using SEM-EDX technique.



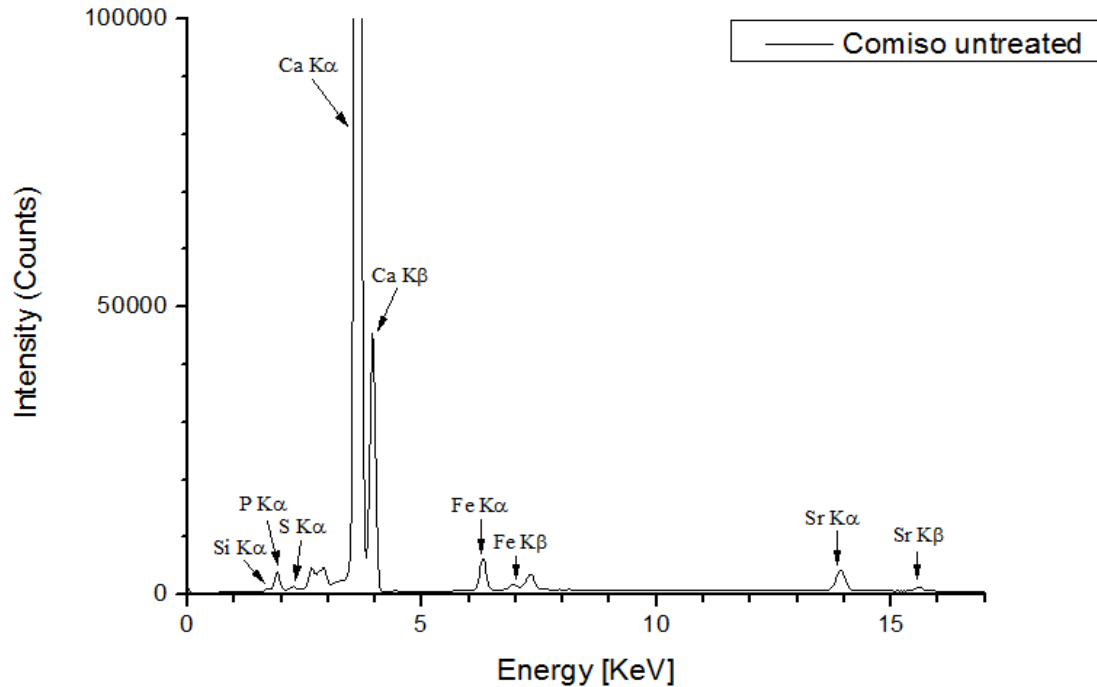
**Fig. 22.** SEM image of untreated Comiso stone sample (magnification x2500).

From the SEM image (*Fig. 22*) surface roughness created by grains of various size could be easily observed along with the porosity of the sample. The elemental analysis showed that the sample is composed of C, O, Ca, Na, Mg, Al, Si, P, S.



**Fig. 23.** Elemental composition of untreated Comiso stone sample

XRF analysis was performed in addition to SEM-EDX measurements in order to compare obtained results. XRF data (Fig. 24) revealed the presence of elements which did not occur in SEM-EDX spectrum, such as Sr and Fe, while Al was detected only in SEM-EDX. The presence of both mentioned elements is also confirmed by petrographic characterization which allowed to observe aluminium silicate and iron crystals using polarized light.



**Fig 24.** XRF spectra of untreated Comiso stone sample.

b. Protective polymeric dispersions

Formulations of different chemical origin: silica-based and fluorine-based were selected in order to compare the final result of the treatment, taking into account a different microscale behaviour at the interface with the stone substrate.

Three different commercial products have been used for this study as protectives for stone objects: silica-based Silo 111 and Wacker 290 and fluorine-based Fluoline HY.

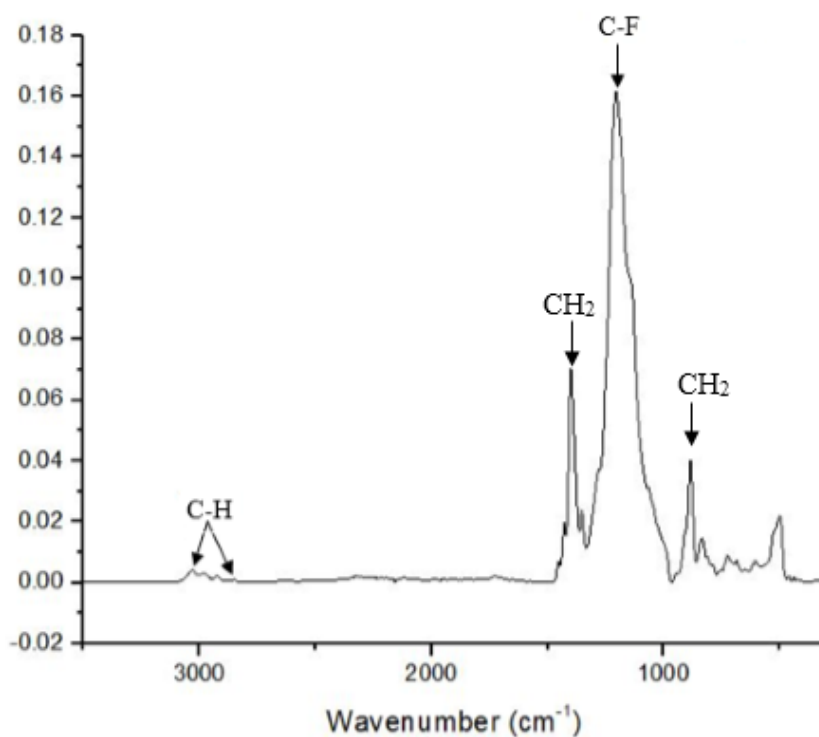
i. Fluoline HY

Fluoline HY – colourless ready-to-use water-oil-repellent protective based on fluorinated copolymers (molecular weight around 400.000 Da). It is a 3% solution in a mixture of acetone and butyl acetate. It

can be used for pre-consolidation and protection of natural and artificial stone materials, plasters and wall paintings, suitable for very porous and absorbent substrates (sandstone, tuff). According to the manufacturer, Fluoline HY is a reversible and UV resistant material, presenting high permeability to water vapour, oil and water repellence even after aging. Furthermore, it has shown in previous applications that it does not alter colours of the stone which it is applied to.

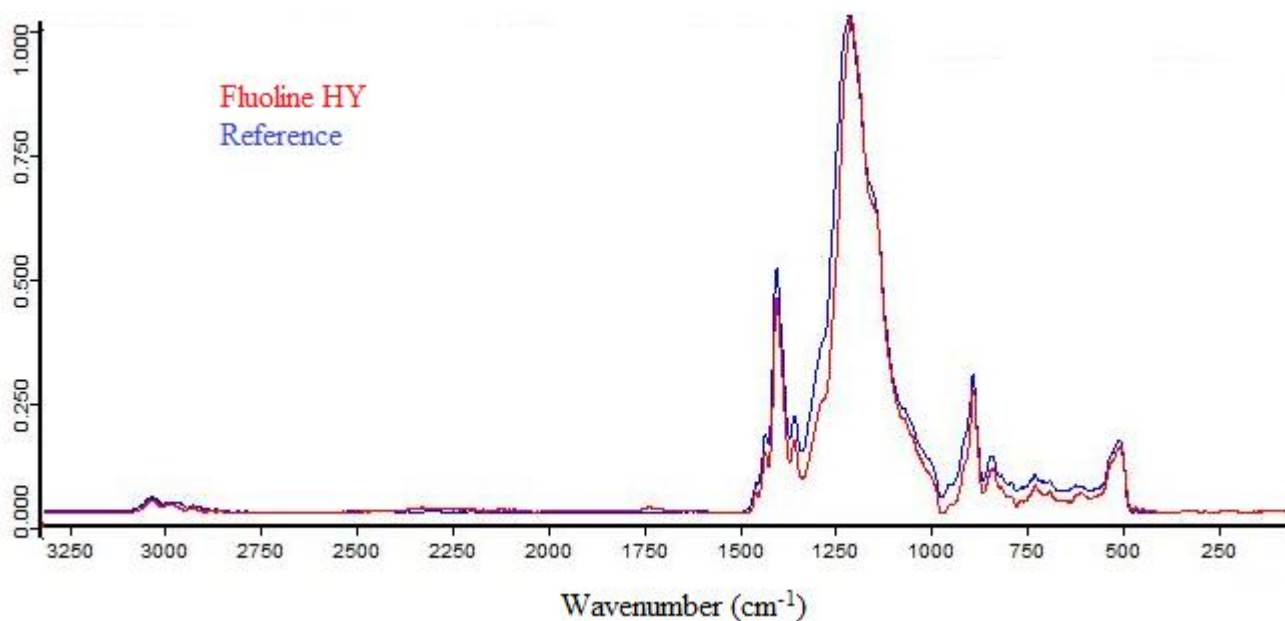
The product is preferably applied by brush at the temperatures not below 5 °C. The yield of the product varies between 1-3 L/m<sup>2</sup>. Due to a low transition temperature it remains always elastic which may lead to absorption of particles which might cause graying of the treated surface. After the treatment with Fluoline HY it is impossible to make other water-based treatment due to high water repellence that this substance provides.

The polymer used in Fluoline HY product was characterized with ATR FT-IR and <sup>19</sup>F ss-NMR. Both techniques were applied in order to determine its chemical composition, after evaporation of the dispersive phase and formation of a homogeneous film of polymer.



**Fig. 25.** Absorbance FT-IR spectrum of Fluoline HY active component

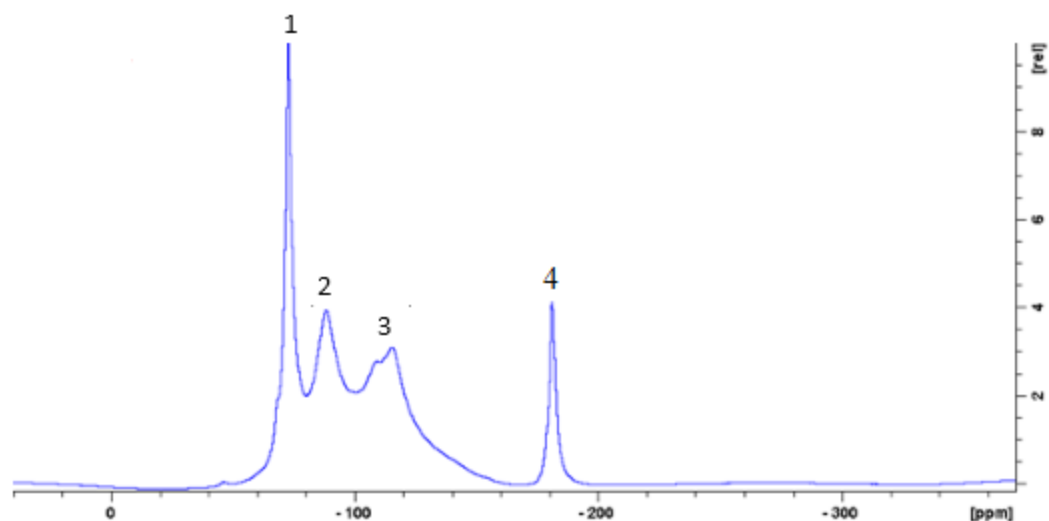
Absorbance spectrum of a film sample is presented in figure 25. Peak observed at  $1208\text{ cm}^{-1}$  could be assigned to C-F stretching vibration. The group of weak bands at the range of  $3030\text{-}2850\text{ cm}^{-1}$  corresponds to C-H stretching vibrations, while peaks at  $1400\text{ cm}^{-1}$  and  $888\text{ cm}^{-1}$  could be associated with  $\text{CH}_2$  wagging and rocking vibrations respectively [61].



**Fig. 26.** Absorbance FT-IR spectra of Fluoline HY active component and reference

The obtained Fluoline HY spectrum was compared to a reference spectrum copolymer of vinylidene fluoride ( $\text{CH}_2\text{CF}_2$ ) and hexafluoropropene ( $\text{CF}_3\text{CFCF}_2$ ) (Fig. 26). The nature of the active component of Fluoline HY has been accredited by comparing fingerprint regions of the spectra ( $1500\text{-}500\text{ cm}^{-1}$ ), which show identical patterns.

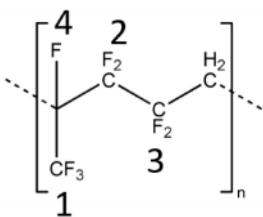
The chemical composition of Fluoline HY active component obtained with FT-IR analysis could be also confirmed by acquiring solid-state (DP)  $^{19}\text{F}$  MAS NMR spectrum (Fig. 27.). Chemical shifts were assigned according to literature [55] and given in table 3.



**Fig. 27.** Solid-state  $^{19}\text{F}$  NMR spectrum of Fluoline HY

Peak 1 (Fig. 27) at -72.8 ppm corresponds to  $\text{CF}_3$  group, peaks 2 and 3 could be assigned to  $\text{CF}_2$  group of both and be detected in the range of -85 to -118 ppm. Peak 4, detected at -181 ppm, corresponds to CF group. These results will be used as a reference to study the possible interactions between product and the substrate after the treatment.

**Table 3.** Chemical shifts of Fluoline HY



Peak number	Chemical shift (ppm)	Nucleus
1	-72.8	$\text{CF}_3$
2	-88.0	$\text{CF}_2$
3	-109.1	$\text{CF}_2$
4	-181.0	CF

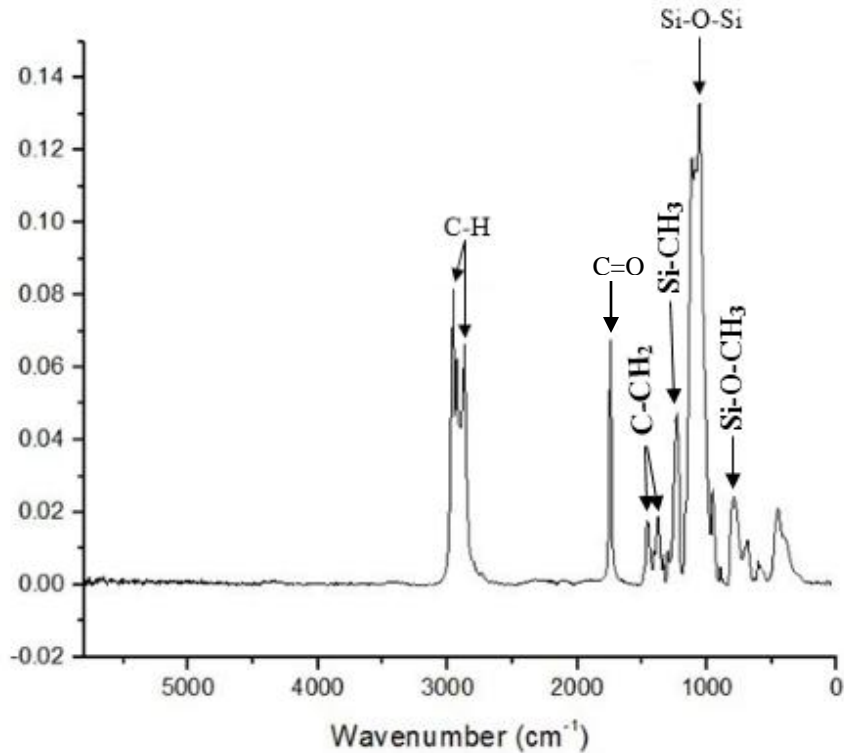
## ii. Silo 111

Silo 111 is a ready to use 10 wt % solution of a mixture of low molecular weight organosiloxane oligomers, dissolved in White Spirit D40. According to the manufacturer, the product should penetrate deep into the substrate, significantly reducing the absorption of water without causing filming effects, chromatic alterations and yellowing over time. The water-repellent effect develops on the surface through a reaction with atmospheric humidity. This material is suitable for the protection of construction materials of monumental works of art, such as: plasters and esteemed frescoes, terracotta, natural

carbonate or silicate based stone or artificial stone, also suitable for every type of absorbent mineral support or very compact materials, like non-degraded marbles.

The surface to be treated must be dry, clean, cured from any efflorescent salts present and the atmospheric temperature must fall between 10°C and 25°C. Furthermore, the surface must not be exposed to direct solar radiation during the treatment. The reaction, needed for water-repellent effect to develop, requires 2-4 days to occur, depending on the atmospheric condition. In this period, treated surface must not be wet. Quantity of product recommended by manufacturer is between 0.3-0.8 L/m<sup>2</sup>.

The chemical composition of the active component of Silo 111 was analysed using attenuated total reflectance FT-IR, obtained on the liquid sample after evaporation of solvent.



**Fig. 28.** Absorbance spectrum of Silo 111 using ATR FT-IR

Silo 111 active component ATR FT-IR spectrum (*Fig. 28*) shows a peak at 1043 cm<sup>-1</sup> corresponds to the absorption bands of Si-O-Si structure. A group of peaks at the range of 2958-2871 cm<sup>-1</sup> indicates the presence of C-H stretching bands, while CH<sub>2</sub> bending vibrations could be observed at around 1460 cm<sup>-1</sup> and 1366 cm<sup>-1</sup>. Peaks at around 785 cm<sup>-1</sup> and 1260 cm<sup>-1</sup> could be assigned to Si-O-CH<sub>3</sub> and Si-CH<sub>3</sub>

structures respectively [62]. A sharp peak at  $1743\text{ cm}^{-1}$ , ascribable to an ester carbonyl group, was not certainly attributed to the polymer itself or to an additive present in the product.

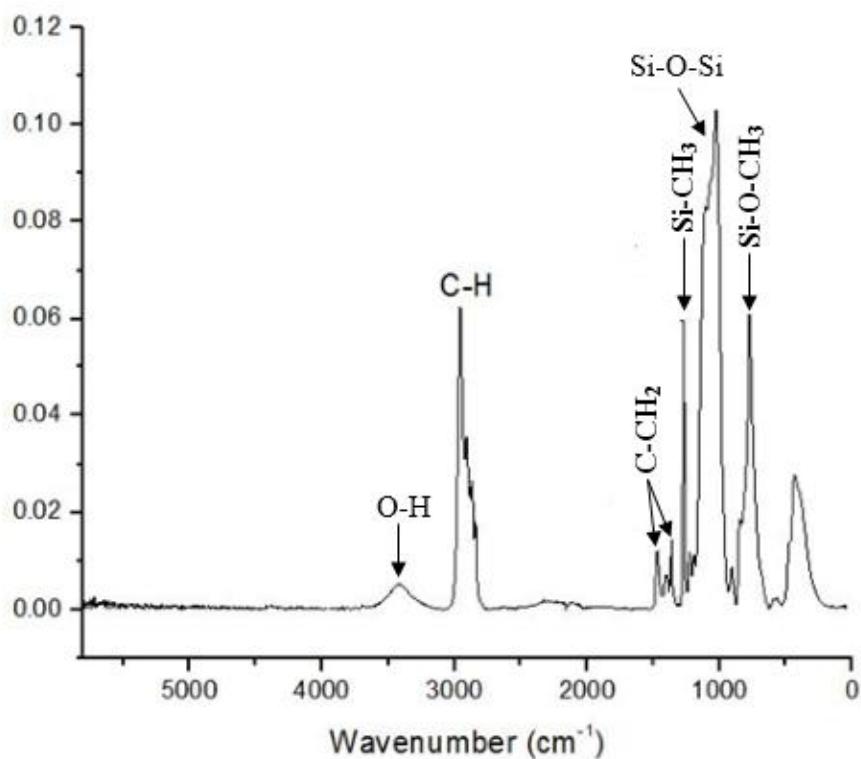
### iii. Wacker 290

Wacker 290 is a solventless silicone concentrate that is based on a mixture of silanes and siloxanes. In order to be used as a water-repellent protective material for stone substrate, Wacker 290 can be diluted in organic solvents: commonly aliphatic hydrocarbons (such as White Spirit) or aromatic hydrocarbons (solvent naphtha). Wacker 290 should be diluted in a weight ratio of 1:11 to 1:15.

If diluted with anhydrous alcohols, such as ethanol or 2-propanol, Wacker 290 could be used in situations where interaction between impregnating substance and solvent-sensitive materials (such as expanded polystyrene, bitumen) cannot be avoided. The alcohol must be completely anhydrous and a dilution ratio of 1:12 pbw is recommended.

Wacker 290 is suitable for impregnation of absorbent, porous, mineral construction materials, such as brickwork, concrete, mineral plasters, mineral-based natural and artificial stone, mineral paints. According to the producer, the special features of this protective substance are: good depth of penetration, high resistance to alkalis, tack-free drying, effectiveness even on damp substrates, rapid development of water repellency. The product reacts with atmospheric moisture or pore water in the substrate, thereby generating the active component while liberating alcohol. According to the manufacturer's recommendations, several layers of the product should be applied, until the substrate is saturated (at least two applications). The requisite quantity of the product depends on the absorbency of the substrate.

The chemical composition of Wacker 290 active component was analysed using attenuated total reflectance FT-IR, after obtaining a film of polymer through solvent casting technique.



**Fig. 29.** Absorbance spectrum of Wacker 290 active component using attenuated total reflectance FT-IR

In figure 29 is presented the ATR FT-IR spectrum of Wacker 290 active component. Characteristic C-H stretching bands could be seen at  $2959\text{ cm}^{-1}$  and C-CH<sub>2</sub> bending vibration bands at  $1465\text{ cm}^{-1}$  and  $1362\text{ cm}^{-1}$ . As it is known from technical sheets provided by the supplier, Wacker is a mixture of silanes and siloxanes, which could be proven by detecting characteristic to siloxane structural units, such as Si-CH<sub>3</sub> and Si-O-Si at  $1270\text{ cm}^{-1}$  and  $1054\text{ cm}^{-1}$  respectively. At  $773\text{ cm}^{-1}$  a signal of Si-O-CH<sub>3</sub> could be detected.



## V. Sample preparation

All selected samples were cleaned with a soft brush, polished with a silicon carbide paper P180, washed in deionized water and dried in the oven at 60 °C until the constant mass was reached (mass difference between two successive weightings did not exceed 0.1 g).

Noto and Comiso stone samples of two sizes (5x5x1 cm and 5x5x2 cm) were treated with different protective polymeric dispersions: fluorine-based Fluoline HY and silica-based Silo 111 and Wacker 290. Two amounts of products were used according to the supplier's recommendations in order to evaluate an influence of the amount of polymer on the protective effect of the product. In the current work it will be referred to these amounts as minimum (min) and maximum (max).

**Table 4.** Recommended quantities of products

Product	Yield (ml/cm <sup>2</sup> )	
	Min	Max
Fluoline HY	0.1	0.2
Silo 111	0.05	0.08
Wacker 290	0.05	0.1

Selected samples were coded before the treatment using the combination of two letters for each name which one stands for the stone type – N for Noto and C for Comiso, while the other stands for the protective product – F for Fluoline HY, S for Silo 111 and W for Wacker 290, adding abbreviations Min or Max with a respect to minimum and maximum amount of applied product (*Table 5*).

**Table 5.** Coded sample names with a respect to the particular product and the applied amounts

Noto stone samples		
Sample name	Product	The amount of product
NF Min	Fluoline HY	Minimum
NF Max		Maximum
NS Min	Silo 111	Minimum
NS Max		Maximum
NW Min	Wacker 290	Minimum
NW Max		Maximum
Comiso stone samples		
Sample name	Product	The amount of product



CF Min	Fluoline HY	Minimum
CF Max		Maximum
CS Min	Silo 111	Minimum
CS Max		Maximum
CW Min	Wacker 290	Minimum
CW Max		Maximum

During the treatment some tendencies were noticed regarding the particular stone type and the product used.

#### Noto stone samples

##### 1. Fluoline HY:

- a. *Minimum amount.* Slight darkening, shininess and film formation can be noticed on the stone's surface.
- b. *Maximum amount.* Absorption of the product was significantly slower than in case of minimum amount. Darkening was visible with a naked eye along with significant film formation and shininess on the sample's surface.

##### 2. Silo 111:

- a. *Minimum amount.* No visible colour changes of the surface were noticed.
- b. *Maximum amount.* The absorption of the product was slower than in the case of minimum amount. No shininess or darkening were present.

##### 3. Wacker 290:

- a. *Minimum amount.* Darkening was visible with a naked eye.
- b. *Maximum amount.* Absorption time was longer than in the case of minimum amount. Very significant darkening could be noticed on the sample's surface.

#### Comiso stone

##### 1. Fluoline HY:



- a. *Minimum amount.* Slight darkening of the surface was visible with a naked eye, no significant film formation was noticed.
  - a. *Maximum amount.* The absorption of product by the sample was slower than in the case of minimum amount. More significant darkening, shininess and formation of a film on the surface could be acknowledged.
2. Silo 111:
- a. *Minimum amount.* An absorption of the product was immediate, no visible colour changes of the surface were noticed.
  - b. *Maximum amount.* Stone sample immediately absorbed the product. No visible colour changes of the surface were noticed.
3. Wacker 290
- a. *Minimum amount.* Stone sample immediately absorbed the product. Slight darkening was visible with a naked eye.
  - b. *Maximum amount.* The absorption of the product was slower than in the case of minimum amount. Significant darkening could be observed on the stone surface.

The treatment revealed that Fluoline HY was absorbed slower by both Noto and Comiso stone samples comparing to absorption time of Silo 111 and Wacker 290. This data could be justified taking into account the different properties of the compound used, being Fluoline HY a dispersion of a much higher molecular weight polymer compared to both Silo 111 and Wacker 290.

## VI. Evaluation of the Effectiveness of the Treatment

### a. Noto stone

#### i. Colorimetry

The chromatic alterations of the surface of Noto stone samples were evaluated comparing  $L^*$ ,  $a^*$  and  $b^*$  colorimetric parameters before (b. t.) and after (a. t.) the treatment with protective polymeric dispersions.

**Table 6.**  $L^*$ ,  $a^*$ ,  $b^*$  parameters of Noto stone samples before and after the treatment

Sample name	$L^*$ (b. t.)	$L^*$ (a. t.)	$a^*$ (b. t.)	$a^*$ (a. t.)	$b^*$ (b. t.)	$b^*$ (a. t.)
NF Min	$82.97 \pm 0.94$	$86.77 \pm 1.87$	$0.45 \pm 0.56$	$1.42 \pm 0.24$	$8.71 \pm 1.32$	$12.05 \pm 0.72$
NF Max	$80.57 \pm 1.62$	$91.34 \pm 1.94$	$1.89 \pm 0.24$	$2.03 \pm 0.5$	$10.26 \pm 0.45$	$12.04 \pm 1.09$
NS Min	$82.54 \pm 1.47$	$81.23 \pm 0.98$	$0.58 \pm 0.62$	$1.22 \pm 0.42$	$9.60 \pm 1.2$	$12.18 \pm 0.74$
NS Max	$80.21 \pm 2.73$	$80.07 \pm 0.67$	$1.63 \pm 0.69$	$1.15 \pm 0.37$	$11.44 \pm 1.57$	$11.66 \pm 0.86$
NW Min	$79.39 \pm 2.46$	$72.88 \pm 1.48$	$1.52 \pm 0.77$	$2.11 \pm 0.52$	$10.62 \pm 1.76$	$15.45 \pm 0.66$
NW Max	$79.86 \pm 1.27$	$74.99 \pm 2.12$	$1.57 \pm 0.26$	$2.62 \pm 0.41$	$10.09 \pm 1.11$	$15.92 \pm 1.15$

It could be seen that values of the lightness coordinate  $L^*$  increased after the treatment with Fluoline HY, remained the same after the treatment with maximum amount of Silo 111 and decreased when minimum amount of Silo 111 and Wacker 290 was used. The red/green coordinate  $a^*$  increased after the treatment in all cases except when maximum amount of Silo 111 was applied. An increase of yellow blue coordinate  $b^*$  values after the treatment could be observed in all samples.

According to the obtained data before and after the treatment,  $\Delta L^*$ ,  $\Delta a^*$ ,  $\Delta b^*$  values were calculated and used for the evaluation of  $\Delta E$ . The total colour difference value can be stated as acceptable when  $\Delta E \leq 5$ .

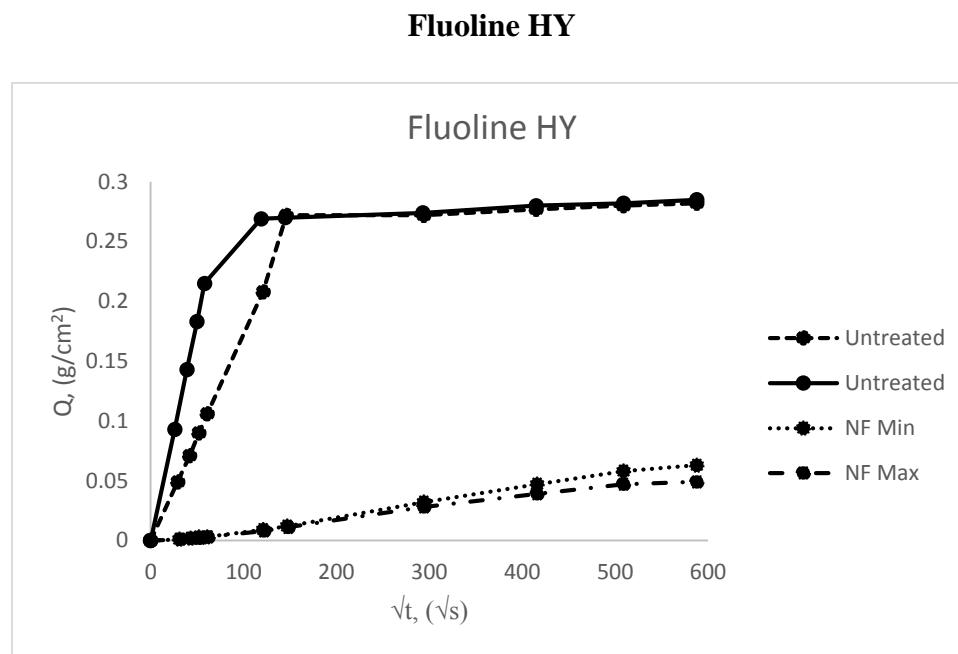
**Table 7.** Total colour difference ( $\Delta E$ ) values of Noto stone samples

Sample name	$\Delta L^*$	$\Delta a^*$	$\Delta b^*$	$\Delta E$
NF Min	$3.80 \pm 2.27$	$0.97 \pm 0.65$	$3.35 \pm 1.50$	$5.60 \pm 1.59$
NF Max	$10.77 \pm 2.83$	$0.15 \pm 0.42$	$1.78 \pm 1.09$	$11.00 \pm 2.79$
NS Min	$-1.31 \pm 1.79$	$0.64 \pm 0.88$	$2.59 \pm 1.47$	$3.56 \pm 1.35$
NS Max	$-0.13 \pm 2.71$	$-0.47 \pm 0.78$	$0.22 \pm 1.81$	$2.95 \pm 1.36$
NW Min	$-6.50 \pm 2.23$	$0.60 \pm 0.67$	$4.83 \pm 1.66$	$8.26 \pm 2.39$
NW Max	$-4.87 \pm 2.71$	$1.05 \pm 0.43$	$5.83 \pm 1.49$	$7.95 \pm 2.20$

$\Delta E$  values (table 7) are acceptable according to the normative only in a case when minimum and maximum amounts of Silo 111 were used. Samples treated with minimum amount of Fluoline HY underwent slight colour changes which not significantly exceeds the acceptable  $\Delta E$  limit.

ii. Liquid water absorption

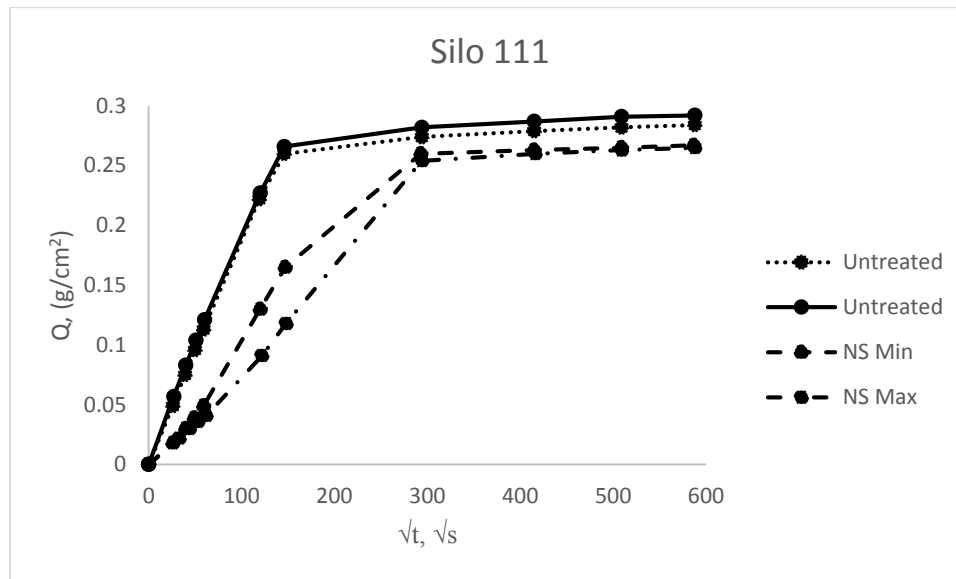
The liquid water absorption by capillarity test was performed on 6 Noto stone samples of the size 5x5x2 cm before and after the treatment with selected protective polymeric dispersions.



**Fig. 30.** Water absorption by capillarity as a function of square root of time of Noto stone samples treated with Fluoline HY

After the treatment, a significant reduction in amount of absorbed liquid water was noticed. At the time  $t^{1/2} = 588 \text{ s}^{1/2}$  the amount of absorbed water per surface area ( $Q$ ) of untreated sample was  $0.285 \text{ g/cm}^2$ . After the treatment with minimum amount of product  $Q = 0.063 \text{ g/cm}^2$ , while with maximum amount  $Q = 0.049 \text{ g/cm}^2$ . From the obtained data it is possible to state that samples treated with maximum amount of product absorb slightly less liquid water than samples treated with minimum amount.

**Silo 111**

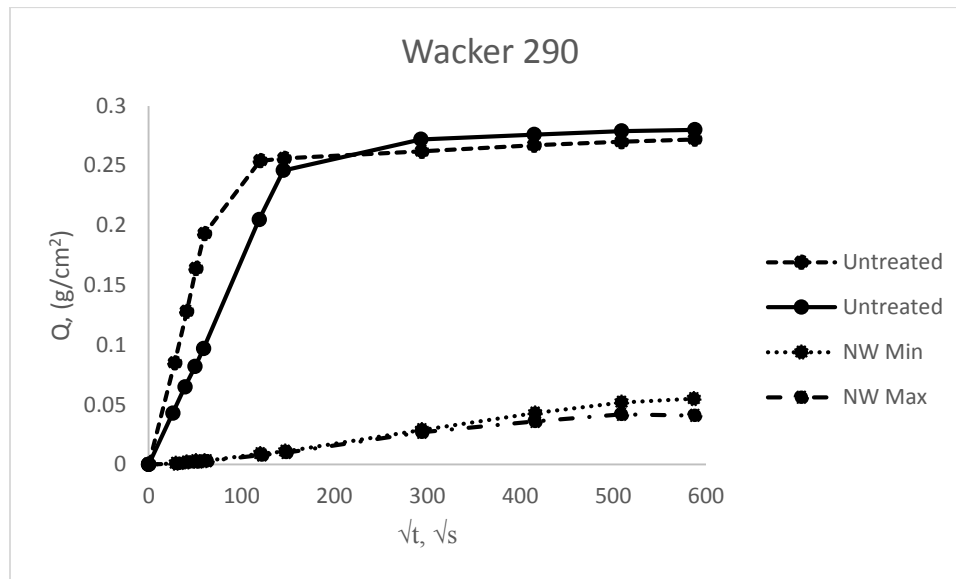


**Fig. 31.** Water absorption by capillarity as a function of square root of time of Noto stone samples treated with Silo 111

No significant changes in amount of absorbed water were noticed after the treatment. When  $t^{1/2} = 588$  s<sup>1/2</sup>,  $Q$  for untreated samples is 0.292 g/cm<sup>2</sup> and 0.294 g/cm<sup>2</sup>, while for samples treated with minimum and maximum amount of product  $Q = 0.265$  g/cm<sup>2</sup>. From the beginning of the test until the test time reached 416 s<sup>1/2</sup>, the sample treated with minimum amount of product showed higher liquid water absorption speed comparing to the one treated with maximum amount. From the time  $t = 416$  s<sup>1/2</sup> liquid water absorption speed became equal for both treated samples.

### Wacker 290

Yield range of this product was 0.05-0.1 ml/cm<sup>2</sup> taking 0.05 ml/cm<sup>2</sup> as minimum and 0.1 ml/cm<sup>2</sup> as maximum amount.



**Fig. 32.** Water absorption by capillarity as a function of square root of time of Noto stone samples treated with Wacker 290

Amount of absorbed liquid water was significantly reduced. At the time  $t^{1/2} \sim 300 \text{ s}^{1/2}$ , for untreated samples  $Q \sim 0.265 \text{ g/cm}^2$ . After the treatment with minimum amount of product  $Q = 0.029 \text{ g/cm}^2$  while with maximum amount  $Q = 0.027 \text{ g/cm}^2$ . According to the obtained data it could be stated that the amount of applied product on the stone surface does not have significant influence for the amount of absorbed liquid water.

### iii. Water vapour permeability

From the test results (*table 8*) it could be seen that water vapour permeability was reduced after the treatment for all tested samples. The lowest reduction occurred when minimum amount of Wacker 290 was used, while the highest - with maximum amount of Silo 111. Treatment with Fluoline HY resulted in similar permeability as Silo 111. Relative water vapour permeability was calculated with a respect to the untreated sample.

**Table 8.** Water vapour permeability values of Noto stone samples

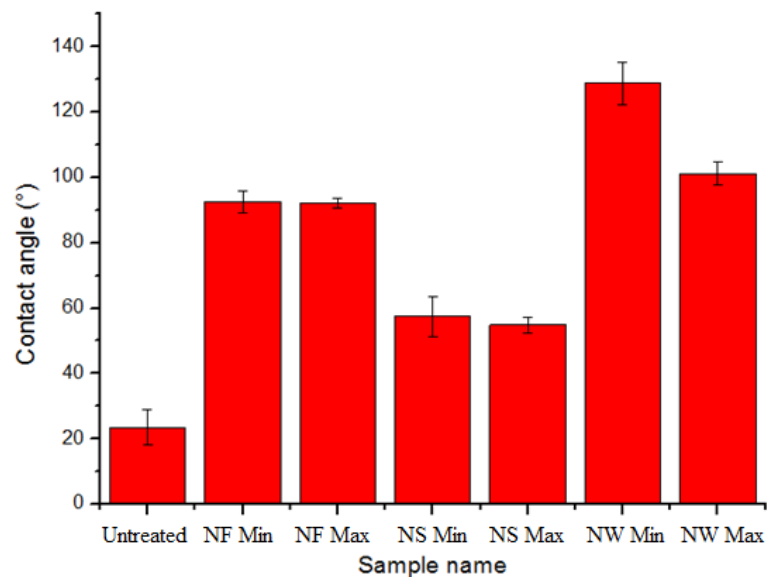
Sample name	Water vapour permeability $\delta_p$ ( $10^{-13} \text{ kg/(m*s*Pa)}$ )	Relative water vapour permeability (%)
Noto untreated	1.64	100
NF Min	1.09	66.8

NF Max	0.641	39.1
NS Min	1.05	63.8
NS Max	0.530	32.4
NW Min	1.34	81.6
NW Max	1.06	65.0

#### iv. Static contact angle

The results of static contact angle measurement are presented in figure 33.

Contact angle value of untreated sample is  $23.43^\circ$ . Samples treated with Fluoline HY and Wacker 290 exhibit contact angle values bigger than  $90^\circ$ , while in case of samples treated with Silo 111 contact angle is much smaller than  $90^\circ$ , which suggests that the sample surfaces are hydrophilic. The exact values of the measured contact angles are presented in the appendix 2.



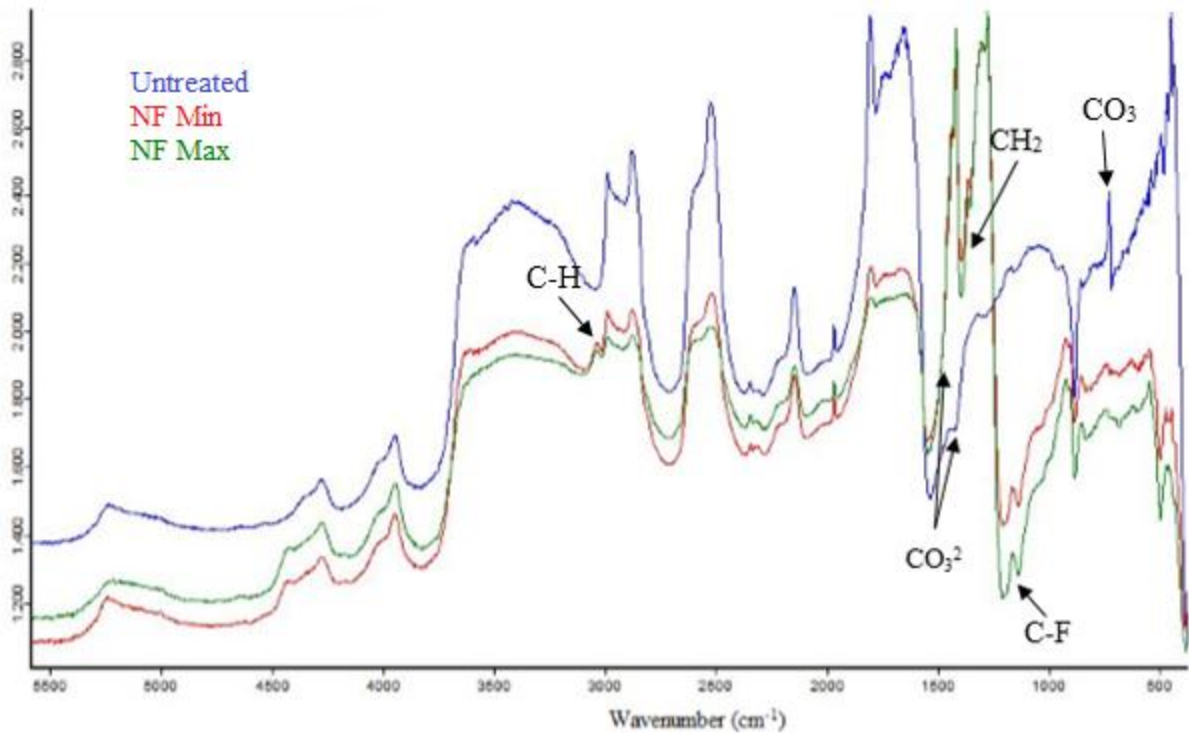
**Fig. 33.** Contact angle values of Noto stone samples

#### v. Total Reflectance FT-IR

Spectra of untreated Noto stone samples were taken as a reference and overlaid to the spectra acquired on samples treated with the three products, in order to see if there can be highlighted changes related to the application of the polymer.

#### FLUOLINE HY

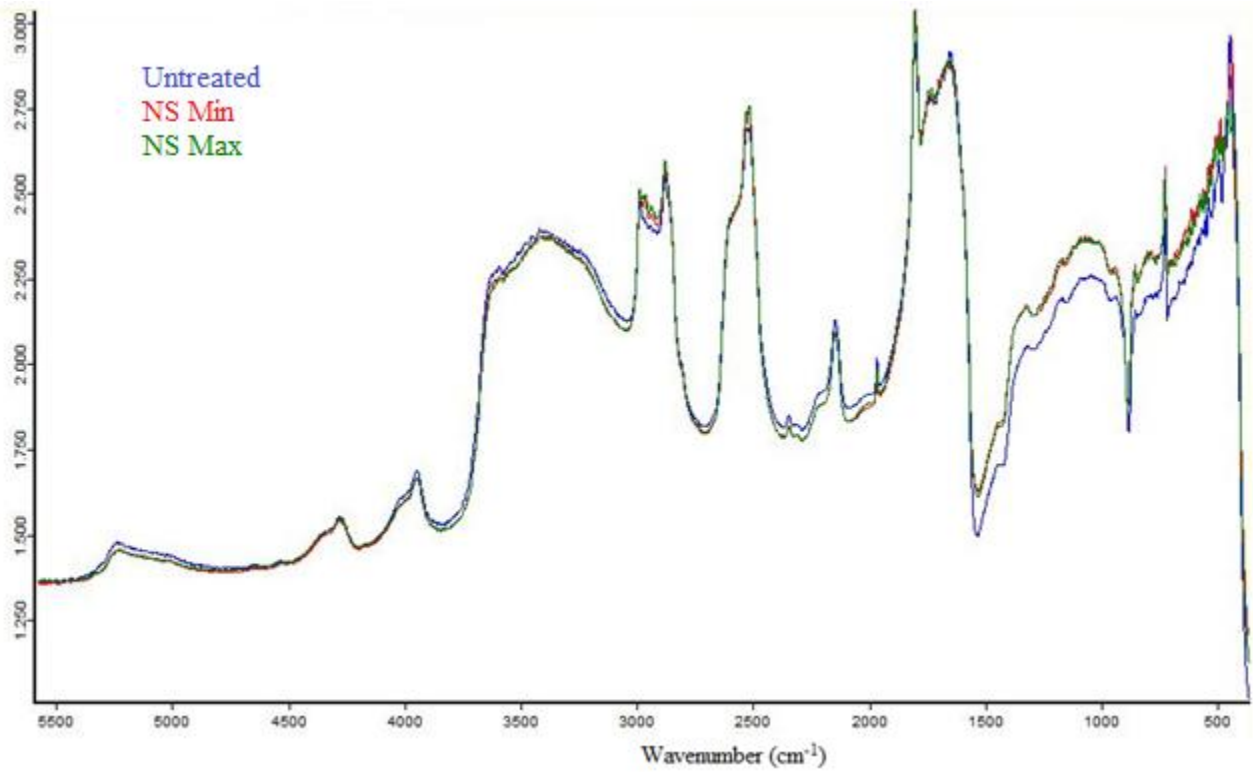




**Fig. 34.** Reflectance spectra of Noto stone samples treated with Fluoline HY

A significant difference between treated and untreated samples occur at around  $1400\text{ cm}^{-1}$ , where is found the characteristic inverted calcite band. In treated samples, this band cannot be observed anymore, since it is covered by the presence of the more intense  $\text{CH}_2$  wagging vibrations at  $1400\text{ cm}^{-1}$  of Fluoline HY active component. [54]. Another difference due to the presence of the polymer can be noticed at  $1383\text{ cm}^{-1}$  and  $3000\text{ cm}^{-1}$ . In fact, those two peaks are present only in treated samples, together with significant changes at the range of  $1222\text{ cm}^{-1}$  and  $1082\text{ cm}^{-1}$  which could be attributed to the C-F stretching vibration of the polymer, which is observed at  $1208\text{ cm}^{-1}$  in the pure film of polymer. The carbonate peak at  $750\text{ cm}^{-1}$  disappears after the treatment.

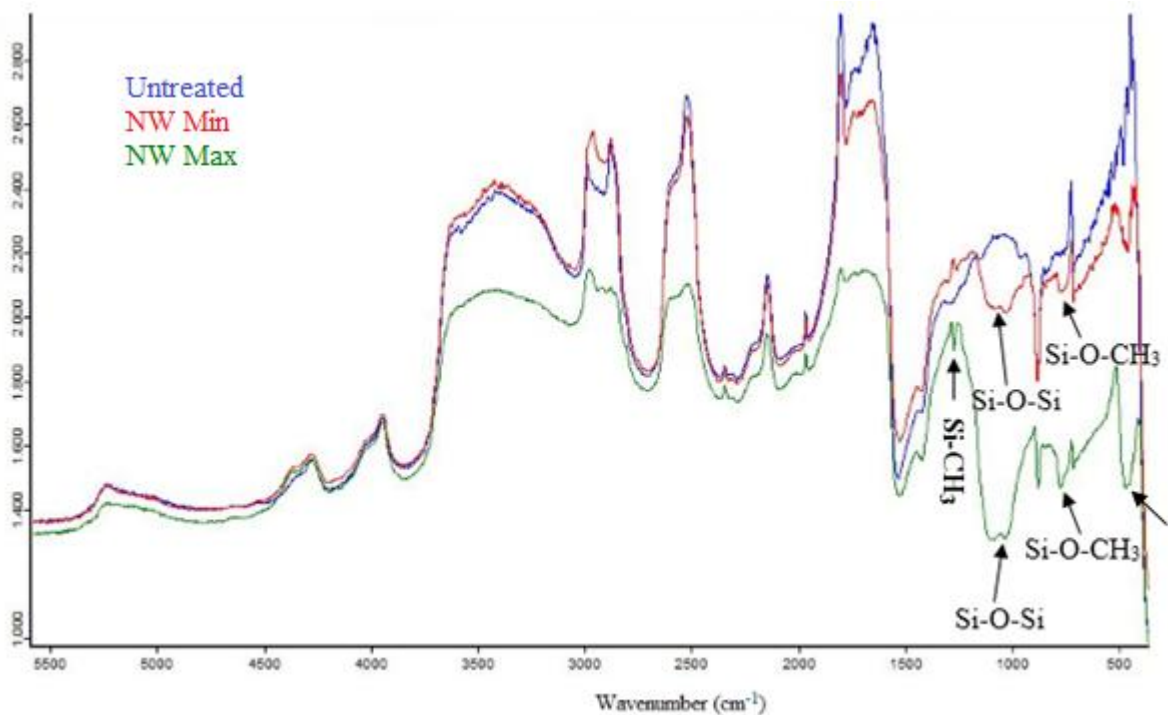
**SILO 111**



**Fig. 35.** Reflectance spectra of Noto stone samples treated with Silo 111

From the comparison of the reflectance spectra of Silo 111 treated Noto stone samples and the reference one (*Fig. 35*), no significant changes were noticed.

## WACKER 290

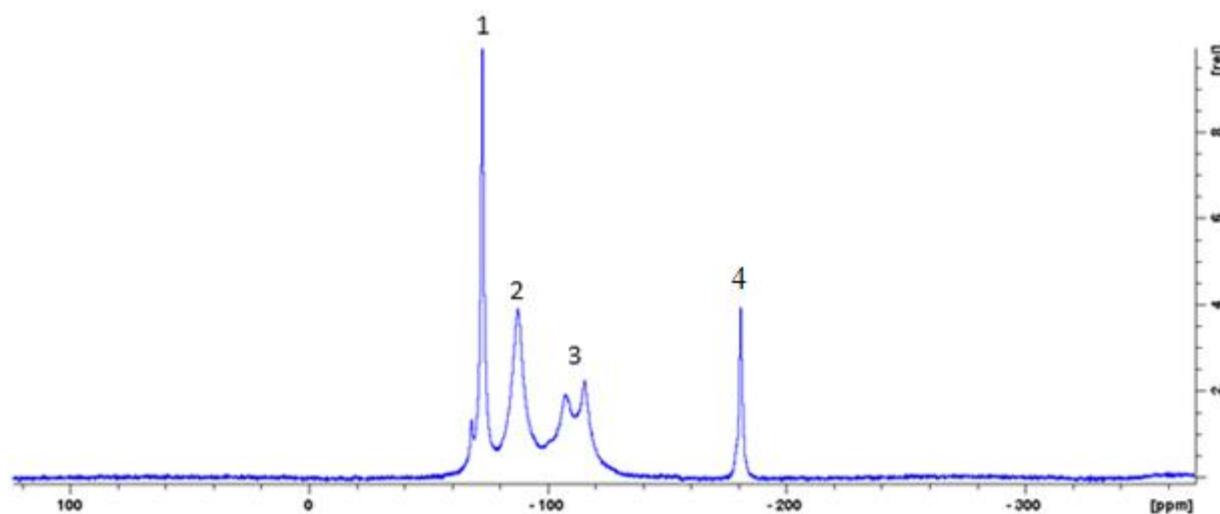


**Fig. 36.** Reflectance spectra of Noto stone samples treated with Wacker 290

The two spectra registered on the samples treated with Wacker 290 show more differences in the fingerprint zone, under  $1500\text{ cm}^{-1}$ , for the great part in the intensity of the peaks observed. Observed changes could be attributed to the different presence of polymer on samples surface, which is more substantial in the NW max sample (*Fig. 34*). Comparing these two spectra with the one of the polymer itself, we can notice how most of the peaks due to the polymer are present, apart from the bending peaks of C-C bonds in the  $1500\text{-}1280\text{ cm}^{-1}$  with the  $1274\text{-}1242\text{ cm}^{-1}$  could correspond to Si-CH<sub>3</sub> vibrations, at  $1104\text{-}1108\text{ cm}^{-1}$  - to Si-O-Si and at  $764\text{-}775\text{ cm}^{-1}$  - to Si-O-CH<sub>3</sub> vibrations. The peak at  $455\text{ cm}^{-1}$  appears in the spectra of treated samples and can be attributed to the presence of product.

#### vi. ss-NMR

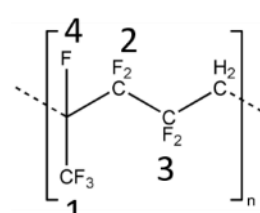
Solid-state  $^{19}\text{F}$  NMR spectrum was obtained on Noto stone sample (NF Max) treated with maximum amount of Fluoline HY (*Fig. 37*). The spectrum was acquired at the rate of 20 kHz. The assigned chemical shifts are presented in table 9.



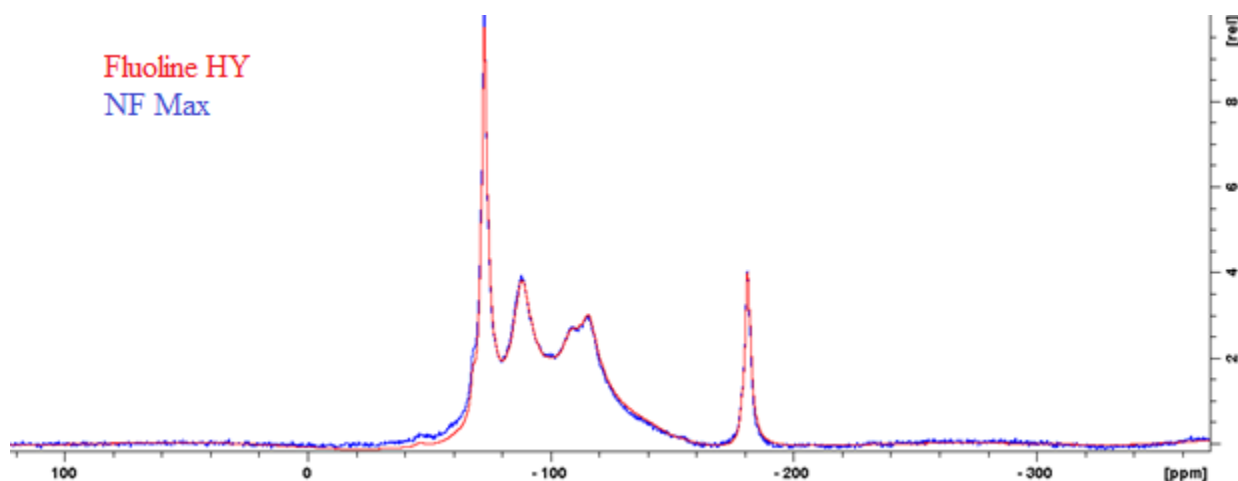
**Fig. 37.** Solid-state  $^{19}\text{F}$  NMR spectrum of Noto stone sample treated with Fluoline HY.

**Table 9.** Chemical shifts of  $^{19}\text{F}$  NMR spectrum of Noto stone sample treated with Fluoline HY

Peak number	Chemical shift (ppm)	Nucleus
1	-68.3	$\text{CF}_3$
2	-72.7	$\text{CF}_2$
3	-107.3	$\text{CF}_2$
4	-181	$\text{CF}$



The obtained spectrum of the sample NF Max was overlaid with the spectrum of Fluoline HY as a reference in order to detect changes which could occur due to the treatment (*Fig. 38*).



**Fig. 38.** Solid-state  $^{19}\text{F}$  NMR spectra of Fluoline HY and Noto stone sample treated with the product

As it could be seen, the spectrum of treated stone sample is identical to the one of Fluoline HY film which suggests that no interactions occurred between product and the substrate. This hypothesis was checked taking into account the relaxation times of  $^{19}\text{F}$  atom of the product and the treated sample (Table 10).

**Table 10.** Relaxation times of  $^{19}\text{F}$  Fluoline HY and NF Max

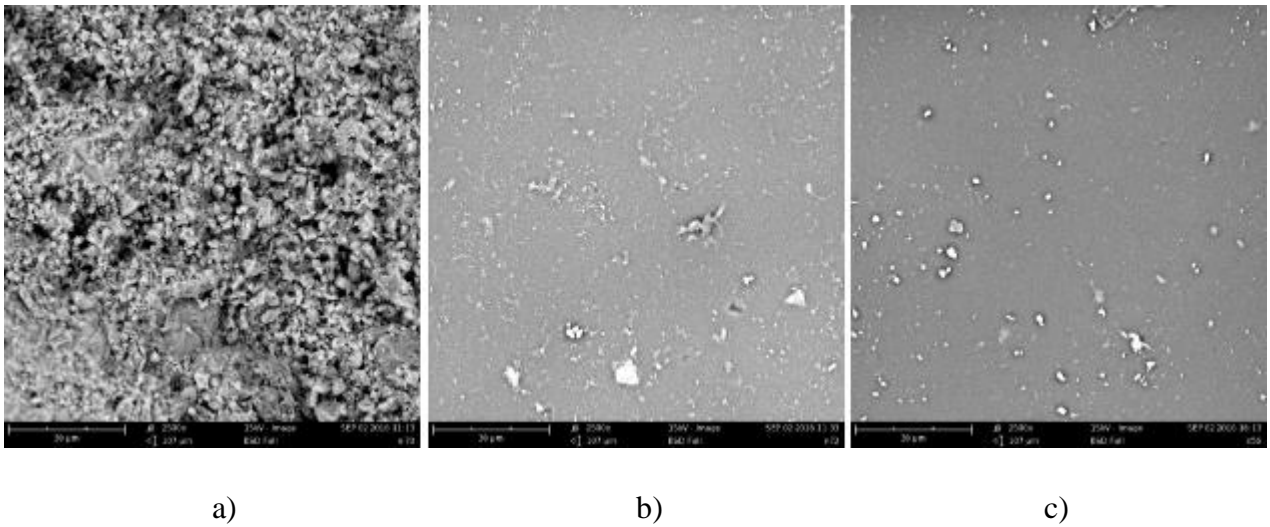
<b>T<sub>1</sub>(F), [s]</b>				
	<b>1</b>	<b>2</b>	<b>3</b>	<b>4</b>
Fluoline HY	$0.657 \pm 0.019$	$0.624 \pm 0.019$	$0.583 \pm 0.017$	$0.619 \pm 0.019$
NF Max	$0.830 \pm 0.025$	$0.670 \pm 0.020$	$0.589 \pm 0.018$	$0.740 \pm 0.022$
<b>T<sub>2</sub>(F), [ms]</b>				
	<b>1</b>	<b>2</b>	<b>3</b>	<b>4</b>
Fluoline HY	$84.9 \pm 2.5$	$35.9 \pm 1.1$	$30.7 \pm 0.9$	$161.9 \pm 4.9$
NF Max	$67.7 \pm 2.0$	$33.5 \pm 1.0$	$27.2 \pm 0.8$	$121.6 \pm 3.6$

#### vii. SEM-EDX

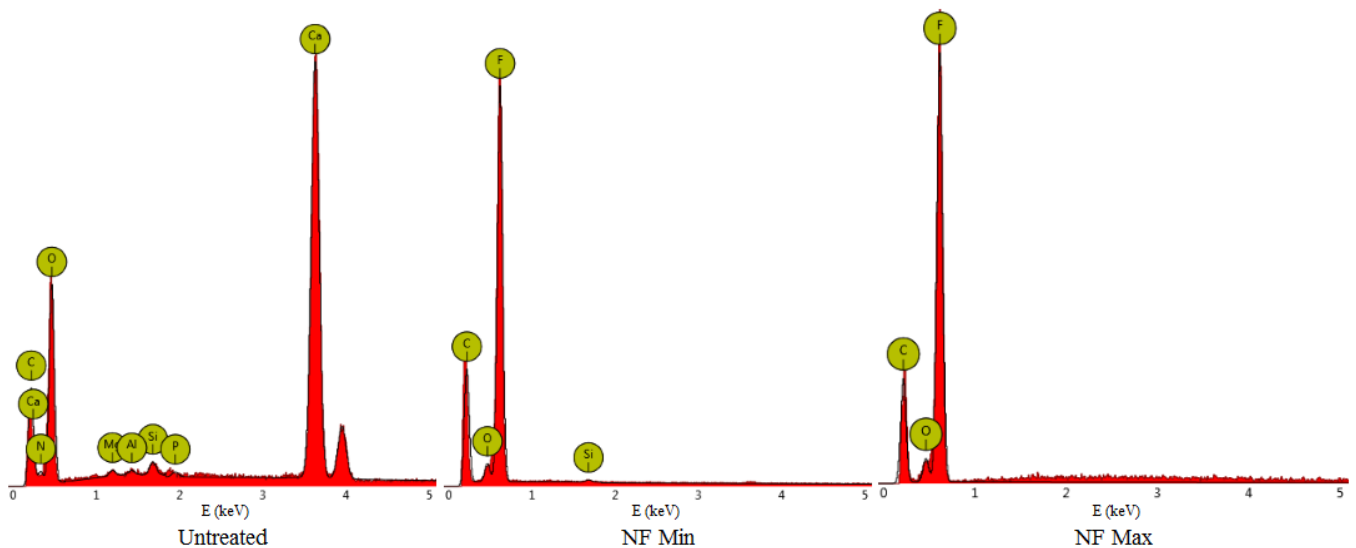
##### *FLUOLINE HY*

Noto stone samples, treated with protective polymeric dispersions were analysed by SEM-EDX in order to get an information about an influence of the treatment on surface morphology and elemental composition of the sample. Obtained results were compared to the untreated sample.

Samples NF Min and NF Max were treated with minimum and maximum amount of Fluoline HY, respectively. Surface morphology of treated samples was compared to untreated one (Fig. 38). Observing the surface of untreated stone sample, grains of different size are clearly visible as well as porosity of the stone, while the surface of treated samples represents completely different situation where grains and pores of the stone are heavily coated with polymer, showing clear film formation on the surface. It is visible that smoother film has formed after the application of maximum amount of product which results in more significant coverage of stone's texture.



**Fig. 38.** SEM image of Noto stone samples (magnification x2500): a) untreated, b) NF Min, c) NF Max.

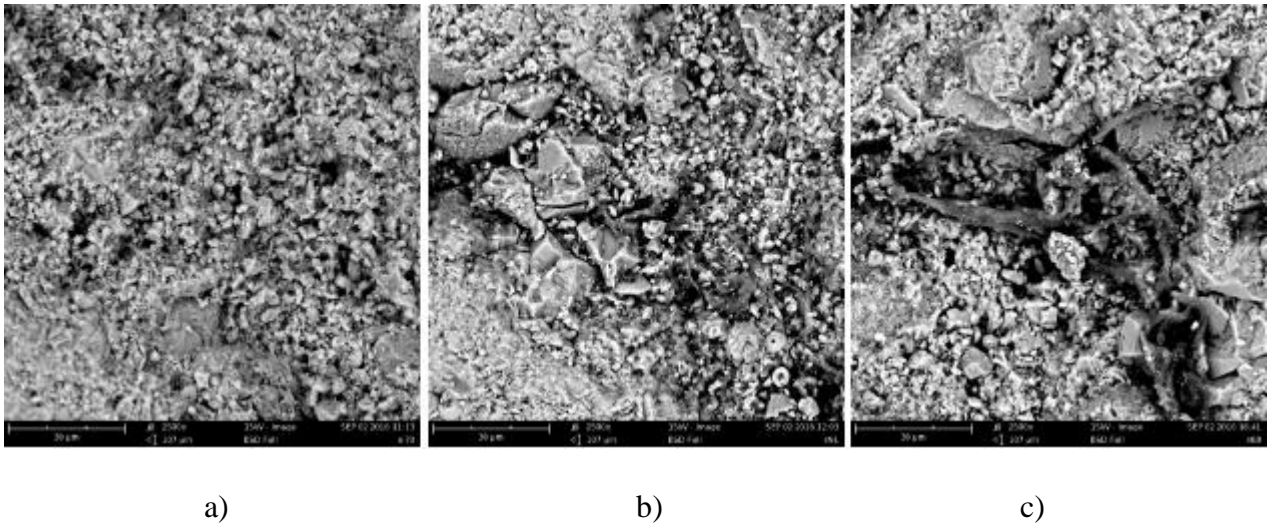


**Fig. 39.** SEM-EDX spectra of Noto stone samples: untreated, NF Min and NF Max

In figure 39 the elemental composition of samples treated with Fluoline HY comparing to untreated sample could be seen. The appearance of fluorine on treated samples, could be stated as a marker of polymer presence. Another change worth mentioning is a disappearance of calcium peak which correlates with surface morphology studies (*Fig. 38*) which proves film formation and a complete coverage of samples' surface.

SILO 111

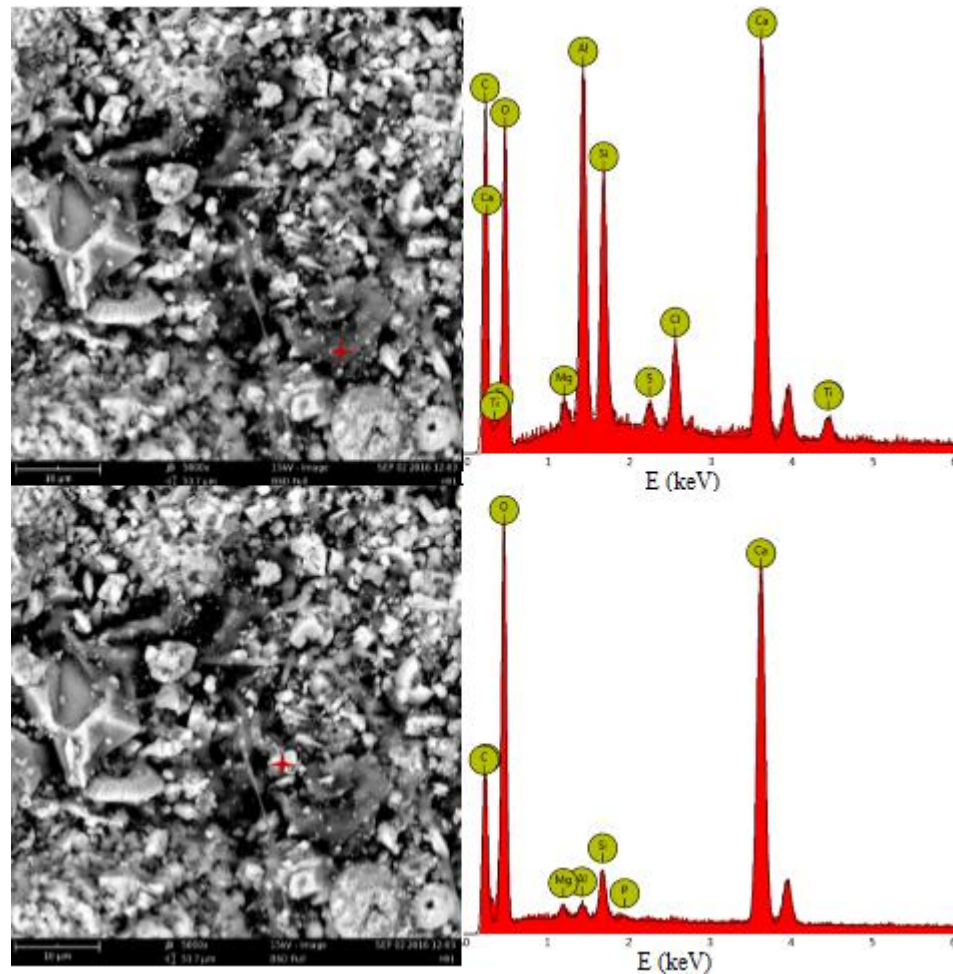
SEM images of samples NS Min and NS Max are presented in figure 39. It is visible that surface morphology of treated samples remains similar to the untreated one, showing no presence of film formation. However, polymer on the surface can be detected after the treatment, concentrated in some points around the grains with minimum amount of product (*Fig. 40. b*), and maximum amount of product (*Fig. 40. c*), where polymer is visible from the dark grey colour and is situated in the cavities of the stone and around capillary walls.



**Fig. 40.** SEM image of Noto stone samples (magnification x2500): a) untreated, b) NS Min, c) NS Max.

Elemental analysis was done on treated samples and it revealed some additional information about the chemical composition of the sample.

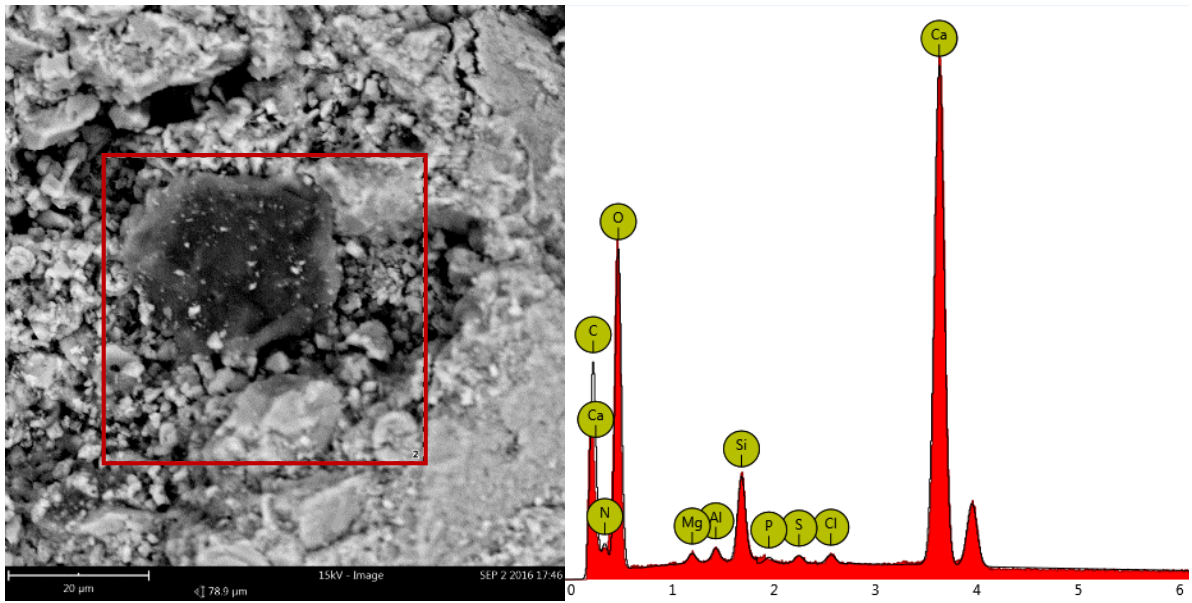
Sample NS Min was analysed with SEM-EDX in two different spots (*Fig. 41*) which showed different appearance in the image, where grey spot refers to polymer area and a bright spot – to sample grain. In the area where the presence of polymer is expected, such elements: C, O, Ca, Ti, Mg, Al, Si, S, Cl and Ti are present, while the spot analysis on a sample grain showed significantly less intensive peak of Si which could be considered as a marker element in order to prove the presence of polymer on the sample's surface.



**Fig. 41.** Spot analysis of sample NS Min with SEM-EDX

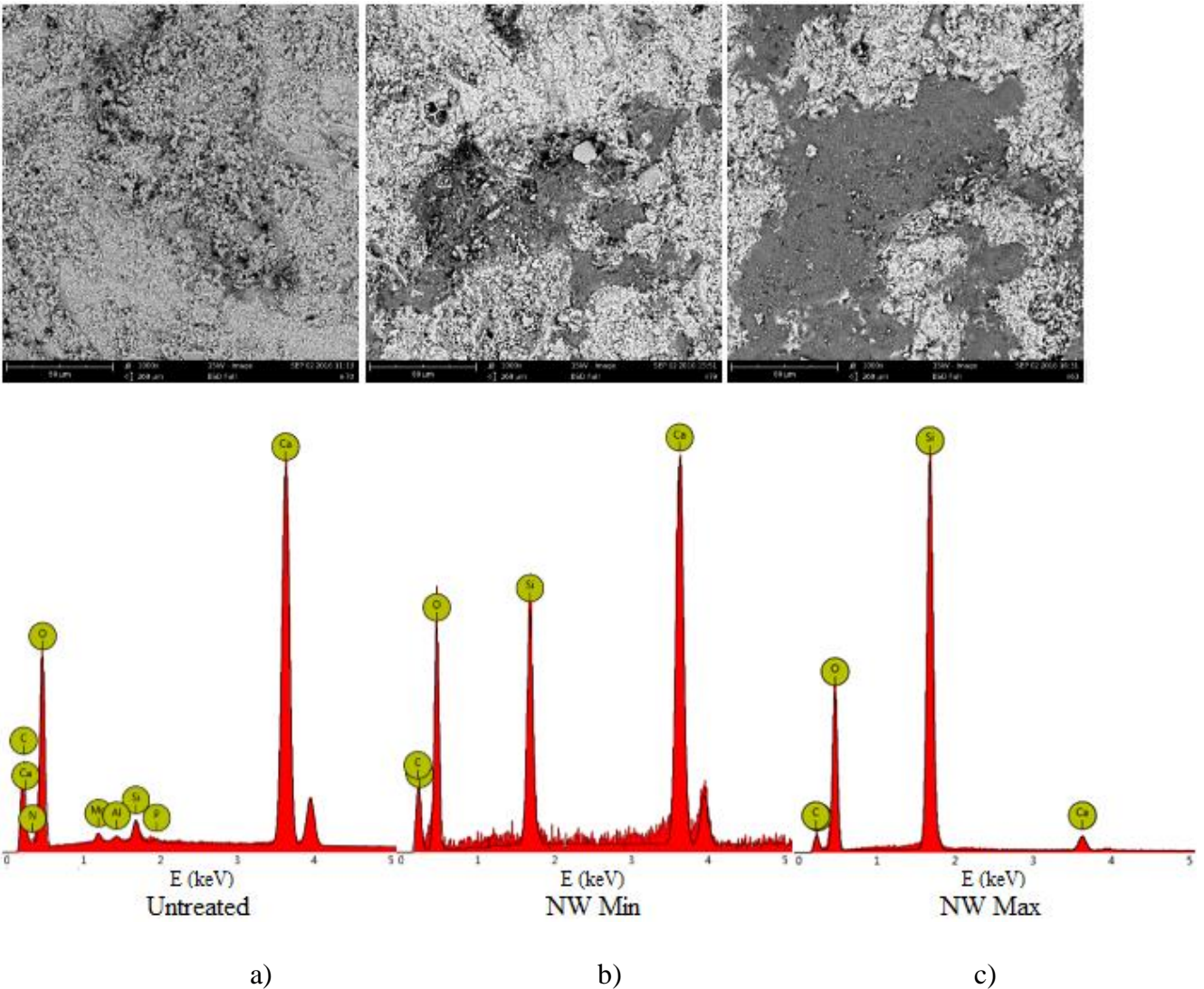
The elemental analysis of the sample NS Max allows to better distinguish chemical differences between different morphological appearance having parts of the surface. The mapping was done in order to see the distribution of detected elements (*Fig. 42*). It could be seen that all elements assigned in figure 41 are present in the spectrum of sample NS Max. The main difference, which should be taken into account is the intensity of Si peak which is lower than in the spectrum on polymer area and higher that in the one obtained on the stone grain. Which could be a valid proof that the distribution of the polymer on the sample's surface is not homogenous.





**Fig. 42.** The spectrum of sample NS Max with SEM-EDX.

Minimum and maximum amount of Wacker 290 protective polymeric dispersion was applied on Noto stone samples NW Min and NW Max, respectively. Surface morphology of treated samples was compared to the untreated sample (*Fig. 43*).



**Fig. 43.** SEM image and elemental analysis of Noto stone samples (magnification x1000): a) untreated, b) NW Min, c) NW Max.

From SEM images the different polymer distribution pattern is visible comparing b) and c) images of figure 43. The wider area of the sample's surface is covered with polymer in the case of maximum amount of product applied, which also results in the reduction of surface roughness. The differences related to the application of the product could be noticed in SEM-EDX spectra as well. It could be seen, that peaks of low concentration elements such as Mg, Al and P disappear due to the presence of the polymer, while Si peak significantly increases after the treatment with minimum and especially with the maximum amount of product, which allows to select silicon as a marker for the presence of Wacker 290 on the sample.

b. Comiso stone

i. Colorimetry

The chromatic alterations of the surface of Comiso stone samples were evaluated comparing L\*, a\* and b\* colorimetric parameters before and after the application of protective polymeric dispersions.

**Table 11.** L\*, a\*, b\* parameters of Comiso stone samples before and after the treatment

Sample name	L* (b. t.)	L* (a. t.)	a* (b. t.)	a* (a. t.)	b* (b. t.)	b* (a. t.)
CF Min	84.79 ± 1.08	79.21 ± 1.08	1.4 ± 0.49	2.36 ± 0.67	13.82 ± 0.7	19.15 ± 1.13
CF Max	81.69 ± 1.29	79.58 ± 1.78	1.7 ± 0.65	2.39 ± 0.6	14.74 ± 1.04	18.91 ± 1.3
CS Min	82.24 ± 0.74	81.85 ± 1.47	1.61 ± 0.41	2.22 ± 0.85	14.68 ± 1.31	16.16 ± 1.51
CS Max	85.38 ± 1.25	82.69 ± 0.81	1.4 ± 0.39	1.09 ± 0.46	13.66 ± 0.86	14.32 ± 0.73
CW Min	84.74 ± 1.28	79.04 ± 0.89	1.7 ± 0.47	1.94 ± 0.71	14.17 ± 0.85	17.49 ± 1.3
CW Max	84.96 ± 1.03	78.16 ± 1.42	1.39 ± 0.39	2.56 ± 0.39	14.62 ± 0.66	19.8 ± 0.92

Table 11 represents a significant decrease in values of lightness coordinate L\* among the samples before and after the treatment in all tested cases, except sample CS Min which exhibits very slight change. Different behaviour could be noticed in red/green coordinate a\*. Samples treated with Fluoline HY and minimum amount of Silo 111 showed significant increase in a\* value, while no significant changes were noticed when Wacker 290 was used. Only the sample treated with maximum amount of Silo 111 exhibited a decrease in a\* parameter. Values of yellow/blue coordinate b\* increased after the treatment in all tested cases.

According to obtained data before and after the treatment,  $\Delta L^*$ ,  $\Delta a^*$ ,  $\Delta b^*$  values were calculated and used for the evaluation of  $\Delta E$  (Table 12).

**Table 12.** Total color difference ( $\Delta E$ ) values of Comiso stone samples

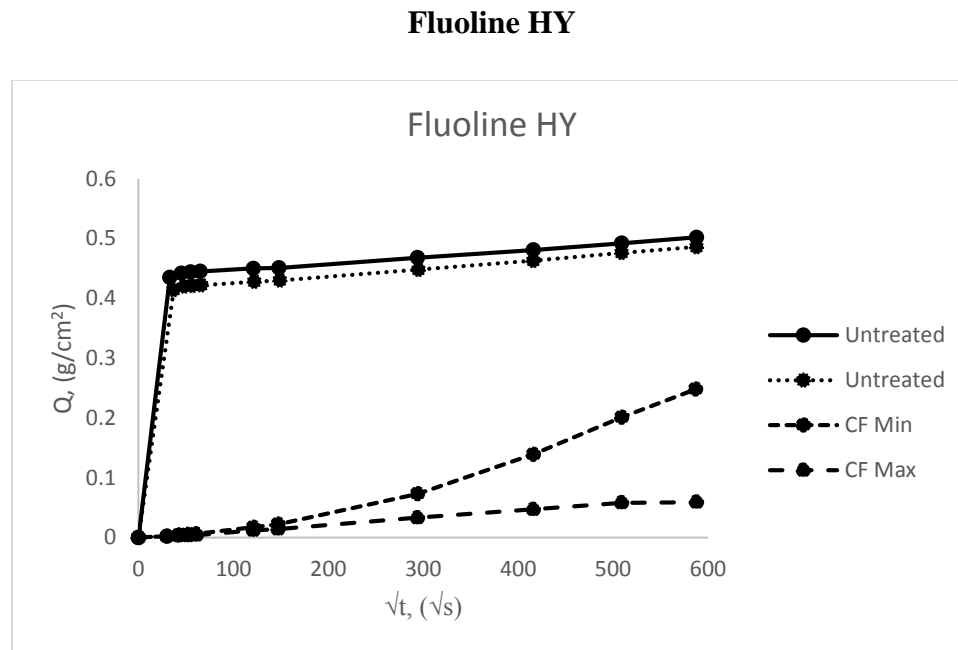
Sample name	$\Delta L^*$	$\Delta a^*$	$\Delta b^*$	$\Delta E$
CF Min	-5.58 ± 1.41	0.96 ± 0.77	5.33 ± 1.63	7.86 ± 1.96
CF Max	-2.11 ± 2.00	0.7 ± 0.7	4.17 ± 1.39	4.95 ± 1.99
CS Min	-0.39 ± 1.68	0.61 ± 0.79	1.48 ± 1.49	2.38 ± 1.54
CS Max	-2.69 ± 1.55	-0.34 ± 0.47	0.66 ± 0.81	2.99 ± 1.39
CW Min	-5.7 ± 1.55	0.24 ± 0.94	3.33 ± 1.45	6.71 ± 1.95

CW Max	$-6.8 \pm 1.87$	$1.18 \pm 0.35$	$5.19 \pm 0.54$	$8.71 \pm 1.54$
--------	-----------------	-----------------	-----------------	-----------------

As it could be seen from table 12, only Fluoline HY, when the maximum amount is used, and Silo 111 gives acceptable  $\Delta E$  values, while the biggest  $\Delta E$  value was obtained after the application of maximum amount of Wacker 290.

ii. Liquid water absorption

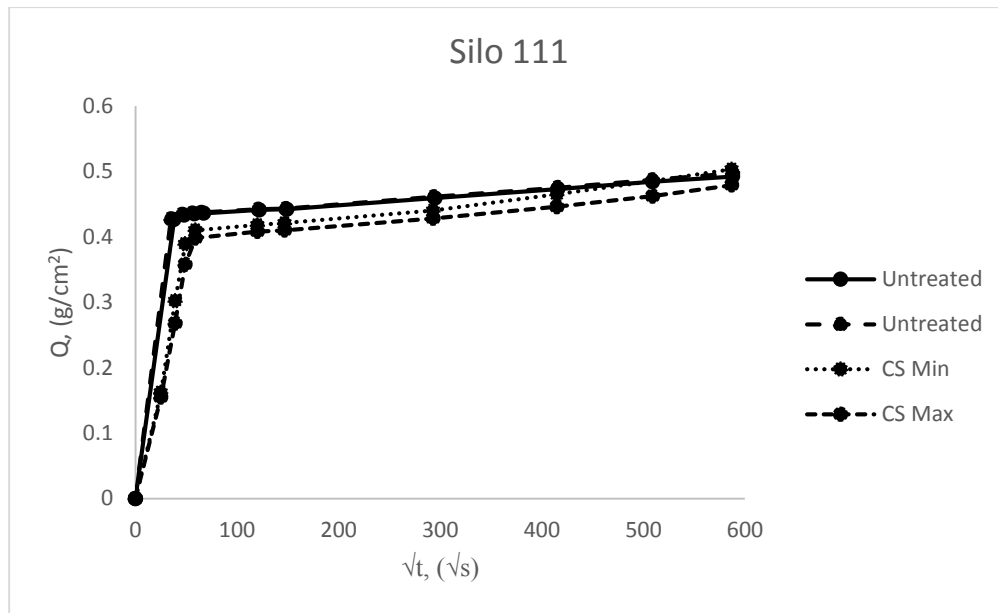
Liquid water absorption by capillarity test was performed on 6 Comiso stone samples of the size 5x5x2 cm before and after the treatment with protective polymeric dispersions.



**Fig. 44.** Liquid water absorption by capillarity as a function of square root of time of Comiso stone samples treated with Fluoline HY

Liquid water absorption after the treatment was reduced significantly comparing with untreated stone samples. When  $t^{1/2}$  is  $587 \text{ s}^{1/2}$ , the amount of water absorbed is  $0.502 \text{ g/cm}^2$  and  $0.486 \text{ g/cm}^2$  of untreated samples,  $0.248 \text{ g/cm}^2$  using minimum amount and  $0.059 \text{ g/cm}^2$  using maximum amount of product. The difference in amount of absorbed liquid water among samples treated with minimum and maximum amount of product started to be significant when  $t^{1/2}$  reached  $150 \text{ s}^{1/2}$ .

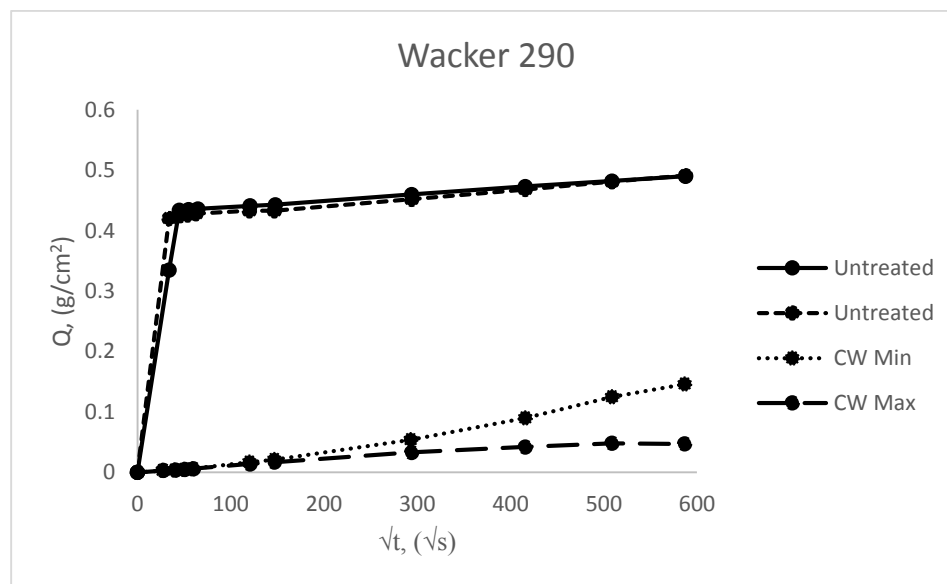
**Silo 111**



**Fig. 45.** Water absorption by capillarity as a function of square root of time of Comiso stone samples treated with Silo111

Significant changes in amount of absorbed water were not noticed when Silo 111 was used. At  $587 \text{ s}^{1/2}$  for untreated sample  $Q$  was  $\sim 0.500$ . After the treatment –  $0.503 \text{ g/cm}^2$  when the minimum amount was used and  $0.479 \text{ g/cm}^2$  when the maximum amount of product was used.

### Wacker 290



**Fig. 46.** Water absorption by capillarity as a function of square root of time of Comiso stone samples treated with Wacker 290

Significant reduction in amount of water absorbed per unit area was observed. Before the treatment, when  $t^{1/2} = 587 \text{ s}^{1/2}$ ,  $Q = 0.491 \text{ g/cm}^2$ . After the treatment, when minimum amount of product was used,  $Q = 0.146 \text{ g/cm}^2$ , in case of maximum amount  $Q = 0.047 \text{ g/cm}^2$ .

iii. Water vapour permeability

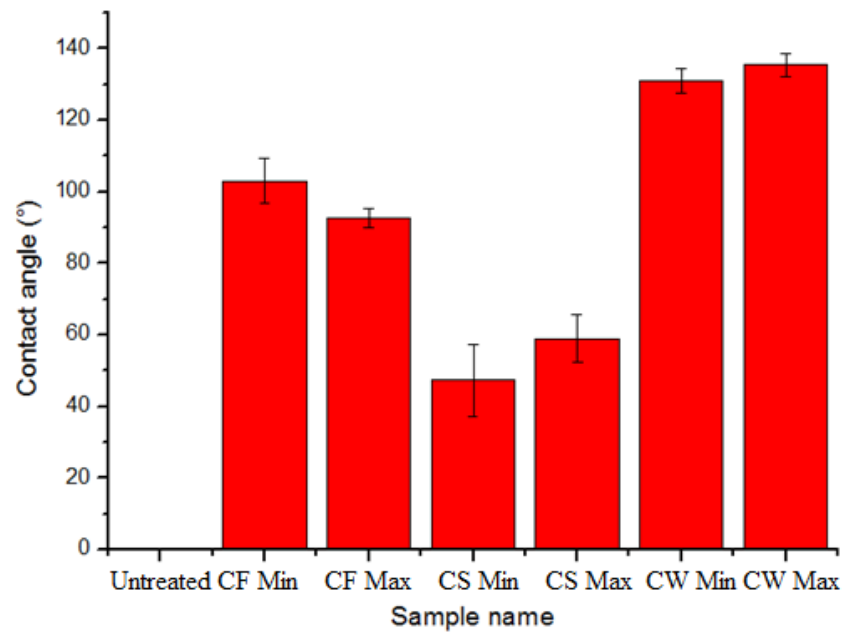
From the results presented in table 13 it could be stated that water vapour permeability was reduced after the treatment with Fluoline HY and Silo 111, while samples treated with Wacker 290 did not exhibit any significant impact. The highest reduction occurred when samples were treated with maximum amount of Fluoline HY, although treatment with minimum amount caused only 6.15 % decrease. The reduction of water vapour permeability after the application of Silo 111 did not depend on the amount of product.

**Table 13.** Water vapour permeability values of Comiso stone samples

<b>Sample name</b>	<b>Water vapor permeability <math>\delta_p</math> (<math>10^{-13} \text{ kg/(m*s*Pa)}</math>)</b>	<b>Water vapor permeability (%)</b>
Untreated	2.73	100
CF Min	2.55	93.45
CF Max	1.36	49.89
CS Min	2.27	76.60
CS Max	2.04	74.76
CW Min	3.20	100.00
CW Max	2.72	99.77

iv. Static contact angle

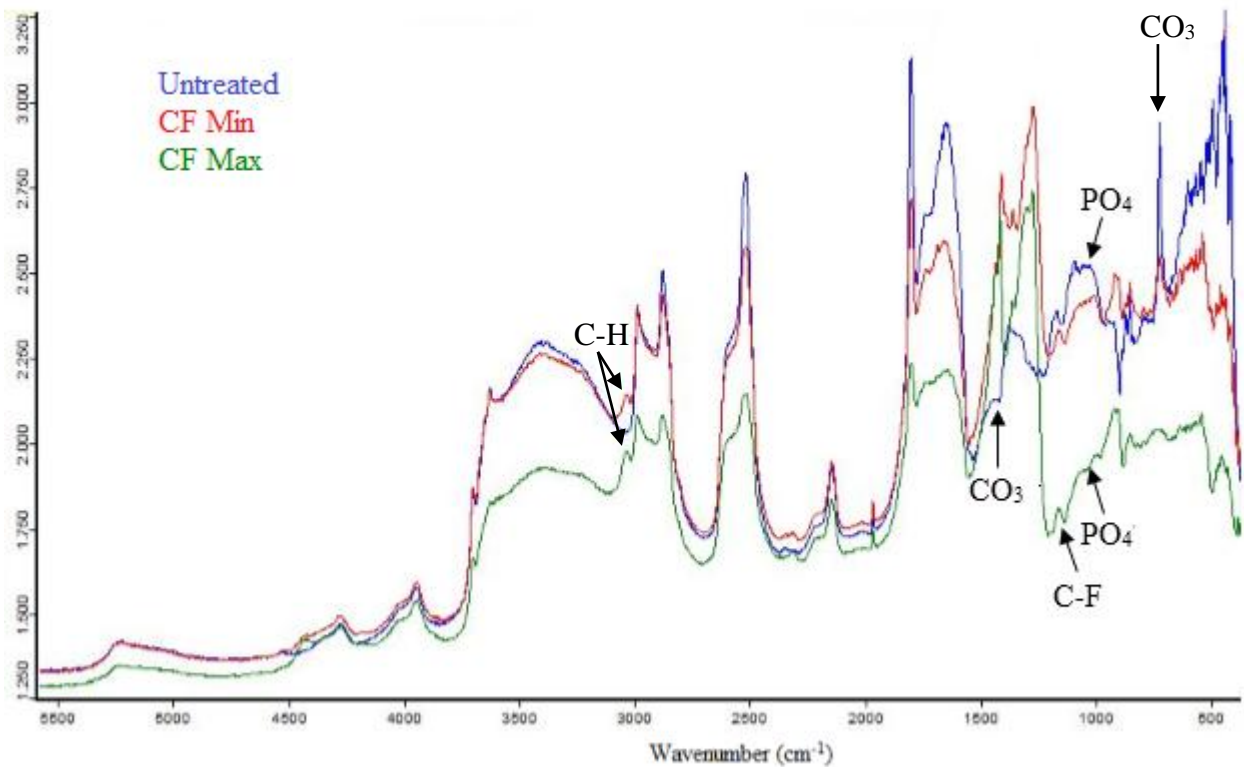
Contact angle values of Comiso stone samples are presented in figure 47. On untreated stone sample the water drop was completely absorbed before 10 seconds, so it was measured a contact angle of  $0^\circ$ . Obtained values exceeded  $90^\circ$  after the usage of Fluoline HY and Wacker.



**Fig. 47.** Contact angle values of Comiso stone samples

v. Total Reflectance FT-IR

**FLUOLINE HY**

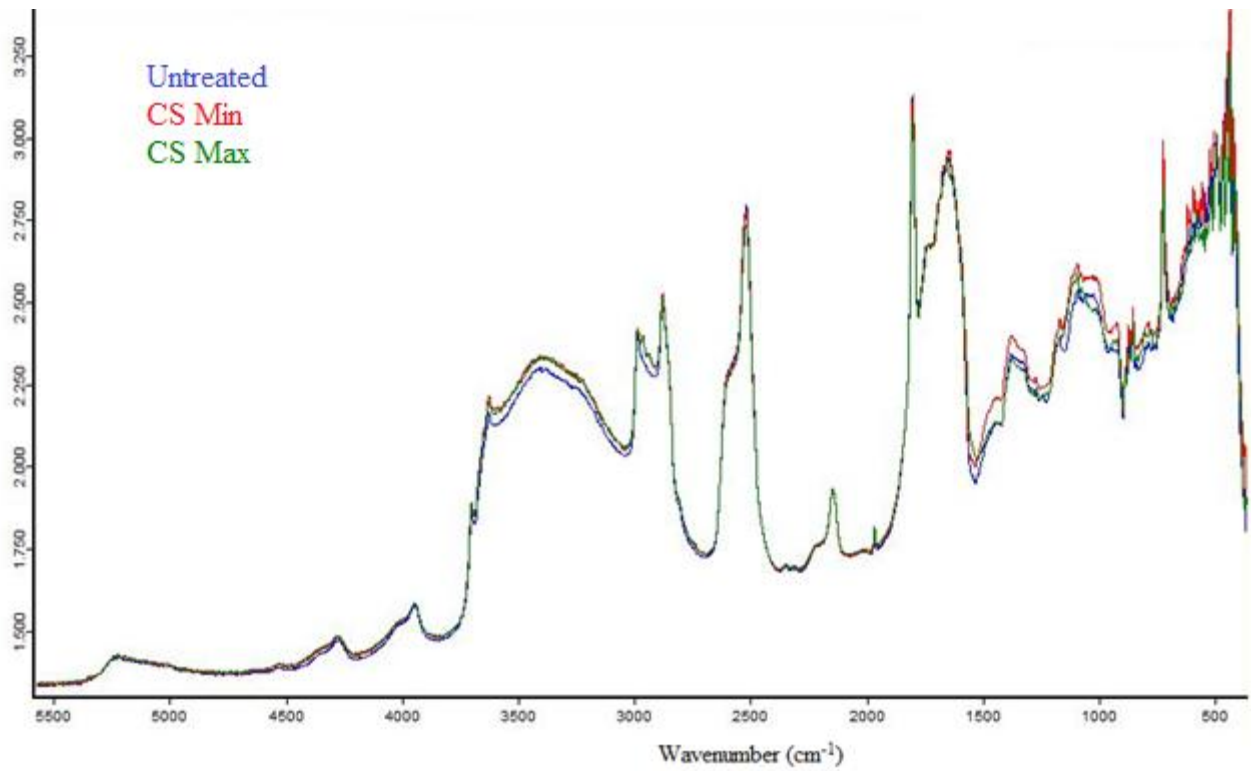


**Fig. 48.** Reflectance spectra of Comiso stone samples treated with Fluoline HY

Comparing the reflectance FT-IR spectra of untreated Comiso stone sample with the ones treated with Fluoline HY, some changes could be observed, such as characteristic calcite band at around  $1400\text{ cm}^{-1}$ , the shape of which became smoother and broader after the treatment. More pronounced differences in spectra could be noticed after the treatment with maximum amount of the product, where more pronounced differences could be observed at the range of  $1207\text{--}1109\text{ cm}^{-1}$  corresponding to C-F stretching vibration (*Fig. 48*).

**SILO 111**

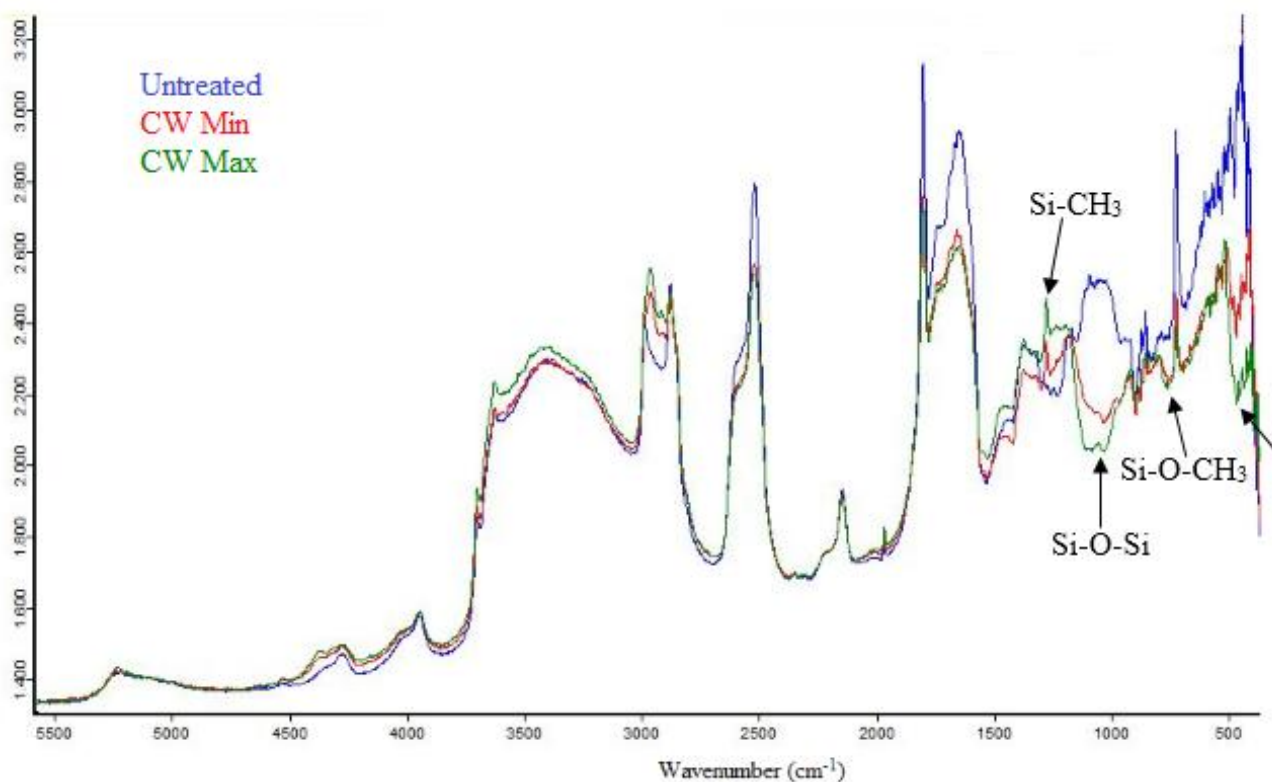




**Fig. 49.** Reflectance spectra of Comiso stone samples treated with Silo 111

The reflectance spectrum of untreated stone sample was compared to the ones treated with Silo 111. No significant changes were observed.

## WACKER 290

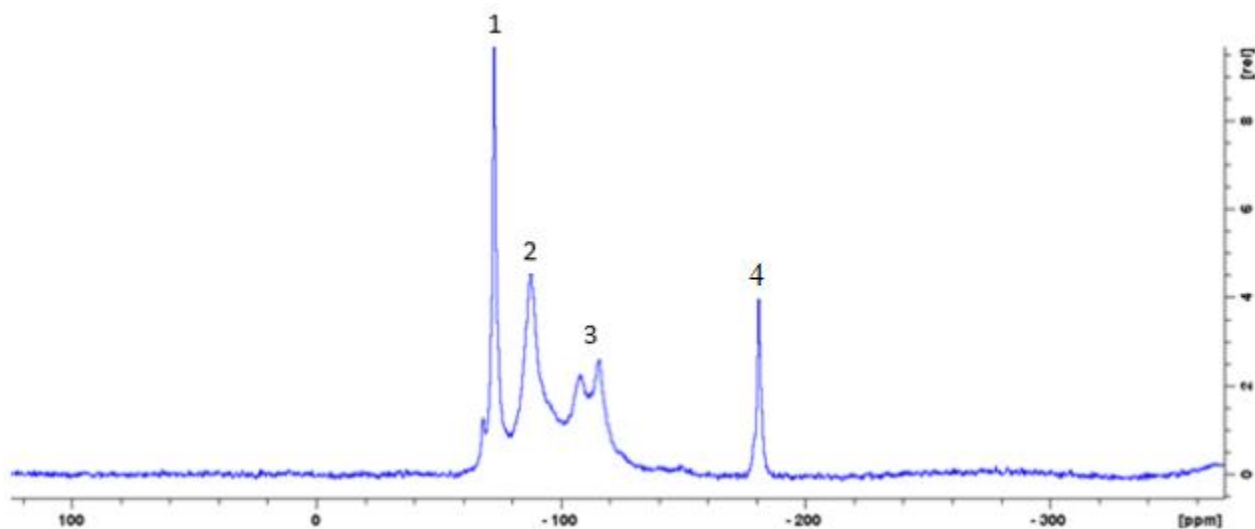


**Fig. 50.** Reflectance spectra of Comiso stone samples treated with Wacker 290

FT-IR reflectance spectrum of untreated Comiso stone sample was overlaid with spectra of samples treated with Wacker 290. Observed changes could be related to the presence of polymer on samples surface, such as differences at a range of 1104-1107  $\text{cm}^{-1}$  and at 749  $\text{cm}^{-1}$  which could be assigned to Si-O-Si and Si-O-CH<sub>3</sub> vibrations respectively. The signal at 455  $\text{cm}^{-1}$  appears after the treatment with both amounts of the product and can be attributed to the presence of polymer on the surface.

#### vi. ss-NMR

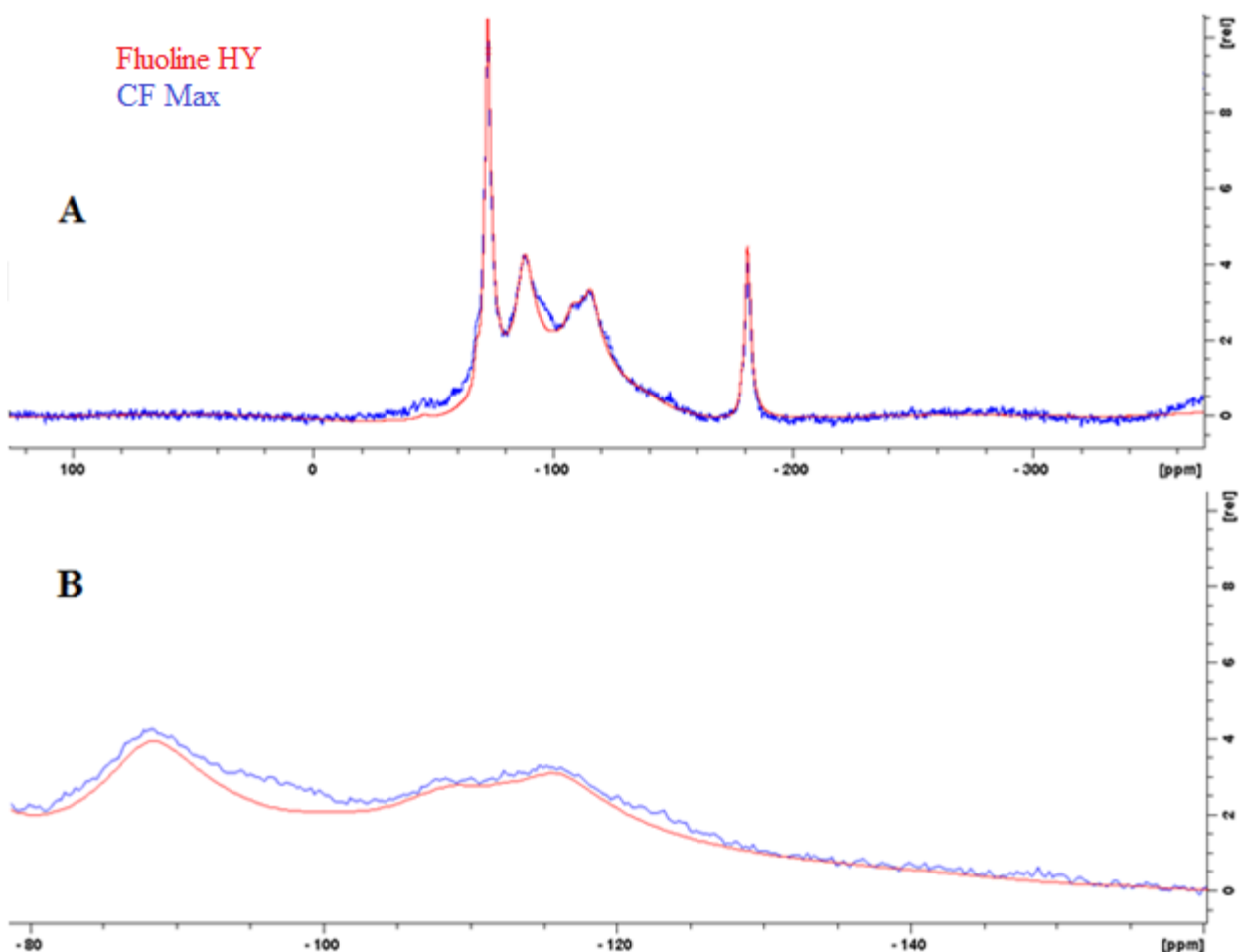
Solid-state DP <sup>19</sup>F NMR MAS spectrum was obtained on Comiso stone sample (CF Max) treated with maximum amount of Fluoline HY (*Fig. 51*) at the rate of 20 kHz. Acquired spectrum was overlaid with the reference spectrum of Fluoline HY (*Fig. 52*).



**Fig. 51.** Solid-state  $^{19}\text{F}$  NMR spectrum of Comiso stone sample treated with Fluoline HY

**Table 14.** Chemical shifts of  $^{19}\text{F}$  NMR spectrum of Comiso stone sample treated with Fluoline HY

Peak number	Chemical shift (ppm)	Nucleus
1	-68.3	$\text{CF}_3$
	-72.7	
2	-87.6	$\text{CF}_2$
3	-107.8	$\text{CF}_2$
	-115.4	
4	-181	$\text{CF}$



**Fig. 52.** Solid-state  $^{19}\text{F}$  NMR spectra of Fluoline HY and Comiso stone sample treated with the product: A - overlapped spectra, B – emphasized areas of distinctive areas

Spectra of Fluoline HY and Comiso stone sample treated with Fluoline HY were overlapped in order to see possible changes due to the treatment (*Fig. 52. A*). Broadening of the spectrum of treated sample could be observed in  $\text{CF}_2$  zone (range from -85 to -118 ppm), new interactions could be seen, possibly due to formation of covalent bonds between C atoms of the polymer and P atoms of carbonate hydroxyapatite [63], which is collaborated by the increase in relaxation times  $T_1$  and  $T_2$  in a  $\text{CF}_2$  zone (peak 2 and 3) comparing to pure polymer (*Table 15*) which suggests the movement reduction of  $\text{CF}_2$  nucleus due to newly formed interactions.

**Table 15.** Relaxation times of  $^{19}\text{F}$  Fluoline HY and CF Max

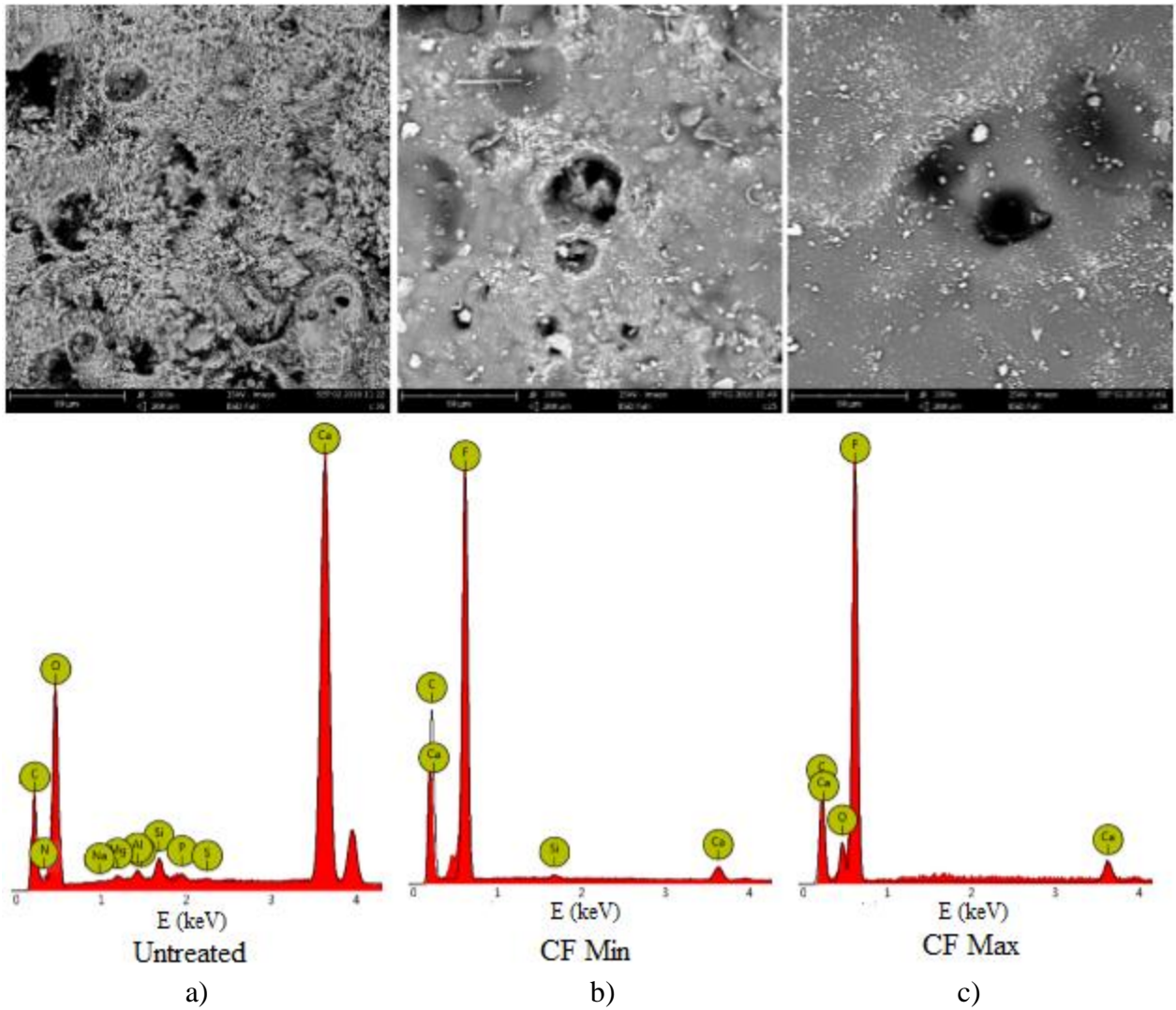
$T_{1F}$ (s)				
	1	2	3	4

Fluoline HY	$0.657 \pm 0.019$	$0.624 \pm 0.019$	$0.583 \pm 0.017$	$0.619 \pm 0.019$
CF Max	$0.693 \pm 0.020$	$0.700 \pm 0.021$	$0.674 \pm 0.020$	$0.562 \pm 0.017$
<b>T<sub>2</sub>F (ms)</b>				
	<b>1</b>	<b>2</b>	<b>3</b>	<b>4</b>
Fluoline HY	$84.9 \pm 2.5$	$35.9 \pm 1.1$	$30.7 \pm 0.9$	$161.9 \pm 4.9$
CF Max	$84.4 \pm 2.5$	$42.3 \pm 1.3$	$40.9 \pm 1.2$	$118.3 \pm 3.5$

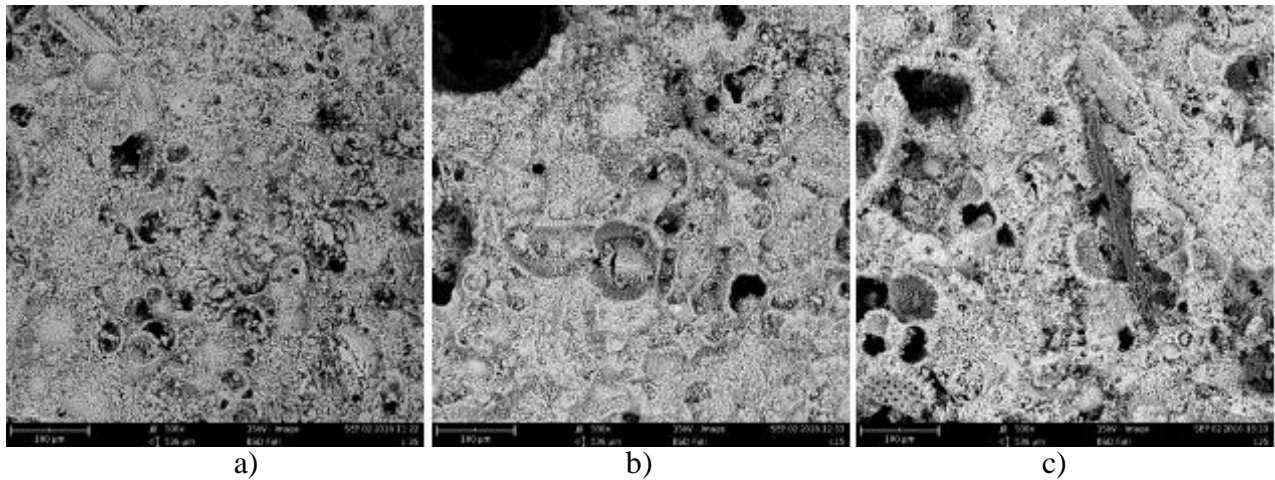
#### vii. SEM-EDX

SEM-EDX measurements were performed on treated Comiso stone samples and changes in the surface morphology and elemental composition were observed.

After the application of Fluoline HY, significant differences could be noticed on the stone surface compared to the untreated sample, such as reduced surface roughness (*Fig. 53*). In the SEM image of CF Min sample, part of the porosity is covered with polymer together with stone grains which still could be distinguished, while the sample treated with maximum amount of product presents different behaviour. Surface texture of the sample CF Max is no longer evident and porous system is filled with polymer. Due to the homogeneous grey colour, it can be stated that Fluoline HY forms a film on the sample's surface. Elemental analysis with SEM-EDX was performed on treated samples with both amounts of the product. It is significant that after the treatment, peaks of minor elements, such as Na, Mg, Al, P, S disappear using both amounts of product, while silicon peak – after the treatment with maximum amount. Appearance of intensive F peak after the treatment are a proof of polymer presence on the surface.

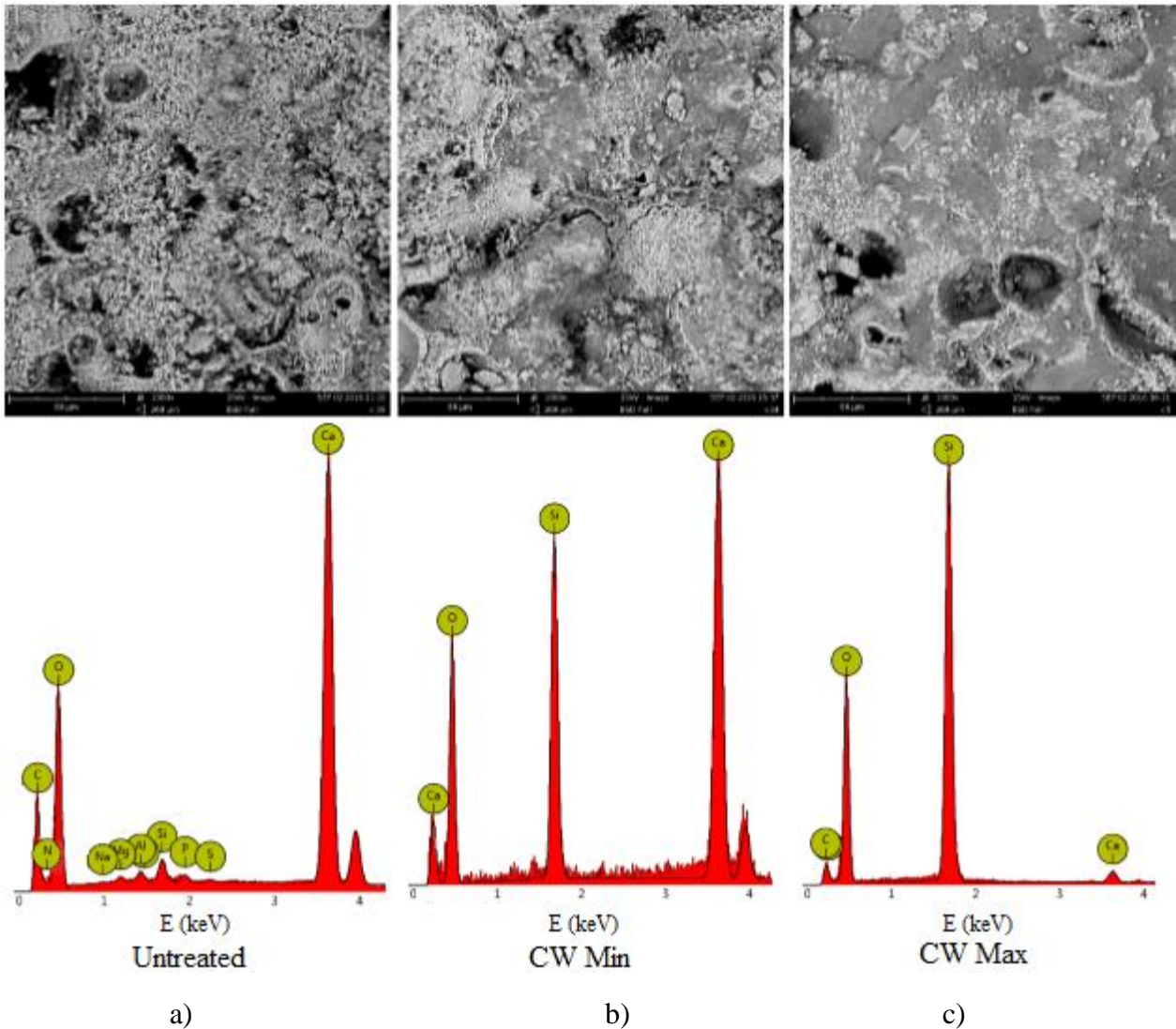


**Fig. 53.** SEM image of Comiso stone samples (magnification x1000): a) untreated, b) CF Min, c) CF Max.



**Fig. 54.** SEM image of Comiso stone samples (magnification x500): a) untreated, b) CS Min, c) CS Max.

Samples CS Min and CS Max were treated with Silo 111. From the SEM image (*Fig. 54*), no significant differences in surface morphology could be observed comparing to the untreated sample. Surface roughness is not reduced and the stone grains are easily distinguishable together with surface porosity.



**Fig. 55.** SEM image of Comiso stone samples (magnification x1000): a) untreated, b) CW Min, c) CW Max.

After the treatment with Wacker 290, some differences in surface morphology and chemical composition could be observed comparing to the untreated Comiso stone sample. In the case of sample CW Min, surface roughness reduction is visible in the grey areas due to the presence of polymer. Along the borders of the grains, polymer layer is cracked and not homogeneously dispersed on the surface. Elemental analysis with SEM-EDX reveals the disappearance of low intensity peaks, such as ones of Na, Mg, Al, P, S and significant increase in the intensity of Si peak. Slightly different situation could be observed after the treatment with maximum amount of Wacker 290. Surface roughness is more



evidently reduced, the distribution of the polymer is more homogeneous than in the previous case, the EDX spectrum presents well pronounced silicon peak which proves the presence of the polymer on stone's surface.

## VII. Samples treated till rejection with Silo 111

Liquid water absorption and static contact angle measurements revealed that Noto and Comiso stone samples treated with Silo 111 did not show any development of hydrophobicity on the surface. According to the technical sheets provided by the supplier, the product is suitable for the protection of natural stone based on carbonate or silicate. XRD analysis results fulfil this requirement as both selected stone types are mainly composed of calcite. The unsuitable amounts of the applied products could be stated as a hypothesis about not satisfying hydrophobic effect. For this reason, Noto and Comiso stone samples were treated with Silo 111 until rejection and colorimetry, liquid water absorption and static contact angle measurements were performed.

### a. Colorimetry

Colorimetric measurements were done on samples C37 and N65, which were coded as CS Rej and NS Rej respectively, before and after the treatment and the values of measured chromatic parameters  $L^*$ ,  $a^*$ ,  $b^*$  and calculated  $\Delta E$  values were compared.

The decrease of  $L^*$  (Table 16) after the treatment until rejection was observed in both stone samples. It states the presence of surface darkening. The red/green coordinate  $a^*$  values increased in both cases after the treatment, however this phenomenon is more noticeable for Comiso stone sample. The change in yellow/blue coordinate  $b^*$  displays similar behaviour to  $a^*$  coordinate but the difference between Comiso and Noto stone samples is not as well defined as in the previous case.

**Table 16.**  $L^*$ ,  $a^*$ ,  $b^*$  parameters of NS Rej. and CS Rej. samples before and after the treatment

Sample name	$L^*$ (b. t.)	$L^*$ (a. t.)	$a^*$ (b. t.)	$a^*$ (a. t.)	$b^*$ (b. t.)	$b^*$ (a. t.)
NS Rej.	$81.14 \pm 1.62$	$76.26 \pm 1.27$	$1.7 \pm 0.31$	$2.61 \pm 0.53$	$10.65 \pm 0.5$	$13.08 \pm 0.97$
CS Rej.	$85.14 \pm 1.26$	$79.12 \pm 1.35$	$1.21 \pm 0.35$	$2.94 \pm 0.64$	$13.45 \pm 0.84$	$17.27 \pm 1.37$

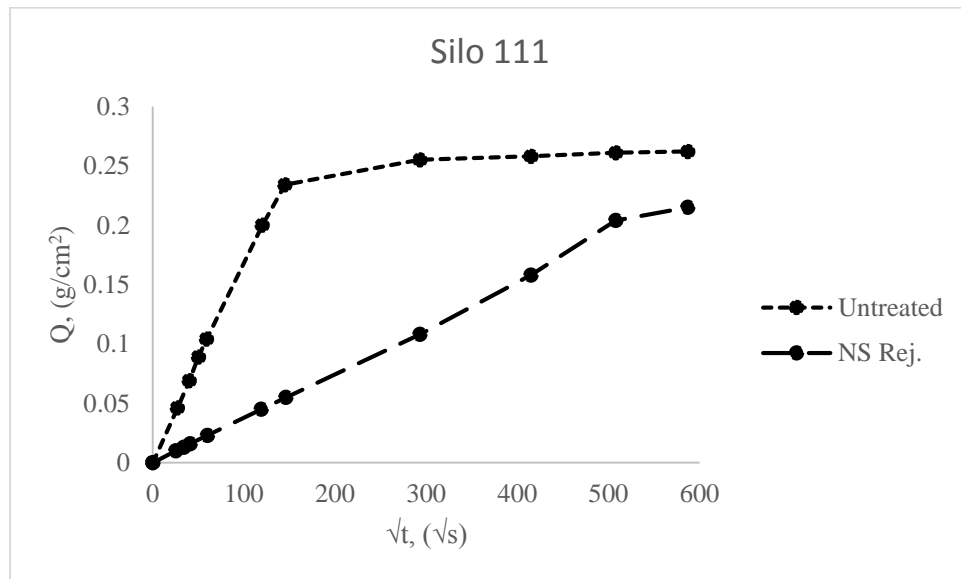
The total colour difference  $\Delta E$  values were calculated and presented in the table 17. The difference between Noto and Comiso stone samples is quite significant, where  $\Delta E$  of Noto only slightly exceeds acceptable value ( $\Delta E \leq 5$ ), while Comiso shows big departure from the acceptable value.

**Table 17.** Total colour difference ( $\Delta E$ ) values of Noto and Comiso stone samples treated till rejection.

Sample name	$\Delta L^*$	$\Delta a^*$	$\Delta b^*$	$\Delta E$
NS Rej.	$-4.88 \pm 2.15$	$0.92 \pm 0.63$	$2.43 \pm 1.14$	$5.68 \pm 2.10$
CS Rej.	$-6.02 \pm 1.71$	$1.73 \pm 0.64$	$3.82 \pm 1.43$	$7.39 \pm 2.10$

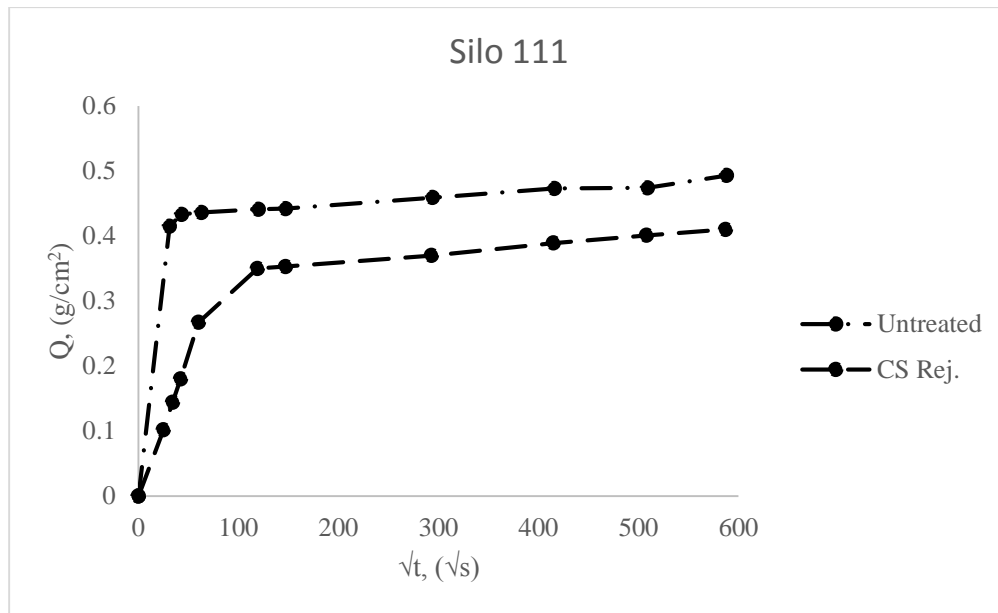
b. Liquid water absorption

Liquid water absorption measurement was performed on samples before and after the treatment following the same methodology as in the section III.d. Results were compared in the form of graphs where amount of absorbed water per surface area plotted versus square root of time.



**Fig 56.** Water absorption by capillarity as a function of square root of time of Noto stone sample treated with Silo 111 till rejection.

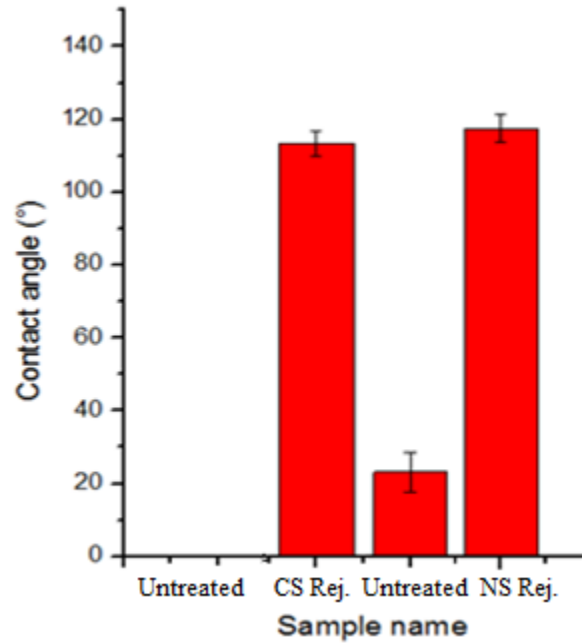
Figure 56 shows significant reduction in the amount of absorbed liquid water per surface area, although the linear increase could be observed until  $t^{1/2} = 500 \text{ s}^{1/2}$ . At the end of the experiment for the untreated sample  $Q = 0.262 \text{ g/cm}^2$ , while for treated  $Q = 0.215$ .



**Fig 57.** Water absorption by capillarity as a function of square root of time of Comiso stone sample treated with Silo 111 till rejection.

Liquid water absorption measurements realized on Comiso stone sample (*Fig. 57.*) show a decrease when sample was treated till rejection. The increase of the amount of absorbed liquid water became stable when  $t^{1/2} = 119 \text{ s}^{1/2}$ . At the end of the experiment for the untreated sample  $Q = 0.493 \text{ g/cm}^2$ , for the sample treated till rejection  $Q = 0.41 \text{ g/cm}^2$ .

c. Contact angle



**Fig 58.** Contact angle values of Noto and Comiso stone samples treated with Silo 111 till rejection. Contact angle values (*Fig. 58.*) show the big increase comparing to untreated samples. For both Noto and Comiso stone samples, contact angle values after the treatment significantly exceeded  $90^\circ$ , which describes the tested surface as hydrophobic.

## VIII. Discussion

Petrographic characterization revealed that both Noto and Comiso stones are biocalcarenes containing bioclastic inclusions, which explains the presence of C-H bonds in FT-IR reflectance spectra of untreated stone samples. According to XRD analysis results it could be stated that both analysed stones are composed mainly of calcite ( $\text{CaCO}_3$ ) with quartz ( $\text{SiO}_2$ ) as a minor phase, however, Comiso stone also contains carbonate hydroxyapatite as a minor phase which is absent in Noto stone.

*Noto stone.* From the obtained values of measured colorimetric parameters of untreated samples, a variability could be noticed among the same group of samples, which shows a colour inhomogeneity within the same stone type. Chromaticity differences could be seen both in red/green coordinate ( $a^*$ ) values and in yellow/blue coordinate ( $b^*$ ) values while lightness coordinate ( $L^*$ ) remains relatively the same among all tested untreated samples.

On the other hand, comparing the same colorimetric parameters after the treatment, more significant differences could be observed. Lightness coordinate  $L^*$  increased for samples treated with Fluoline HY. As it was pointed out in a sample preparation section (V.), shininess and film formation were visible with a naked eye after the treatment: and the increase of the lightness coordinate proves this statement.  $L^*$  remains the same for samples treated with minimum and maximum amounts of Silo 111 and it could be related to small  $\Delta E$  value for both samples which proves that the product did not cause unacceptable chromatic alterations on the stone surface. The decrease of  $L^*$  was observed on samples treated with Wacker. It confirms the darkening of the surface which was visible with a naked eye after the treatment.

The total colour difference  $\Delta E$  results show that the acceptable values by European normative were achieved when minimum and maximum amounts of Silo 111 were used. The highest  $\Delta E$  was noticed in case of Fluoline HY maximum amount.  $\Delta E$  value was just slightly exceeding 5 when minimum amount of Fluoline HY was used. After the treatment with Wacker 290 total colour difference was higher than accepted value. It is important to note that using both amounts, caused chromatic alterations on the stone surface were similar – around 8, which shows that changes in chromatic parameters are not significantly dependent on the amount of applied product.

From liquid water absorption results, when Fluoline HY was used as a protective substance, amount of absorbed liquid water decreased significantly showing the same behaviour with both amounts of

product. Contact angle measurements have also confirmed that Noto stone sample's surface became hydrophobic after the treatment. Despite this, water vapour permeability test revealed that porosity was reduced after the treatment with both amounts, more specifically, in the case of maximum amount, the reduction of permeability was around 27 % higher than minimum amount while liquid water absorption curves remained similar. Obtained results could propose the hypothesis of the film formation on the surface, which was confirmed by surface morphology studies with SEM, where in the case of both treated samples with Fluoline HY, the reduction in surface roughness and porosity was clearly visible. The presence of the polymer was also proven with reflectance FT-IR technique, presenting new peaks which appeared in the spectra after the treatment and are characteristic to fluorinated polymers, such as C-F, CH<sub>2</sub> and C-H. Solid-state <sup>19</sup>F NMR analysis showed no changes in the spectrum and relaxation times after the treatment comparing to the untreated sample, which proves that no interactions and formation of new chemical bonds occur.

According to liquid water absorption curves, after the treatment with Silo 111, the surface properties in terms of hydrophobicity remained similar to untreated samples. The fact that surface remained hydrophilic was further confirmed by static contact angle measurement, when the obtained values did not exceed 90 °. It brought about the idea that the product was not present on the surface of the sample but confined inside the samples, result confirmed by water vapour permeability results. In fact, when minimum amount of Silo 111 was used for the treatment, water vapour permeability was equal to 66.75 %, while in the case of maximum amount – only 32.39 %, which leads to think that porosity of samples is actually reduced by the product. SEM imaging technique showed that the polymer is concentrated in cavities of the stone sample and around the walls of capillaries, reducing pore diameter. This phenomena explains the significant reduction in water vapour permeability and the reason of its invisibility in the reflectance FT-IR spectrum, due to low penetration in this type of material of infrared radiation used.

Liquid water absorption results of Wacker 290 show a situation very similar to the one with Fluoline HY. After the treatment with both minimum and maximum amounts, the significant decrease in amount of absorbed water could be noticed, moreover expressing similar behaviour. The surface hydrophobicity has been proven by contact angle values as well. Water vapour permeability results show that when minimum amount was used, the percentage of water vapour permeability reduction is significantly lower than in case of Fluoline HY and Silo 111. Surface morphology analysis with SEM shows inhomogeneous distribution of the polymer, where bigger surface area is covered with a product in the

case of maximum amount applied. The presence of the polymer on the sample's surface was also confirmed by EDX analysis, presenting well pronounced silicon peaks which could be attributed to the silica-based polymer. Characteristic groups to this kind of material such as Si-O-Si, Si-CH<sub>3</sub>, Si-O-CH<sub>3</sub> were also observed in reflectance FT-IR spectra.

*Comiso stone.* From obtained colorimetry results, it could be seen that measured parameters vary among untreated samples, revealing colour inhomogeneity within the same stone type. Comparing the obtained values, some differences could be observed before and after the treatment. The decrease in lightness coordinate L\* can be noticed in all tested samples after the treatment. The lowest difference was calculated when minimum amount of Silo 111 was used, which supports the previous observation. Total colour difference  $\Delta E$  was not bigger than acceptable value using both amounts of Silo 111.

Significant decrease in L\* parameter was observed after the usage of Wacker 290 and Fluoline HY minimum amount, confirming the surface darkening visible with a naked eye. It is important to note, that L\* parameter decreased significantly less after the treatment with maximum amount of Fluoline HY than with minimum, while in both cases darkening was visible with a naked eye. This phenomenon could be explained by the fact that film formation and shininess was noticed on the surface of sample treated with maximum amount, while these effects were absent utilising minimum amount. Total colour difference  $\Delta E$ , in this case did not exceed the accepted value, despite the shininess observed due to the presence of polymer, while the opposite result was observed in the case of minimum amount where no shininess and film formation was noticed.

After the treatment with Wacker 290, darkening of the stone surface was confirmed also by  $\Delta E$  value, which after the application of maximum amount of product was the biggest comparing to other products used on Comiso stone.

Liquid water absorption measurement showed well expressed differences between treated and untreated stone samples when Fluoline HY was used. The amount of absorbed water decreased significantly after application of the product, although showing slightly better result after the application of maximum amount of product. The fact that surface became hydrophobic was confirmed by static contact angle measurement since obtained values exceeded 90° in both cases. Although, water vapour permeability measurement showed a significant difference in terms of porosity obstruction, when treatment with minimum amount closed the porous system less than 10 %, while in case of maximum amount it was



reduced twice than for untreated sample. SEM images could propose an explanation for this phenomena, showing the open porosity after the treatment with minimum amount of product, even though the surface roughness was significantly reduced and the presence of polymer on the surface was clearly visible and confirmed by EDX and reflectance FT-IR measurements. Drastic reduction of water vapour permeability of the sample treated with maximum amount of Fluoline HY can be explained with SEM images, where the polymer film on the surface is very well pronounced by significantly reduced stone surface roughness and porosity. Solid-state  $^{19}\text{F}$  NMR analysis showed the differences in the spectrum of sample treated with maximum amount of Fluoline HY comparing to the pure product spectrum. It could be hypothesized that covalent bond has formed among carbon of  $\text{CF}_2$  group of the polymer and phosphorus of carbonate-hydroxyapatite because it is the main difference between chemical composition of Comiso and Noto stones' samples, where the latter does not contain carbonate-hydroxyapatite crystals.

Different situation was observed when Silo 111 was used for the treatment, as no significant difference in amount of absorbed liquid water was noticed between treated and untreated samples. After the static contact angle measurement, obtained values did not exceed  $90^\circ$  proving the absence of surface hydrophobicity. As in the case of Noto stone, the proposed idea could be that the product is not on the surface but migrated deeper into stone capillaries. The reduction of water vapour permeability for around 25 % comparing to untreated samples could support this statement along with the absence of characteristic siloxanes' peaks in reflectance FT-IR spectra of treated samples. In addition to that, surface morphology analysis with SEM imaging confirms scarce distribution of the polymer on the surface.

After the treatment with Wacker 290, liquid water absorption was significantly reduced, revealing that slightly better result was achieved by using maximum amount of product. Obtained contact angle values were relatively the same, being much higher than  $90^\circ$ . This and significant reduction in absorbed liquid water confirms the development of hydrophobicity on the samples surface. Water vapour permeability measurement showed no closing of the stone porous system as in both cases it remained equal to the one of untreated sample. This statement was confirmed by SEM imaging, which showed the open stone's surface porosity even though the surface roughness was significantly reduced, making polymer presence evident.

*Treatment until rejection with Silo 111.* Noto and Comiso stone samples treated until rejection with Silo 111 expressed different results than with the amounts suggested by the supplier. After the treatment, darkening visible with a naked eye was noticed on both samples. Decrease in lightness coordinate was also observed, though it was not significant when both recommended amounts were used on Noto stone and minimum amount of product was applied on Comiso stone sample. Obtained  $\Delta E$  exceeded the acceptable value in both samples treated till rejection, which is opposite to the results obtained using recommended amounts.

From liquid water absorption measurements it could be seen that the amount of absorbed water was significantly reduced on Noto stone comparing to untreated sample, while on Comiso stone the reduction appeared as well but was not well defined. Performed static contact angle measurement revealed that both Noto and Comiso stone samples developed hydrophobicity on their surfaces as contact angle values exceeded  $90^\circ$ ; this was not observed after the usage of recommended amounts. These results lead to the idea that the increased amount of applied product caused formation of a polymeric network on the stone substrate, resulting in an appreciable hydrophobic coating. Obtained results could be taken as a legitimate reason to start a deeper testing of the best amount of product to apply on these particular stone types.

## IX. Conclusions

In this work the effectiveness of three commercial polymeric dispersions (Fluoline HY, Silo 111, Wacker 290) was evaluated on Noto and Comiso stone samples using different surface and bulk analysis techniques.

Untreated stone samples were characterized using optical microscopy, mercury intrusion porosimetry, XRD and XRF techniques. Noto stone appeared to be a low porosity biocalcarene classified as a wackestone and a biomicrite, while Comiso stone was described as porous biocalcarene, classified as a grainstone and biosparite. Both stones are composed of calcite as a major and quartz as a minor phase, in addition to that Comiso stone also contains a carbonate hydroxyapatite as a minor phase.

Liquid water absorption measurement was used to evaluate the effect of the product on the amount of absorbed liquid water. Fluoline HY and Wacker 290 significantly reduced samples' ability to absorb liquid water on both stone types while Silo 111 did not show any impact.

Chromatic alterations were evaluated according to calculated total colour difference  $\Delta E$  values. Acceptable results (when  $\Delta E \leq 5$ ) were obtained when Silo 111 was used on both stones and Fluoline HY minimum amount on Comiso stone.

Reduction in water vapour permeability was observed in all tested cases. The biggest porosity obstruction occurred when maximum amount of Silo 111 and Fluoline HY was used for the treatment of Noto stone samples. In case of Comiso stone samples, the biggest reduction was observed with maximum amount of Fluoline HY. The smallest changes in water vapour permeability were achieved when Wacker 290 minimum amount was used for the treatment of Noto stone, while for Comiso stone – minimum amount of Fluoline HY and both amounts of Wacker 290.

The most promising results in terms of developed hydrophobic effect and water vapour permeability were achieved on both Noto and Comiso stone samples using Wacker 290, although it caused chromatic alterations on the stone surface after the application of recommended amounts of product by the supplier. As it could be seen, liquid water absorption, water vapour permeability and static contact angle measurement results were not strongly dependent on the amount of product used, further investigations

should be done in order to find optimum product amount which would result in development of hydrophobic effect and reduction in chromatic alterations.

Silo 111, when applied on both Noto and Comiso stone samples, did not result in expected hydrophobic effect after the application of recommended amounts, while opposite results were achieved after sample treatment till rejection, which proves the necessity of further investigations in order to find suitable amount of product to be applied.

Fluoline HY formed a film on the stones' surface and caused porosity reduction after its application on Noto and maximum amount of product on Comiso stone samples.

The interactions were observed by solid-state NMR after the treatment of Comiso stone with Fluoline HY, which could be hypothesized as a formation of covalent bond between the elements of the polymer and carbonate-hydroxyapatite component of Comiso stone, while no such phenomena were observed in case of Noto stone.

Further investigations needs to be done on protective polymeric dispersions, for example the incorporation of inorganic nanoparticles, in order to eliminate or reduce undesirable properties.

## **Acknowledgement**

I would like to thank Prof. Eugenio Caponetti for the supervision and the given opportunity to do my master thesis project at the University of Palermo.

I also would like to thank Dr. Sillvestro Antonio Ruffolo for the co-supervision and a possibility to do mercury intrusion porosimetry measurements and petrographic characterization of samples in the laboratory of the University of Calabria.

The exceptional gratitude goes to Vincenzo Renda for the supervision throughout the entire process, help with solving problems, performing measurements, for support, priceless lessons and advices that I will never forget.

I want to thank to Alberto Spinella for the solid-state NMR measurements and help with the interpretation of the results.

Maria Luisa Saladino for the help with XRD measurements and follow up.

Francesco Lopresti for SEM-EDX and contact angle measurements.

I am also very thankful to my ARCHMAT colleagues Whitney Jacobs, Carla Soto, Ivona Posedi, Indre Zalaite, Diego Badillo, Guilhem Mauran, Aman Maldewo, Milan Markovic, Dela Kuma, Rana Abboud, Dauren Adibekov, Francisco Centola, Elisaveta Demidova, Leonor Costa and Drita Abazi for making this journey unforgettable.

## Bibliography

1. Camuffo D. Physical weathering of stones. *Sci Total Environ*, 167, 1995, p. 1-14.
2. Lee C. H., Lee M. S., Suh M., Choi S. W. Weathering and deterioration of rock properties of the Dabotap pagoda (World Cultural Heritage), Republic of Korea. *Environ Geol*, 47, 2005, p. 547–557.
3. Domasłowski W. Preventive conservation of stone objects. Torun, 2003, ISBN 83-231-1645-8
4. Ciantia M. O., Castellanza R., di Prisco C. Experimental study on the water-induced weakening of calcarenites. *Rock Mech Rock Eng*, 48, 2015, p. 441-461.
5. Zanardinia E., Abbruscato P., Ghedini N., Realini M., Sorlini C. Influence of atmospheric pollutants on the biodeterioration of stone, *Int Biodeter Biodeg*, 45, 2000, p. 35-42.
6. Soluble salts and deterioration of archaeological materials. *Conserve O Gram*, 6/5, 1998
7. Cataldo R., De Donno A., De Nunzio G., Leucci G., Nuzzo L., Siviero S. Integrated methods for analysis of deterioration of cultural heritage: the Crypt of “Cattedrale di Otranto”. *J Cult Herit*, 6, 2005, p. 29-38.
8. Gomez-Herasi M., Benavente D., Alvarez de Buergo M., Fort R. Soluble salt minerals from pigeon droppings as potential contributors to the decay of stone based cultural heritage. *Eur. J. Mineral*, 16, 2004, p. 505-509.
9. Pavlík Z., Žumár J., Pavlíková M., Černý R. Interaction of building stones with inorganic water-soluble salts. *International Journal of Chemical, Molecular, Nuclear, Materials and Metallurgical Engineering*, 6, 2013, p. 328-333.
10. Moropoulou A., Kouloumbi N., Haralampopoulos G., Konstanti A., Michailidis P. Criteria and methodology for the evaluation of conservation interventions on treated porous stone susceptible to salt decay. *Prog Org Coat*, 48, 2003, p. 259–270.
11. Warscheid Th., Braams J. Biodeterioration of Stone: a Review. *Int Biodeter Biodeg*, 46, 2000, p. 343-368.
12. Tomaselli L., Lamenti G., Bosco M., Tiano P. Biodiversity of photosynthetic micro-organisms dwelling on stone monuments. *Int Biodeter Biodeg*, 46, 2000, p. 251-258.
13. Sterflinger K. Fungi: their role in deterioration of cultural heritage. *Fungal. Biol.*, 24, 2010, p. 47-55.
14. Chen J., Blume H., Beyer L. Weathering of rocks induced by lichen colonization - a review. *Catena*, 39, 2000, p. 121-146.
15. Pozo-Antonio J. S., Ramil A., Rivas T., López A. J., Fiorucci M. P. Effectiveness of chemical, mechanical and laser cleaning methods of sulphated black crusts developed on granite. *Constr Build Mater*, 112, 2016, p. 682-690.

16. Senesi G. S., Carrara I., Nicolodelli G., Milori D. M. B. P., De Pascale O. Laser cleaning and laser-induced breakdown spectroscopy applied in removing and characterizing black crusts from limestones of Castello Svevo, Bari, Italy: A case study. *Microchemical J*, 124, 2016, p. 296–305.
17. Aibeo C., Cavallin T., Egel E., Favaro M., Kamenova V., Nodari L., Patelli A., Pavlov A., Pavlova I., Schalm O., Scopece P., Simon S., Storme P., Verga Falzacappa E., Voltolina S. Preliminary assessment of atmospheric plasma torches for cleaning of architectural surfaces. *3<sup>rd</sup> European Workshop on Cultural Heritage Preservation, EWCHP 2013*.
18. Sanmartín P., Cappitelli F., Mitchell R. Current methods of graffiti removal: A review. *Constr Build Mater*, 71, 2014, p. 363-374.
19. Pozo-Antonio J. S., Rivas T., Fiorucci M. P., López A. J., Ramil A. Effectiveness and harmfulness evaluation of graffiti cleaning by mechanical, chemical and laser procedures on granite. *Microchemical J*, 125, 2016, p. 1–9.
20. Licchelli M., Malagodi M., Weththimuni M., Zanchi C. Anti-graffiti nanocomposite materials for surface protection of a very porous stone. *Appl. Phys. A*, 116, 2014, p. 1525-1539.
21. Pinho L., Mosquera M. J. Titania-Silica nanocomposite photocatalysts with application in stone self-cleaning. *J. Phys. Chem. C*, 115, 2011, p. 22851-22862.
22. Ferreira Pinto A. P., Delgado Rodrigues J. Stone consolidation: The role of treatment procedures. *J Cult Herit*, 9, 2008, p. 38-53.
23. Baglioni P., Rodorico G., Ching-chih C. Nanoparticle technology saves cultural relics: potential for a multimedia digital library. *Online Proceedings of DELOS/NSF Workshop on Multimedia Contents in Digital Libraries*, 2003.
24. Delgado Rodrigues J., Ferreira Pinto A. P. Laboratory and onsite study of barium hydroxide as a consolidant for high porosity limestones. *J Cult Herit*, 19, 2016, p. 467-476.
25. Chelazzi D., Poggi G., Jaidar Y., Toccafondi N., Giorgi R., Baglioni P. Hydroxide nanoparticles for cultural heritage: consolidation and protection of wall paintings and carbonate materials. *J. Colloid Interface Sci.*, 392, 2013, p. 42-49.
26. Remzova M., Sasek P., Frankeova D., Slizkova Z., Rathousky J. Effect of modified ethylsilicate consolidants on the mechanical properties of sandstone. *Constr Build Mater*, 112, 2016, p. 674-681.
27. Sassoni E., Graziani G., Franzoni E. An innovative phosphate-based consolidant for limestone. Part 1: Effectiveness and compatibility in comparison with ethyl silicate. *Constr Build Mater*, 102, 2016, p. 918-930.
28. Sassoni E., Graziani G., Franzoni E. An innovative phosphate-based consolidant for limestone. Part 2: Durability in comparison with ethyl silicate. *Constr Build Mater*, 102, 2016, p. 931–942.

29. Borgia G. C., Bortolotta V., Camaiti M., Cerrib F., Fantazzinic P., Piacenti F. Performance evolution of hydrophobic treatments for stone conservation investigated by MRI. *Magnetic Resonance Imaging*, 19, 2001, p. 513–516.
30. Laurenzi Tabasso M. Acrylic polymers for the conservation of stone: advantages and drawbacks. *APT Bulletin*, Vol. 26, No. 4, 1995, p. 17-21.
31. Favaro M., Mendichi R., Ossola F., Simon S., Tomasin P., Vigato P. A. Evaluation of polymers for conservation treatments of outdoor exposed stone monuments. Part II: Photo-oxidative and salt-induced weathering of acrylic-silicone mixtures. *Polym. Degrad. Stab.*, 92, 2007, p. 335-351.
32. Colas A., Corning D. Silicones: preparation, properties and performance. Dow Corning, Life Sciences, 2005, Form No. 01-3077-01.
33. Sadat-Shojai M., Ershad-Langroudi A. Polymeric coatings for protection of historic monument: opportunities and challenges. *J. Appl. Polym. Sci.*, 112, 2009, p. 2535-2551.
34. Smith D. W., Iacono S. T., Boday D. J., Kettwich S. C. Advances in fluorine-containing polymers. Oxford University Press, 2012, ISBN 978-0-8412-2792-7.
35. Amcduri B., Boutevin B. Well architecture fluoropolymers: synthesis, properties and applications, 1-st edition. Elsevier Ltd., 2004, ISBN: 0-08-0443885.
36. Liu S., Liu X., Latthe S. S., Gao L., An S., Yoon S. S., Liu B., Xing R. Self-cleaning transparent superhydrophobic coatings through simple sol–gel processing of fluoroalkylsilane. *Appl Surf Sci*, 351, 2015, p. 897-903.
37. UNI EN 15886, Conservation of cultural property - Test methods - Color measurement of surfaces (2010).
38. UNI EN 15801, Conservation of cultural property - Test methods - Determination of water absorption by capillarity (2010).
39. UNI EN 15803, Conservation of cultural property - Test methods - Determination of water vapor permeability (2010).
40. UNI EN 15802, Conservation of cultural property - Test methods - Determination of static contact angle (2010).
41. La Russa M. F., Belfiore C. M., Fichera G. V., Maniscalco R., Calabro C., Ruffolo S. A., Pezzino A. The behaviour to weathering of the Hyblean limestone in the Baroque architecture of the Val di Noto (SE Sicily): an experimental study on the “calcare a lumachella” stone. *Constr Build Mater*, 77, 2015, p. 7-19.
42. Bonforte A., Catalano S., Maniscalco R., Pavano F., Romagnoli G., Sturiale G., Tortorici G. Geological and Geodetic Constraints on the Active Deformation Along the Northern Margin of the Hyblean Plateau (SE Sicily). *Tectonophysics*, 640–641, 2015, p. 80–89.



43. Baronio G., Binda L., Tedeschi C., Tiraboschi C. Characterisation of the materials used in the construction of the Noto Cathedral. *Constr Build Mater*, 17, 2003, p. 557-571.
44. Binda L., Tiraboschi C., Baronio G. On-site investigation on the remains of the Cathedral of Noto. *Constr Build Mater*, 17, 2003, p. 543-555.
45. Tringali S., De Benedictis R., La Rosa R., Russo C., Bramante A., Gavarini C., Valente G., Ceradini V., Tocci C., Tobriner S., Maugeri M., Binda L., Baronio G. The reconstruction of the Cathedral of Noto. *Constr Build Mater*, 17, 2003, p. 573-578.
46. La Russa M. F., Barone G., Belfiore C. M., Mazzoleni P., Pezzino A. Application of protective products to “Noto” calcarenite (south-eastern Sicily): a case study for the conservation of stone materials. *Environ Earth Sci*, 62, 2010, p. 1263-1272.
47. Anania L., Badala A., Barone G., Belfiore C. M., Calabro C., La Russa M. F., Mazzoleni P., Pezzino A. The stones in monumental masonry buildings of the “Val di Noto” area: new data on the relationships between petrographic characters and physical–mechanical properties. *Constr Build Mater*, 33, 2012, p. 122-132.
48. La Russa M. F., Rovella N., de Buergo A. M., Belfiore C. M., Pezzino A., Crisci G. M., Ruffolo S. A. Nano-TiO<sub>2</sub> coatings for cultural heritage protection: the role of the binder on hydrophobic and self-cleaning efficacy. *Prog Org Coat*, 91, 2016, p. 1-8.
49. Bergamonti L., Alfieri I., Lorenzi A., Predieri G., Barone G., Gemelli G., Mazzoleni P., Raneri S., Bersani D., Lottici P. P. Nanocrystalline TiO<sub>2</sub> coatings by sol–gel: photocatalytic activity on Pietra di Noto biocalcarene. *J Sol-Gel Sci Technol*, 75, 2015, p. 141-151.
50. Basics of Polarizing Microscopy. Retrieved from: [http://research.physics.berkeley.edu/yildiz/Teaching/PHYS250/Lecture\\_PDFs/polarization%20microscopy.pdf](http://research.physics.berkeley.edu/yildiz/Teaching/PHYS250/Lecture_PDFs/polarization%20microscopy.pdf)
51. Dunham R. J. Classification of Carbonate Rocks According to Depositional Texture. In: Ham, W.E., Ed., Classification of Carbonate Rocks, AAPG, Tulsa, 1962.
52. Folk R. L. Practical petrographic classification of limestones. American Association of Petroleum Geologists Bulletin, 43, 1959.
53. Ahr W. M. Geology of carbonate Reservoirs. The Identification, Description, and Characterization of Hydrocarbon Reservoirs in Carbonate Rocks. A John Wiley & Sons, Inc., Hoboken, New Jersey, 2008, ISBN 978-0-470-16491-4.
54. Madejova J., Komadel P. Baseline Studies of the Clay Minerals Society Source Clays: Infrared Methods. *Clays Clay Miner.*, 49, 5, 2001, p. 410-432.
55. Isbester P. K., Brandt J. L., Kestner T. A., Munson E. J. High-Resolution Variable-Temperature <sup>19</sup>F MAS NMR Spectroscopy of Vinylidene Fluoride Based Fluoropolymers. *Macromolecules*, 31, 1998, p. 8192-8200.

56. Polyvinylidene Fluoride and its Blend: Miscibility and Crystallization Studies by FT-IR Spectroscopy. Retrieved from: [http://shodhganga.inflibnet.ac.in/bitstream/10603/37801/6/015\\_chapter%205.pdf](http://shodhganga.inflibnet.ac.in/bitstream/10603/37801/6/015_chapter%205.pdf)
57. Bergamonti L., Alfieri I., Lorenzi A., Montenero A., Predieri G., Barone G., Mazzoleni P., Pasquale S., Lottici P. P. Nanocrystalline TiO<sub>2</sub> by sol-gel: characterisation and photocatalytic activity on Modica and Comiso stones. *Appl Surf Sci*, 282, 2013, p. 165-173.
58. Cardiano P., Sergi S., Lo Schiavo S., Piraino P. In situ polymerization of 3-glycidoxypropyl trimethoxysilane (GLYTS) as a new tool for stone conservation. *Annali di Chimica*, 93, 2003.
59. Cameotra S. S., Dakal T. C. Carbonatogenesis: microbial contribution to the conservation of monuments and stone artwork. *Conserv. Sci. Cult. Herit.*, 12, 2012, p. 79-108.
60. Ahmed G. S., Gilbert M., Mainprize S., Rogerson M. FT-IR analysis of Silane Grafted High Density Polyethylene. *Plastics, Rubber and Composites*, 38 (1), 2009, p. 13 – 20.
61. Ricci C., Miliani C., Brunetti B. G., Sgamellotti A. Non-invasive Identification of Surface Materials on Marble Artifacts With Fiber Optic mid-FT-IR Reflectance Spectroscopy. *Talanta*, 69, 2006, p. 1221-1226.
62. Poli T., Elia A., Chiantore O. Surface Finishes and Materials: Fiber-optics reflectance spectroscopy (FORS) Problems in Cultural Heritage Diagnostics. *e-PS*, 6, 2009, p. 174-179.
63. Dolbier Jr. W. R. Guide to Fluorine NMR for Organic Chemists. John Wiley & Sons, Inc., New Jersey, USA, 2009.
64. Ohta N., Robertson A. R. Colorimetry. Fundamentals and applications. John Wiley & Sons Ltd, 2005, SBN-13 978-0-470-09472-3 (HB).
65. Carey F. A., Giuliano R. M. Organic Chemistry 8th Edition. McGraw-Hill, 2010, ISBN-10: 0073402613.
66. Derrick M. R., Stulik D., Landry J. M. Infrared spectroscopy in conservation science. The Getty Conservation Institute Los Angeles, 1999, ISBN 0-89236-469-6.
67. Theophanides T. Infrared Spectroscopy - Materials Science, Engineering and Technology. InTech, 2012, ISBN 978-953-51-0537-4.
68. Chércoles Asensio R., San Andrés Moya M., de la Roja J. M., Gómez M. Analytical characterization of polymers used in conservation and restoration by ATR-FT-IR spectroscopy. *Anal. Bioanal. Chem.*, 395, 2009, p. 2081–2096.
69. Capitani D., Di Tullio V., Proietti N. Nuclear Magnetic Resonance to characterize and monitor Cultural Heritage. *Prog. Nucl. Magn. Reson. Spectrosc.*, 64, 2012, p. 29–69.
70. Bastone S., Spinella A., Chillura Martino D. F., Tusa S., Caponetti E. More insight into characterization of the waterlogged wooden part of Acqualadroni Roman Rostrum by solid-state NMR. *Microchem. J.*, 124, 2016, p. 831-836.

71. Blumich B., Casanova F., Perlo J., Presciutti F., Anselmi C., Doherty B. Noninvasive testing of art and cultural heritage by mobile NMR. *Accounts Chem. Res.*, Vol. 43, No. 6, 2010, p. 761-770.
72. Goldstein J. I., Newbury D. E., Echlin P., Joy D. C., Lyman C. E., Lifshin E., Sawyer L., Michael J. R. Scanning electron microscopy, 3-rd edition. Kluwer Academic/Plenum Publishers, New York Boston, Dordrecht, London, Moscow, 2003, ISBN: 0-306-47292-9.
73. Kazmiruk V. Scanning Electron Microscopy. InTech, Rijeka, 2012, ISBN 978-953-51-0092-8.
74. Krinsley D. H., Pye K., Boggs S. Jr., Tovey N. K. Backscattered Scanning Electron Microscopy and Image Analysis of Sediments and Sedimentary Rocks. Cambridge University Press, New York, 1998, ISBN 0-521-45346-1.
75. Schreiner M., Melcher M., Uhler K. Scanning electron microscopy and energy dispersive analysis: applications in the field of cultural heritage. *Anal. Bioanal. Chem.*, 387, 2007, p. 737-747.
76. Tuduce Traistaru A., Sandu I. C. A., Timar M. C., Dumitrescu G. L., Sandu I. SEM-EDX, Water Absorption, and Wetting Capability Studies on Evaluation of the Influence of Nano-Zinc Oxide as Additive to Paraloid B72 Solutions Used for Wooden Artifacts Consolidation. *Microsc. Res. Tech.*, 76, 2013, p. 209-218.
77. Janssens K. Non-destructive Micro Analysis of Cultural Heritage Materials, 1-st edition. Elsevier Science, 2004, ISBN 9780080454429.
78. Muller R. O. Spectrochemical Analysis by X-ray Fluorescence. Plenum Press, New York, 1972, ISBN-13: 978-1-4684-1799-9.
79. Calza C., Anjos M. J., Buen M. I., Mendonca de Souza S., Brancaglioni A. Jr., Lima T. A., Lopes R. T. XRF applications in archaeometry: analysis of Marajoara pubic covers and pigments from the sarcophagus cartonnage of an Egyptian mummy. *X-Ray Spectrom.*, 36, 2007, p. 348-354.
80. Shackley M. S. X-Ray Fluorescence Spectrometry (XRF) in Geoarchaeology. Springer New York Dordrecht Heidelberg London, 2011, ISBN 978-1-4419-6885-2.
81. Wheeler B. D. Analysis of limestones and dolomites by X-ray fluorescence. *The Rigaku Journal*, Vol. 16, No. 1, 1999, p. 16-25.

## X. Appendix

### *Appendix I.* Characterization techniques

#### **Colorimetry**

Colorimetry is a common technique used in the field of cultural heritage because it is a non-invasive and non-destructive method which provides information about colour and its change due to various factors, such as treatment with protective formulations, atmospheric pollution, previous restoration practices, etc.

Better understanding of the color vision phenomena can be achieved by opponent-colors theory which states that retina of the human eye consists of three types of photoreceptors which respond to red-green, yellow-blue and white-black opponencies and all colors can be characterized by the degree of response of these photoreceptors to the color [64].

#### **Liquid water absorption by capillarity**

The phenomena of water transportation can be easier understood when the capillary system of stone is taken into account. Capillary rising of liquids strongly depends on the size of pores inside the stone as it can rise up to different levels. The height of capillary rising can be expressed by the equation (13):

$$h = \frac{2\delta}{r * d * g} \quad (13),$$

where:

$\delta$  – surface tension of water (N/m),

$r$  – radius of the capillary tube (m),

$d$  – water density (kg/m<sup>3</sup>),

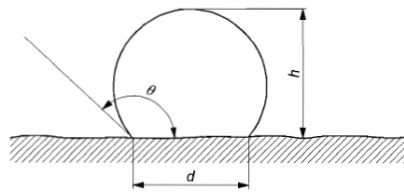
$g$  – acceleration of gravity (m/s<sup>2</sup>).

As the equation (13) shows, the higher water level in stone capillaries will be achieved in case of fine pores because of smaller radius value rather than in coarse pores. This phenomena has led to the

classification of capillaries according to pore radius: micropores are of a diameter smaller than 2 nm, mesopores - between 2 and 50 nm, macropores – diameter greater than 50 nm [3].

### Static contact angle

When a drop of water enters in contact with a solid surface, the static contact angle is evaluated as the angle  $\theta$  (in degrees) formed between the surface of the sample and the water drop, at the contact point (*Fig. 11*), where:  $d$  – a diameter of the contact surface in mm,  $h$  – height in mm,  $\theta$  – static contact angle in degrees. It represents the hydro-repellency of the surface due to adhesion and cohesion forces between the liquid and the surface. If cohesion forces inside the liquid drop are stronger than the adhesion forces between solid and liquid, a spherical form of the drop will be observed with a contact angle greater than  $90^\circ$  and the surface could be considered as hydrophobic. On the other hand, if static contact angle is lower than  $90^\circ$ , the surface could be considered as hydrophilic.



**Fig. 11.** Scheme of static contact angle [40]

### Fourier transformed infrared spectroscopy (FT-IR)

Infrared spectroscopy (IR) is an important analysis technique used to determine the structure of materials at molecular level, due to the possibility to identify the presence of certain atom groups within the molecule, both organic and inorganic. IR spectroscopy is based on the ability of chemical bonds of absorbing energy by vibrating in characteristic ways when subjected to IR radiation [65]. This technique can be used to analyse both organic and inorganic materials, in solid, liquid or gaseous phases, with the exception of metals, due to strong reflection of electromagnetic waves. There are several techniques by which an IR spectra could be obtained and they must be chosen depending on the particular sample to be analysed. For example, transmission method, in which the IR beam is studied after passing through the sample, can be used to investigate samples of all physical phases but in many cases requires a preliminary preparation of the sample and dilution with KBr to obtain a low concentration of the chemical species to analyse, in order to avoid complete absorption of the IR radiation from the sample.

The reflection method, in which the IR beam is analysed after being reflected by the sample, is mainly used for surface analysis of solid specimens [66].

The above mentioned reflectance IR spectroscopy can be used to analyse samples which are difficult to investigate by transmittance method. Light might undergo three types of reflection due to the interaction of sample surface with electromagnetic radiation: internal, specular and diffuse reflection, depending on the characteristics of the sample surface. Internal reflection spectroscopy, also known as attenuated total reflection (ATR) spectroscopy is based on total internal reflection phenomenon. ATR technique is commonly used to analyse opaque materials and thin films. Specular reflection occurs when the incident radiation is directly reflected by the sample and results in mirror-like reflection when the reflection angle is the same as incident radiation angle. Specular reflection IR spectroscopy is used for the samples with a smooth surface. Diffuse reflection IR spectroscopy (DRIFT) is based on analysis of IR radiation diffused by the sample and is associated with the reflection from rough surfaces. This technique is used for analysis of powders and solid samples [67].

Due to the possibility to examine materials of different chemical origin, IR spectroscopy is widely applied in the field of cultural heritage. One of relatively common applications is the characterization of conservation products based on polymers. ATR-FT-IR has been proven to give excellent results for this purpose as it allows the analysis of materials made of synthetic polymers which have different characteristics and also allows identification of additives [68].

### **Solid state nuclear magnetic resonance (ss-NMR)**

Nuclear magnetic resonance (NMR) spectroscopy is an analysis technique which is based on the ability of atom nuclei to behave like a magnet when subjected to a magnetic field, generated by using a superconductive magnet. This technique gives information about the molecular composition of the substance. Due to the experimental setting, ss-NMR is a micro-destructive technique, since the material to be analysed should be placed inside the instrument where the magnetic field is homogeneous and the sample should be preliminarily ground to assure homogeneity in the sample under examination.

The most often applied types of NMR spectroscopy are  $^1\text{H}$  and  $^{13}\text{C}$  because hydrogen and carbon are the most common elements in organic molecules and the analysis of their isotopes can provide researchers of NMR spectra rich in information about their chemical environments [65].

NMR spectroscopy has found its application in medicine, science and technology. It is also becoming more and more common in the field of cultural heritage as well but its application is rather recent due to the fact that it was possible to analyse materials only in the liquid phase which would require changing of molecular structure of such materials as parchment, leather, paper, wood, etc. However, the development of solid state NMR solved above mentioned problems making NMR a powerful tool for the analysis of materials belonging even to cultural heritage [69]. In particular, analysis of relaxation times of the NMR active nuclei, possible with an expert use of ss-NMR and exploitation of dipolar coupling effects, can give strong indication about interactions involving non-covalent bonds and interphase phenomena, in this way giving information about the conservation state of an artefact [70].

However, the instrumentation is large and expensive and obtaining an NMR spectrum requires sampling, which carries some limitations in its application for the analysis of cultural heritage. Although, some researches and trials of mobile NMR instruments have been already done which makes it promising technique in the future for the analysis of cultural heritage as it is portable and non-invasive [71].

### **Scanning electron microscopy (SEM)**

Scanning electron microscopy (SEM) is a widely used investigation technique which provides information about surface morphology of organic and inorganic materials, together with their elemental composition when coupled with a EDX analyser. The principle of SEM is the irradiation of the area to be analysed with a finely focused electron beam. The interaction of an electron beam with the sample causes the occurrence of different types of secondary emissions, such as secondary electrons, and X-rays, which are collected by the analyser together with backscattered electrons. In terms of imaging, the most important signals are secondary and backscattered electrons as they vary depending on the surface topography of the sample, which results in the possibility of evaluating microstructural characteristics of solid objects by providing high resolution images, because of the low lateral resolution of this technique. In addition to that, as a result of electron irradiation, characteristic secondary X-rays are emitted, which give information about qualitative and quantitative elemental composition [72].

In order to get a deeper insight into the working principle of this technique, it is important to understand the electron-atom interaction processes. The interaction occurs not only on the surface but also inside the matter. The electron interaction with the sample consists of Coulomb attraction with positive charged

nuclei, and repulsion with electrons from the sample. As a result, changes in momentum or energy of electrons can be experienced and entering electron beam can scatter elastically or inelastically and generate backscattered and secondary electrons respectively [73].

SEM imaging has found its application in various fields, such as geology, as it allows to obtain data about the size, shape, distribution of grains, mineralogy and porosity of fine particles [74], cultural heritage for the material characterization of various objects of artistic importance [75], studies of the distribution and penetration pathways of protective materials on the surface of the object [76].

### **X-ray fluorescence (XRF)**

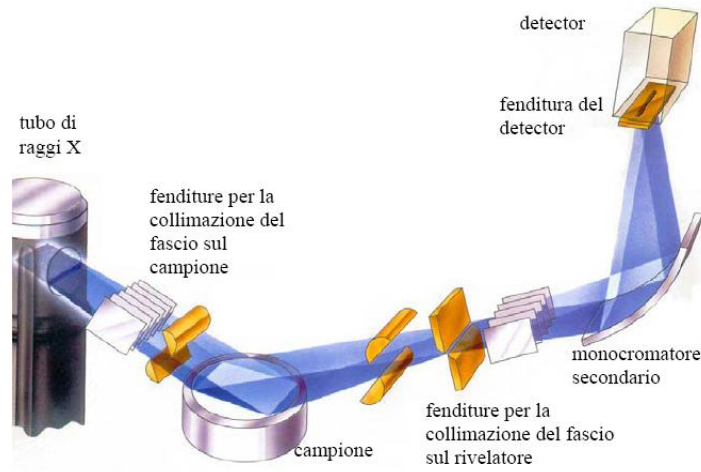
X-ray fluorescence spectrometry (XRF) is a non-invasive and non-destructive analysis technique and one of the most used methods in the field of cultural heritage for qualitative and semi-quantitative analysis. It is based on the ionization of the atoms of the material to be examined by a beam of primary X-rays. The principle of this technique is that a beam of monochromatic X-ray photons is used to expel an inner shell electron to the continuum when an atom is exposed to the necessary amount of energy. The excited atom then tends to return to the ground state filling the gap left by the expelled electron with an electron from a neighbouring outer shell, whose place then is occupied by another electron from an outer shell [77]. At every step, since electrons go from higher energy levels into lower energy levels, the excess energy has a probability to be emitted in form of X-ray photons. Each transition, labelled with a specific letter such as K, L, M, etc., is characteristic for each element and by measuring the energy of the emitted radiations a particular element can be identified [78].

A wide variety of XRF technique application examples in the field of archaeometry can be found, for instance, an investigation of the composition of metal alloys, sculpture, coins, pigments in paintings, ceramics, manuscripts and others [79]. One of the main reasons of such popularity is its non-destructive nature, together with the fact that samples remain unchanged after exposure to X-rays for the time requested for the analysis. In fact, the measurement requires only minimum sample preparation, such as basic cleaning from dirt, and is very fast (few seconds) [80]. Although, some limitations in the usage of this technique can be observed, such as peak overlaps, Compton scattering from low atomic number elements and other effects that introduce spectral artefacts. Moreover, the intensity of analytical lines can be affected by particle size, structural differences among samples, absorption and enhancement effects [81].



## X-ray diffraction (XRD)

X-Ray Diffraction (XRD) is a technique that is used to obtain information about phases, structure, composition and dimension of crystallites in mono and polycrystalline materials.



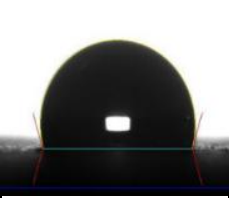

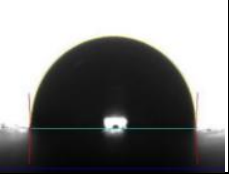
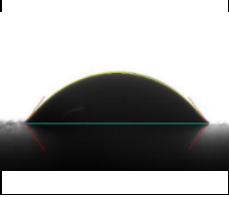


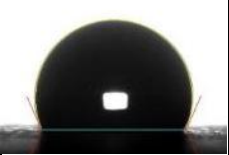


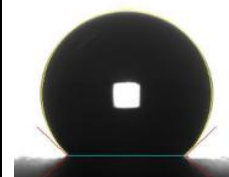


**Figure 12. Powder diffractometer scheme.**

The technique used for the analysis of samples is powder diffraction: the sample is constituted by a high number of crystallites oriented casually. It is a relatively simple technique that gives structural information averaged statistically on a wide spatial region. Diffraction pattern is made of a series of peaks due to reflections, each of which is generated by diffraction from the plane family  $h k l$ . If there are present more crystalline phases, it is possible to identify them, since reflections from each of them are additive.

Through this technique it is possible to identify a material in the crystalline state in which it is found, since it is examined diffraction of the radiation caused by interaction with atoms placed regularly in lattice planes. Constructive interference of diffracted radiation enables to evaluate interplanar distances  $d_{hkl}$  of lattice planes through Bragg's law from the measurement of diffraction angles  $\theta$ . Distance values  $d_{hkl}$  are characteristic features of each lattice planes families; determination of these values, connected with Miller index  $h k l$  of the planes from which they are generated, enables to determine cell parameters of the unit cell of crystalline phase under exam.

*Appendix 2.* Contact angle measurements data of Noto and Comiso stone samples

Sample name	Product	Amount	Image	Average	
C62	-	-		0	
C74	Fluoline HY	Min		$102.91 \pm 6.32$	
C72	Fluoline HY	Max		$92.78 \pm 2.62$	
C50	Silo 111	Min		$47.25 \pm 10.06$	
C61	Silo 111	Max		$58.93 \pm 6.81$	
C37	Silo 111	Rejection		$113.42 \pm 3.47$	
C63	Wacker 290	Min		$131.00 \pm 3.29$	
C84	Wacker 290	Max		$135.33 \pm 1.98$	



N9	-	-		$23.43 \pm 5.47$	
N37	Fluoline HY	Min		$92.55 \pm 3.41$	
N33	Fluoline HY	Max		$92.13 \pm 1.50$	
N17	Silo 111	Min		$57.40 \pm 6.22$	
N18	Silo 111	Max		$54.85 \pm 2.48$	
N65	Silo 111	Rejection		$117.79 \pm 3.88$	
N6	Wacker 290	Min		$128.80 \pm 6.48$	
N15	Wacker 290	Max		$101.13 \pm 3.43$	